THE UNIVERSITY OF CHICAGO

ENGINEERING THE IMMUNE SYSTEM TO IMPROVE VACCINES: CHEMICAL APPROACHES TO MODULATING INNATE IMMUNITY

A DISSERTATION SUBMITTED TO

THE FACULTY OF THE DIVISION OF THE PHYSICAL SCIENCES

IN CANDIDACY FOR THE DEGREE OF

DOCTOR OF PHILOSOPHY

DEPARTMENT OF CHEMISTRY

BY

BRADLEY STUDNITZER

CHICAGO, ILLINOIS

MARCH 2023

Table of Contents

List of Figures

Acknowledgements

I am so grateful to the many people who have supported me throughout my PhD. To my PhD advisor, Professor Aaron Esser-Kahn, I cannot thank you enough for the support and guidance you've given me the last five years. To the rest of my thesis committee, Professor Bozhi Tian and Professor Bryan Dickinson, thank you so much for your support and scientific guidance. I want to thank the entire Esser-Kahn lab for being an amazing place to do science. To Britteny Cassaidy, Matt Rosenberger, Jainu Ajit, Jeremiah Kim, Seong-Min Kim Vicente Mateus, and Adam Weiss, thank you for being amazing colleagues and even better friends.

Outside of the lab, there are numerous friends I would like to thank: Norman Zhao for our jerk chicken nights; Matt Zajac for our gym sessions; Tim Grabnic for being the best Baseliner captain and point partygoer; Kate Henn for being my CorePower buddy. To the former apartment members of 5491, I could not think of a better group of roommates with whom to bunker down for COVID; to Nathaniel Durfee for being the best mashed potato maker, to Adam Weiss for being an amazing Baseliners co-captain and Yoop fanatic, and to Ben Soloway for being my burrito buddy and tennis pal #rollfords.

To my Shorefamily, Sarah Willson and Adam Antoszewski, I want to thank you both for being my best friends throughout my graduate school experience. We had so many fun times and fond memories, including friends' dates, Michigan trip, feeding Rudy, and countless inside jokes. Sarah is such a kind, caring roommate, who would drive my passport to O'Hare at the most inconvenient time. To Adam, who has been my best friend since day one of the program. Starting with 1st year social events, to 2nd year TV watch sessions, to 3rd year COVID Facetimes and beyond, I cannot express how much your friendship means to me. To my parents, Debbie and Eliot, and siblings, Josh, Sam, and Dara, who have been a huge support through this entire

process (and long before), thank you. Your encouragement and support mean the world to me. Lastly, to Kendall, my most amazing partner – thank you for everything. You are always so kind, supportive, and fun in all the most perfect of ways. I cannot wait for what the future has in store for us. Cheers.

Abstract

This thesis focuses on modulating the innate immune responses with chemical tools with two specific goals: (1) to improve vaccines by determining the best way to elicit immune signaling from the cells with the strongest signaling capability and (2) to better understand the biological mechanisms that lead to allergic contact dermatitis and provide potential therapeutics to treat this condition. Vaccines are one of the best ways to prevent disease in humans and animals; by this prevention of disease, vaccines extend survival and improve quality of life. Vaccines work by educating the immune system to recognize a particular pathogen without risk of getting the disease. Vaccines rely on antigen presenting cells to signal to adaptive immune cells to generate a robust and specific protective response. In this work, I isolate and characterize first-responding dendritic cells (FRs), a subset of dendritic cells that (1) show increased responses to pathogen associated molecular patterns, (2) facilitate adaptive immune responses by providing the initial paracrine signaling, and (3) can be selectively targeted by vaccines to modulate both antibody and T cell responses *in vivo*. Additionally, by targeting the FRs with a synergistic TLR agonist formulation, we demonstrate that we can enhance the FR cytokine response for TNF-α, IL-6, and IL12-p70. Additionally, we reduce bulk population cytokines using a brefeldin loaded liposome that selectively targets FRs, ablating their signaling function. These results demonstrate the importance of FRs in generating large scale immune responses necessary to provide robust antibody protection against disease, and how these FRs can be targeted by vaccines to optimize results.

Allergic contact dermatitis (ACD) is a condition in which an individual has an inflammatory response to small compounds called contact allergens. ACD is estimated to affect up to 20 % of the USA's population and is characterized by a sensitization phase and elicitation

phase. ACD is the most common occupational hazard in the United States, resulting in millions of dollars of productivity loss per year. In this work, we identify honokiol as the first known compound to reduce both sensitization and elicitation to dinitrochlorobenzene, a model hapten. Additionally, we identify IRF-3 is a key inflammatory transcription factor in the ACD response. These findings promise to enable novel classes of therapeutics for ACD.

Preface

Portions of Chapter 2 have been reproduced with permission from: Deak, P.; Studnitzer B.; Ung, T.; Steinhardt, R.; Swartz, M.; Esser-Kahn, A. Isolating and targeting a highly active, stochastic dendritic cell subpopulation for improved immune responses. Cell Reports. 41 (5), 111563, 2022.

Chapter 1: Introduction

1.1 Introduction to Vaccines

Vaccines are one of the best ways to prevent disease in humans and animals; by this prevention of disease, vaccines extend survival and improve quality of life.[1] Vaccines work by educating the immune system to recognize a particular pathogen without risk of getting the disease.[2,3] Vaccines are typically designed empirically, containing a live or attenuated form of the pathogen.[4,5,] This design has been successful for a handful of diseases, leading to eradication of diseases such as diphtheria and small pox; however, it presents certain challenges for other diseases. [6,7,8] For example, some inactivated pathogens do not elicit a strong protective immune response that is desired for vaccines.[9] Additionally, there are other important factors, such as side effects or storage requirements, that could make a vaccine fail in clinical trials. To overcome these challenges, it is important to have a clear picture of the biological framework for how the body responds to these vaccines, as well as adaptable tools that can effectively modulate the protection induced by the vaccine.

1.2 Innate and Adaptive Immune System

There are two branches of the immune system: the innate immune system and the adaptive immune system. Both parts of the immune system are critical in preventing disease and are linked to each other via feedback mechanisms. The innate immune system is the body's initial line of defense against a pathogen; it acts swiftly and non-specifically.[10] Innate immune cells detect exposure to a pathogen via pattern recognition receptors (PRRs) that recognize pathogen associated molecular patterns (PAMPs). PRR detection of a pathogen is a key early step in the immune response to protect the body from the pathogen.[11] After PRR activation,

chemical signals, such as cytokines and chemokines, are released to the surrounding environment. These chemical signals recruit antigen presenting cells (APCs), such as dendritic cells, macrophages, and B cells, to the site of infection.[12,13] APCs become activated by PAMPs, and start phagocytosing pathogens, as well as cellular debris.[10] Protein fragments of the phagocytosed material are processed and expressed on the major histocompatibility complex (MHC) on the cell surface. The presentation of the protein fragments on the surface acts as a signal to indicate which antigens the APC has encountered.[14] This surface presentation, commonly known as antigen presentation, is the crucial link between the innate and adaptive immune systems. In addition to presenting antigen, the APCs expression other surface receptors that are necessary for costimulation, such as CD40 and CD86. These costimulatory proteins are important for the APC's ability to signal to and activate T cells.[5]

After activation, the APC travels to the lymph node, where it will eventually encounter a T cell that has a T cell receptor (TCR) that recognizes the MHC-peptide complex on the APC. The costimulatory proteins on the APC are secondary signals to the T cell that induce the T cell to expand, resulting in more T cells that express the same TCR on their surface. This T cell expansion increases the chances that a T cell with this TCR encounters a B cell that has encountered the same pathogen as the initial APC, and therefore is presenting the same antigen as that initial APC. When this T cell discovers such a B cell, the B cell proliferates and differentiates into memory B cells and plasma B cells. Memory B cells remain in circulation for an extended period of time and provide a memory response to a specific pathogen. Plasma B cells produce antibodies that bind to and neutralize a specific pathogen, helping to prevent infection.

1.3 Pattern Recognition Receptors

There are multiple subclasses of pattern recognition receptors (PRRs) that allow the immune system to recognize and react to pathogen-associated molecular patterns (PAMPs). Some of these subclasses of PRRs include nucleotide-binding oligomerization domain (NOD), retinoic acid-inducible (RIG) receptors, C-type lectin receptors (CLRs), and toll-like receptors (TLRs). When PRRs recognize a PAMP, a signaling cascade is induced, resulting in immune activation. PRR activation by PAMPs can often lead to strong and effective immune responses.

TLRs are the best characterized PRRs; they recognize PAMPs that are ubiquitously expressed on pathogens. As a result, TLRs are actively being studied as target receptors for vaccine adjuvants. There are 10 different TLRs in humans that recognize different PAMPs, but TLRs share some common structural motifs.[15] TLRs contain a horseshoe-shaped motif comprised of several leucine-rich repeat units (LRRs). Two TLRs are able to form a constitutive dimer around these LRRs. TLRs dimerize as either homodimers or heterodimers.

TLRs are found in two different locations of the cell. Certain TLRs, such as TLR 1, 2, 4, 5, and 6, are found on the cell surface. These TLRs recognize PAMPs that are generally found on the surface of a pathogen, such as bacterial cell membrane and cell wall components. Other TLRs, such as TLR 3, 7, 8, and 9, are found in the endosome. These endosomal TLRs recognize PAMPs that are found inside of a pathogen, such as RNA or DNA. After PRR activation, a signaling cascade is generated leading to activation of immune transcription factors, such as Nuclear factor kappa-light-chain-enhancer of activated B cells (NF-kB) and interferon regulating factor (IRF).[16,17] By transcribing cytokines, chemokines, and cell surface receptors, these transcription factors help orchestrate the overall immune response.

1.4 NF-kB and IRF: Key immune Transcription Factors

NF-kB and IRF each represent a family of pleotropic transcription factors that regulate a large array of genes involved in immune and inflammatory responses.[18,19] The canonical activation of NF-kB happens via PRR signaling.[20] Upon activation, NF-kB translocates into the nucleus where it controls the transcription of over 400 immune genes.[21] The specific transcriptional activity of NF-kB is dictated by the particular receptor that was activated. NF-kB consists of two subunits – one subunit is a DNA binding domain, and the other subunit is a transcriptional activator domain. These subunits dimerize to bind a specific DNA sequence, activating transcription.[22] As a result, NF-kB activity results in pro-inflammatory signals, such as cytokines and cell surface markers, that dictate the large scale immune response that can lead to long-term immunity.[23,24] Some pro-inflammatory genes controlled by NF-kB include TNF-α, IL-6, CD86, MHC1, and TLR2.[25]

Similar to NF-kB, IRFs are a class of transcriptional factors that regulate immune responses that are activated by PRR signaling. Each IRF has distinct biological activity, but overall, IRFs are known to be the key antiviral transcription factors.[19] Upon activation, IRFs regulate a class of cytokines known as interferons (IFNs). There are two types of IFNs. Type 1 interferons, such as IFNα and IFNβ, that limit the spread of viral agents via promoting antigen presentation and natural killer cell activity, while restraining pro-inflammatory pathways. Additionally, they activate the adaptive immune system by promoting the development of antigen specific T and B cell responses.[26] Type II IFN expression results in nitric oxide production – a known antiviral agent –, as well as dendritic cell maturation and MHC II

presentation.[27] Overall, the activity of NF-kB and IRF help determine the scale and nature of an immune response.

1.5 Heterogeneity in the Immune System

The bulk output of an immune response represents the combined behaviors of a highly diverse ensemble. Many unique subsets of cells work together to fight a range of potential threats and maintain long-term memory. [28,29] The interplay between these groups of cells establishes checks and balances, which is essential to the function of the immune system. Measuring the immune response in bulk populations does not capture the unique contributions of individual cells, particularly when behaviors are highly heterogeneous, or driven by rare cell types.[30]

To study the diversity of the response, "top down" approaches have been employed to break down a system into distinct subpopulations based on the expression of cell surface markers. This approach has allowed for cataloging major immune cell types and establishing functional divisions. For example, multiple subsets of dendritic cells exhibit pathogen specificity, unique cytokine profiles, and antigen specific cell pairing.[31] A major drawback of this approach is that it depends on pre-selection of known cell markers, creating bias in experiments and focuses studies on cell surface classification. Moreover, cells in each bin get averaged in the analysis of the experiment, blurring the heterogeneity within bins.[32]

To circumvent these issues, "bottom up" approaches have been developed that study genetic and protein processes at a cellular level. Single cell RNA profiling is a method of profiling the individual response of cells to immune stimulation. Two common RNA profiling approaches are RNA-FISH and single cell RNA-Seq. RNA-FISH has been used to probe RNA expression and spatial orientation, while single-cell RNA-Seq helps uncover structure in cellular

heterogeneity that can identify novel cell types.[33] RNA profiling has allowed researchers to determine that stochastic cytokine signaling, such as IFN-β, and IFN-γ, from a limited number of cells can shape an immune response.[34,35] Studying protein composition and activity can also elucidate individual cell function. Fluorescent based techniques and flow cytometry techniques, such as CyTOF, are useful tools for studying protein roles that affect immune response.[36] For example, a small subpopulation of CD8+ T cells maintain high levels of CD25 after acute viral infection, leading to long-lived memory cells.[37] Overall, these single cell profiling techniques are crucial for studying the heterogeneity of the immune system.

1.6 Heterogeneity of Dendritic Cells

Dendritic cells (DCs), named for the dendrites that extend from the cell, are key immune cells, as they link the innate and adaptive immune system. They have an important role in recognizing PAMPs, presenting antigen, via MHCs and facilitating adaptive immune responses.[38] For dendritic cells, functional heterogeneity is critical in the complex process of initiating adaptive immune responses. Dendritic cells are broken down into four main subsets based on transcriptional and surface markers: plasmacytoid DCs (pDC), type 1 classical DCs (cDC1), type 2 classical DCs (cDC2), and monocyte-derived DCs (mo-DCs).[31] pDCs are master regulators of type I interferons, making them specialists at responding to viral infection.[39,40] cDC1s are characterized by a high intrinsic ability to cross present antigens via MHCI.[41] cDC1s also excrete high levels of IL-12, promoting Th1 and natural killer responses.[42] cDC2s have high levels of PRRs and secrete high levels of cytokines, such as TNF-α, IL-6, and IL-10.[43] cDC2s are potent activators of helper and cytotoxic T cell subsets.[44,45,46,47] Mo-DCs, unlike other DCs, remain at the site of inflammation, expand resident populations, and release inflammatory signals.[48] Each subpopulation of DC has a nuanced, integral role in the immune system.

Even within subtypes, DC populations have heterogeneous responses to immune stimulation. For example, in bone marrow derived DCs, a stochastically arising and small population of high IFN-β secreting cells was observed; and in pDCs, a similar stochastic response for IFN-α release was identified via single-cell mRNA sequencing.[35,49] Moreover, DC functionality varies by tissue location, even within the same lymphoid structure.[50,51] These studies suggest that DCs exist in a range of phenotypes and functionalities that is not captured by the subclasses of DCs. This work aims to provide a clearer picture of the how heterogeneity in DC populations affects the overall immune response.

1.7 History of Vaccines

Throughout history, vaccines have taken a multitude of forms. As early as 430 BC, it was identified that people who survived smallpox did not get reinfected with the disease. From this observation, it was deduced that our bodies have complex mechanisms that allow us to remember past infections. This idea led to the innovation of the first vaccine, where a small amount of small pus material was transferred from an infected person to a non-immune patient – a process named inoculation –. The pus material was scratched into the skin, with the idea that the patient would have a mild, yet protective infection. An issue with this initial vaccine, was inoculation resulted in illness that would last weeks to months.[52]

The second generation of a smallpox vaccine came from Edward Jenner in the 1700s. Jenner noted that milkmaids who had previously been infected with cowpox did not show symptoms upon infection with smallpox. This intriguing connection resulted in an improved inoculation procedure. Instead of inoculating with smallpox, Jenner inoculated with cowpox, a much less severe disease.[52] From Jenner's cowpox inoculation, we learned that less harmful diseases could be used to protect against more severe diseases. Eventually, this idea manifested

into the concept that pathogens could be attenuated by adapting them into other species before inoculation to make them less infectious before injecting these pathogens into humans for vaccines.[53] For example, Albert Sabin used a rodent-adapted polio virus to use as a vaccine against polio. Later, Jonas Salk discovered that chemically inactivating a virus could also lead to long-lasting immunity, while improving the safety of the vaccine.[54,55]. These innovations were critical for the development of many modern vaccines.

1.8 Vaccine Types

There are four main categories of vaccine as denoted by the World Health Organization. These categories are live attenuated, inactivated, toxoid, and subunit vaccines.[56] Live attenuated vaccines are vaccines that consist of a weakened form of a live virus. This attenuation is achieved by passage through a foreign host. A pathogen can be attenuated *in vitro* using tissue culture or *in vivo* through embryonated eggs or live animals.[57,58] The foreign host selects for a host-optimized virus, with the virus eventually becoming so optimized for the host that it loses infectiousness to humans. This attenuation process makes it easier for the human immune system to eliminate the pathogen but keeps the necessary components of the pathogen that lead to a strong memory response. Live attenuated vaccines result in strong immune activation, because an intact virus is administered.[33] These vaccines are typically low cost, as they contain just the virus, and no additional components. One major disadvantage of the live attenuated vaccine is that the virus can mutate back to an infectious variant, which can be of issue to immunocompromised patients. As a result, immunocompromised people are not recommended to receive a live attenuated vaccine; as such, they rely on herd immunity to be protected from the pathogen. Another disadvantage of the live attenuated vaccine is that it needs to be stored in a proper environment for the virus to remain viable. These storage issues present problems for

shipping and maintaining the vaccine during distribution.[59] Some examples of live attenuated vaccines are tuberculosis, yellow fever, and measles.

Inactivated vaccines are composed of a pathogen that has been inactivated using heat or a chemical method, such as using formaldehyde. This inactivation results in a non-infectious pathogen that can safely be used in vaccination. Unlike the live attenuated vaccine, immunocompromised people are recommended to receive an inactivated vaccine, because there is no fear of infection. An inactivated vaccine often requires a booster, as inactivation reduces the overall scale of immune response induced by the vaccine. Some examples of an inactivated vaccine are the seasonal influenza vaccine and the pertussis vaccine.[57]

The toxoid vaccine is another class of vaccine that is made of inactivated components. In this instance, the toxin that generated by the pathogen is inactivated by heat or formaldehyde. As a result, immunity is developed against the toxin produced by the pathogen and not the pathogen itself. The tetanus vaccine or the diphtheria vaccine are examples of this type of vaccine.[57]

A subunit vaccine consists of a protein or sugar (or set of proteins/sugars) produced by a particular pathogen. This protein or sugar acts as the antigen in this type of vaccine. The antigen is usually expressed in a different virus or bacteria creating a recombinant pathogen. Since the antigen is expressed and purified in a laboratory setting, the subunit vaccine is favored over the other types of vaccine, because it has increased control over purity, dosage, and reproducibility of antibody generation.[57] Additionally, a subunit vaccine typically has better shelf-stability than other types of vaccines. One major drawback of the subunit vaccine is that the antigen in the subunit vaccine is generally not immunogenic, so adjuvants, or immuno-stimulatory compounds, must be added to the vaccine in order to elicit an immune response. Determining the appropriate adjuvant for a specific subunit vaccine is a complex and poorly understood process, which leads

to issues in clinical trials of subunit vaccines. If the adjuvants are too strong or too weak, the vaccine will either induce strong side effects or not be protective, respectively, resulting in a failure of clinical trial.[60] An example of a subunit vaccines is the COVID-19 vaccine.

1.9 Vaccine Development and Adjuvants

There is an ongoing need to develop new vaccines for disease that threaten public health, such as HIV and malaria, as well as emerging diseases, such as new coronavirus variants. However, most vaccines are empirically derived with little understanding of their mechanism of action. This lack of understanding makes it difficult to design novel, effective vaccines. A vaccines effectiveness is dictated by its composition. A vaccine has two main components: an antigen and an adjuvant. Since an antigen alone typically has low immunogenicity, an adjuvant is added to a vaccine that increase the immune response, leading to improved protection.[61]

Ideal adjuvants have a long shelf-life, are biodegradable, inexpensive, and promote the desired immune response against the antigen of interest.[61,62] Currently, there are very few adjuvants that are approved by the FDA for use in humans.[63] The most common adjuvant is alum, an amorphous aluminum salt. The adjuvanticity of alum was discovered in 1920, when its addition to vaccines lead to increased effectiveness. Although there are many immunostimulatory compounds, alum was the only FDA approved adjuvant for use in humans for many years.

Recently, additional adjuvants have been approved for use in humans in the United States.[63] MF59 is an oil-in-water emulsion composed of squalene. This adjuvant improves immune cell infiltration and aids in transport of antigen to the lymph node. Other adjuvants use synthetic PAMP-like compounds that activate TLRs. For example, AS04 is composed of

monophosphoryl lipid A (MPLA), a TLR4 agonist, and alum, leading to an improved immune response. While these approved adjuvants have aided vaccine development against a handful of diseases, there are many diseases that cannot be vaccinated against with current vaccine technologies; new and improved adjuvants need to be generated to protect against these diseases.

Historically, adjuvants have been formulated using a single immune agonist. Recently, adjuvants that are composed of multiple types of immune agonists have shown promise. One example of this type of adjuvant is AS01B, which consists of MPLA and QS-21, a natural component found in the Quillaja Saponaria tree.[64] This adjuvanting strategy has elicited some success, because it induces an enhanced immune response, known as immune synergy, which can improve the protectiveness of vaccines.

1.10 Adjuvants and PRR Synergies

With the need for new adjuvants that generate a specific immune response, PAMPs are being utilized as adjuvants to increase immunogenicity without increasing toxicity. Natural pathogens contain more than one type of PAMP. To better mimic pathogenic composition, multiple agonists have been used in an adjuvant to synergistically enhance the immune response. These improved responses can also result in reduced amounts of adjuvant and antigen used in a vaccine.[65,66] Synergistic adjuvants can also dictate the type of response generated by simultaneous activation of specific PRRs. TLR agonists are at the forefront of adjuvant development; because TLR activation can result in a strong cellular Th1 response, which many subunit vaccines lack.[67,68]

The discovery of synergies between multiple PRRs has led to incorporation of multiple agonists in vaccine formulation. For example, simultaneous TLR4 and TLR7 activation results

in a synergistic expression of various pro-inflammatory cytokines, such as IL-1β and IL-6.[69] Because of this synergy, this TLR combination has been targeted by adjuvants in influenza models, resulting in a long-lasting, Th1/Th2 balanced response.[70] In another example of synergy, TLR 2 and TLR9 have been stimulated in mice to induce strong protection against lung infection from a bacteria that causes pneumonia.[71] Since TLR synergy has resulted in improved protection, research efforts have targeted these receptors with chemically and spatially-linked vaccine delivery systems, with the goal of inducing even more protective responses.

1.11 Vaccine Delivery Systems

Vaccine delivery systems can influence the spatial and temporal organizations of the adjuvant and antigen, resulting in an altered immune response to the vaccine. Common delivery systems include unlinked formulations, chemically conjugated formulations, and nanoparticle (or microparticle) formulations. In an unlinked formulation, adjuvant and antigen are dissolved into a solvent and injected as is. There is no chemical modification or encapsulation process in this type of formulation. The unlinked formulation is the most rudimentary type of formulation and is often used to initially test the efficacy of an adjuvant.

In a chemically conjugated formulation, an agonist is chemically bonded to another agonist and/or antigen to spatially link the molecules. Since PAMPs in pathogens are spatially linked, chemically linking these molecules can attempt to mimic the spatial orientation of these compounds in a pathogen. In one study, TLR2, TLR4, and TLR9 agonists were linked via different sized PEG linkers showing that the spatial distance between agonists can alter the immunogenicity of a system.[11,72] Evaluation of these linked system indicates that the specific combination of agonist, as well as steric interactions, impact the immune response to these systems. Developing more potent and effective immunostimulants via linkage has led to

incorporation of these compounds in vaccine formulations. The first example of this was CL429, which activates TLR2 and NOD2.[73] CL429 was used to adjuvant an HIV-1 subunit vaccine that resulted in higher antibody titers when compared to each of the individual agonists or a free mixture equivalent of both agonists. Covalently linked PRR-agonist research was further explored with the development of a triagonist molecule that is composed of TLR 4, TLR 7, and TLR 9 agonists.[74,75] This molecule increased the antibody response to vaccinia virus antigen and elicited a balanced Th1/Th2 response compared to the unconjugated agonists. These studies on covalently linked agonists demonstrate that the spatial orientation of an adjuvant has a large impact on the immune response

Nanoparticles are common vaccine delivery system. With these particle formulations, molecular cargo, such as adjuvant and antigen, can either be loaded in the interior of the particle or attached to the surface of the particle, allowing for spatiotemporal control of delivery. There are many chemical and immune factors that make particle formulation an attractive option. First, encapsulated vaccine cargo can have improved stability, since it is protected from chemical degradation until it has reached an immune cell, and particle formulations help facilitate DC uptake.[76] By facilitating DC uptake, these particles help shepherd the vaccine to the cells that will maximize their immunological impact, resulting in enhanced cross-presentation.[77,78] When formulating particles, it is important to consider the size of the particles, because size influences uptake and cargo release, altering the immune response.[79]

Two common types of particles used in vaccine delivery are microspheres, often made from poly(lactic-co-glycolic acid) (PLGA), and liposomes, made from lipids. These particles are engineered to be roughly the size of bacteria.[80] PLGA is a biodegradable, biocompatible, and most importantly FDA approved, plastic polymer that has been used multiple research efforts for

vaccine formulations.[81] Another advantage of PLGA, is that PLGA degrades in physiological conditions over weeks, which leads to a slow time release of molecular cargo. If applied appropriately, this slow time-release of cargo can remove the need for a patient to receive a second injection or booster vaccine.[82] PLGA has been used to enhance MHCI and MHCII presentation by over 50-fold compared to soluble antigen and can improve cross presentation with 1000-fold lower concentration of soluble agonist. [83,84] Another type of plastic microsphere that has been used in vaccine research is a polystyrene (PS) microsphere. The PS microsphere can be coated with a siloxane core that reduces immunogenicity of the particle and allows for covalent attachment of PRR agonists.[85] This PS formulation has been used to isolate and target a highly active dendritic cell subpopulation that improves immune responses.[86]

Liposome nanoparticles have become an important vaccine delivery system. A key advantage of liposomes is their versatility and plasticity. Liposome composition can be chosen to achieve desired features such as charge, size, and location of cargo.[87] Depending on the chemical properties of the cargo, hydrophilic compounds can be entrapped within the aqueous inner space, whereas hydrophobic compounds can be intercalated into the lipid bilayer.[88] Additionally, antigen can be attached to the liposome surface by adsorption of chemical linking.[89] Subunit liposome vaccines have been used to improve antibody response in a HIV-1 gp41 (N-MPR) model in mice.[90] Liposomes can also be formulated as mRNA vaccines, which have been used to attenuate pulmonary fibrosis.[91] The choice of formulation is important to a vaccine's efficacy. Covalent linking of adjuvant/antigen and particle formulation can be ways to improve the antibody response of a vaccine.

1.12 Synergistic Vaccine Delivery: Design and Efficacy and Challenges

In an attempt to mimic the spatial orientation of pathogens, synergistic adjuvants have been included in microsphere and liposome delivery systems.[92,93] Both PLGA particles and liposomes have been developed to encapsulate or adsorb dual or tri combinations of agonist.[94,95,96] Mice immunized with multi-agonist formulations have demonstrated distinct change in the immune response compared to the use of one agonist or antigen alone. These immune responses include high avidity antibodies and balanced Th1/Th2 responses, while having an improved safety profile compared to commercial adjuvant systems.[97,98,99,100] By improving long-term protection and safety, a handful of synergistic adjuvants have been employed in clinical trials. Some of these adjuvants include AS01 and AS02, which target TLR4 and NLRP3, AS15, which targets TLR4 and TLR9 and CAF09 which targets TLR3 and Mincle receptor.[101]

With the advances of synergistic adjuvants in the clinic, new adjuvant development should employ the knowledge gained from clinical and fundamental synergistic studies. Researchers have begun to apply the immunogenicity profiles of pathogens to engineer improved vaccines. For example, *M. tuberculosis* activates TLR 2, 4, and 9.[102] Combining all three agonists into an adjuvant may improve *M. tuberculosis* vaccines. Improved adjuvant design and vaccine efficacy will also need approaches that control the dose and time release of synergistic cargo, target specific cellular compartments and cell types, and study single cell expression profiles *in vivo*. These capabilities can be incorporated into new technologies by using covalent chemistries and nanoparticulate systems.

Depending on the disease, there are clear readouts, such as bacterial clearance, reduced parasite burden, and tumor volume. In addition, vaccines can be tracked, using techniques such

as luminescence and PET imaging, to visualize vaccine biodistribution and correlate a vaccine's bio-physicochemical properties to its efficacy. These measures of vaccine efficacy need to be monitored to ensure sustained protective responses in challenge studies and clearance of the target pathogen. Correlating synergistic vaccine formulations to these measures of efficacy will provide a more comprehensive understanding of the relationship between vaccine composition, resulting immune responses, and adjuvant and vaccine efficacy.

With all new adjuvant and formulation technologies, it is crucial to consider the safety profile of the vaccination materials.[103] For example, the amount of systemic cytokines, cell viability, and off-targets effects should be monitored. Several considerations, including formulation and administration route, can drastically alter the immune response. Particulate formulation or additives, such as oil-in-water emulsions, can enhance the immune response and may be an alternative approach to develop potent adjuvants, while avoiding toxic side effects.[104,105] In addition, simply changing the administration route can change what immune cells are targeted and the responses elicited, providing another method to obtain improved immune responses. With these considerations in mind, the application of immune synergies to modulate the immune response is a powerful tool for novel and more rational adjuvant discovery, thereby impacting future development of safer and more effective vaccines. In this work, we use particle delivery systems to enhance immune response to vaccines by targeting stochastically active DCs.

1.13 Setting the Stage: Allergic Contact Dermatitis

Allergic contact dermatitis (ACD), or contact dermatitis, is a chronic skin disorder accompanied by clinical symptoms of rashes, itchiness, and inflammation in the lesion area that affects an estimated 20 % of the population.[106,107,108] Additionally, as of 2021, there were 9.2

million cases of ACD in children, with 217,000 cases of ACD resulting in emergency room visits. When comparing reported allergic information in 2021 to 2014 the percent of skin allergies in children has increased from 11.7 % to 12.6 %, indicating that ACD is becoming a larger issue in the United States.[109] Contact dermatitis is currently the largest occupational work hazard in the United States, accounting for 20% of occupational health incidents, resulting in significant economic loss.[110,111,112]

Currently, treatments for ACD are focused on reducing symptoms after allergies have been developed. The most common methods for treating ACD is to apply either topical corticosteroids or emollients. To treat ACD, topical corticosteroids are applied to the site of inflammation.[113] Topical corticosteroids are powerful anti-inflammatory compound that are a cheap and effective method of reducing inflammation in ACD. However, they do not completely irradicate inflammation, and repeated usage of these compounds can result in a variety of negative side-effects, including muscle atrophy, bone loss, and diabetes.[114,115,116,117] Emollients are less common than corticosteroids as a treatment for ACD. They are applied directly to the skin and provide a film of protection against exposure to contact allergens. In addition to providing a physical barrier, emollients often include anti-inflammatory compounds to mitigate inflammation.[118]

1.14 Hypersensitivity Reactions

Allergic reactions are defined by an exaggerated immunological response to an antigen or allergen. These responses are broken down into four different hypersensitivity reactions, in which the immune system gets activated in a way that damages the body rather than protecting it. Type I, II, and III hypersensitivity reactions result in immediate inflammation, while type IV hypersensitivity has delayed inflammation.[10,119]

Type I hypersensitivity is the most common type of allergic response and occurs upon exposure to allergens such as dust mites or pollen.[120,121] Type I allergens react with allergen-specific IgE antibodies on the FcεRI receptor of mast cells, resulting in the release of granules that contain inflammatory mediators such as histamine. Symptoms of type I hypersensitivity are often mild, such as runny nose, sneezing, but in some cases, symptoms can be more serious, such as breathlessness and asphyxiation. [122]

Type II hypersensitivity is characterized by an antibody response after a small, reactive small molecule binds to the cell's surface. A type II hypersensitivity allergen, such as penicillin, binds to a red blood cell to form an antigen-cell complex, stimulating B cells to produce IgG or IgM antibodies against the new antigen.[123] If severe, this antibody response can activate the complement system or an enzymatic cascade. These responses are cytotoxic, ultimately killing the host's red blood cells, which can result in local tissue damage.[124]

Similar to type II hypersensitivity, Type III hypersensitivity is also mediated by antibodies that recognize self-antigens. In contrast, type III hypersensitivity occurs when chemically reactive small molecules covalently bind soluble proteins as opposed to the surface of the cells. As a consequence, the antibodies bind these antigen-protein complexes to form immune complexes that can activate the complement system.[125,126] Type III hypersensitivity reactions can typically be seen as serum sickness and Arthus reaction.[119]

Unlike other models of hypersensitivity, type IV hypersensitivity is mediated by allergen-specific T cells.[127,128] Type IV hypersensitivity is induced when an allergen or a chemically reactive compound penetrates the skin and reacts with human proteins to generate haptens. Although the exact process of hapten recognition is still unclear, activated dendritic cells migrate to the lymph node to stimulate proliferation of hapten-specific T-cells.[129] Upon re-exposure to

haptens, inflammation in the form of rash and swelling can be observed. Allergic contact dermatitis (ACD) is considered to be a type IV hypersensitivity reaction but type IV hypersensitivity can also occur in inflammatory and autoimmune disease as well as in tissues and/or organ transplantation.[130]

1.15 Pathology of Allergic Contact Dermatitis

ACD results from bodily exposure to small, reactive molecules called haptens, which are commonly found in cosmetic and fragrance products. Repeated exposure to these haptens induces a delayed type IV hypersensitivity response, in which the immune system has an exaggerated inflammation response accompanied by clinical symptoms of rash, itchiness and inflammation.[106]

This type IV hypersensitivity response is broken down into two distinct phases: the elicitation phase and the sensitization phase. The sensitization phase occurs after initial exposure to a hapten. The hapten react with epidermal proteins, such as HSP90, to form a haptenated protein.[131] These haptenated proteins are recognized by pattern recognition receptors on skin resident dendritic cells (DCs), resulting in a pro-inflammatory response.[132] These DCs release cytokine and chemokine signals to recruit immune cells, such as T cells and neutrophils that are critical for sensitization.[106,107]

These DCs present haptenated peptide to naïve T cells. These T cells become activated, proliferate, and differentiate into hapten-specific T cells.[106] Re-exposure to the same hapten can induce skin inflammation and pro-inflammatory cytokines, which are key characteristics of the elicitation phase.[108]

1.16 Contact Allergens: An Overview

Contact allergens are a group of chemical compounds that cause ACD. There are thousands of known contact allergens; and these allergens share three common identifying characteristics.[106,133] First, contact allergens are low-molecular weight organic compounds. It is not well understood why the small compound size is important, but it is hypothesized that the smaller compounds can more easily penetrate the skin and react with proteins to form an allergen-protein complex, a key initial step in the development of contact dermatitis.[134] Second, contact allergens are strongly electrophilic compounds. Contact allergens commonly have aldehydes, epoxides, or aromatics in their structure. These structural groups react with nucleophilic amino acids, such as lysine or cysteines on proteins to form an allergen protein complex.[135] Lastly, the contact allergens must elicit a response from the innate immune system. This adjuvanticity of a contact allergen is key to distinguishing it from other common toxic chemicals. Some examples of contact allergens are dinitrochlorobenzene (DNCB), eugenol, citral, and cinnamaldehyde.[136,137,138,139]

Exposure to contact allergens can happen because of occupational, geographical, or habitual reasons. In the workplace, DNCB is a strong contact allergen and, it is a common byproduct of many industrial processes, which can result in ACD for workers that encounter it.[139,140] Additionally, exposure to certain plants that inhabit particular geographic regions can also induce contact dermatitis. For example, poison oak and the lacquer tree produce known contact allergens.[141,142] People can also be exposed to allergens based on habits or choice of products that they use.[143,144] Many contact allergens have floral or fruity aromas; consequently, they are commonly used in fragrance products.[109] For example, citral is used in soaps and shampoos because of its strong lemony scent. Instance of ACD is increasing in the USA and

worldwide and is thought to be a result of increased exposure to contact allergens via increased industrial processing and inclusion of contact allergens in household products.[109]

1.17 *In vitro* and *in vivo* Methods to Study ACD

Among the thousands of known contact allergens, DNCB is one of the best studied contact allergens. Early work in the contact allergen field established that DNCB on its own is not immunogenic; it must bond to a carrier protein to elicit a response.[145,146] This work helped to establish DNCB as a model contact allergen for scientific study. DNCB has consistently been used to elicit contact hypersensitivity in mice in a type of assay, called a local lymph node assay (LLNA).[147,148,149,150] The general protocol for this assay is to apply a contact allergen, such as DNCB, to the shaved abdomen of a mouse for 2 days. After 3 days of rest, the same contact allergen is applied to the dorsum of the ear for 4 days. This LLNA has helped elucidate the roles of specific immune cells, such as neutrophils and CD4+ T cells, cytokines, such as TNF-α and IL-6 in ACD.[151,152]

Although the LLNA is an effective way to study ACD, there is a need perform faster and cheaper studies on ACD. Additionally, manufacturing industries wanted to identify contact allergens before incorporating these compounds in their product.[153] As a result, some *in vitro* assays have been developed to identify and evaluate the potency of chemical sensitizers. A few of these methods include the direct peptide reactivity assay, the human cell-line activation test and IL-8 secretion from THP-1 cells.[154] The direct peptide reactivity assay (DPRA) is a way to predict sensitization by incubating test compounds with peptides containing a lysine or cysteine residue. Liquid chromatography-mass spectrometry is then used to determine whether a protein-compound adduct has formed; the formation of this adduct classifies a compound as a contact

allergen with 54 % accuracy. A key limitation of the DPRA is that it fails to reproduce the physiological conditions of the skin.[155,156]

As an improvement on the DPRA, cellular assays were developed that rely on phenotypic changes of antigen presenting cells as markers of skin sensitization. The human cell-line activation test (h-CLAT) looks at upregulation of CD54 and CD86 as markers for skin sensitization after incubating the THP-1 cells with contact allergen. [157,158,159,160] Upregulation of these surface proteins is important for ACD, because CD54 is an adhesion surface molecule that is involved in MHCII presentation, and CD86 is a costimulatory molecule that provides necessary signals for T cell activation and proliferation.[161,162] Upregulation of these cell surface proteins has been linked to sensitization with roughly 75 % accuracy. [163,164] In addition to the h-CLAT, IL-8 secretion in THP-1 cells has been used to predict the sensitization potential of compounds with roughly 80 % accuracy Additionally, stronger chemical sensitizers were linked with higher levels of IL-8 secretion, indicating that IL-8 secretion could not only indicate whether a compound is a sensitizer, but also could indicate the relative sensitization potential of a given compound.[165,166] IL-8 was chosen as a readout because it is a strong proinflammatory cytokine with a key role of recruiting neutrophils to the site of infection, providing a first line of defense against infection.[167,168] In ACD, neutrophils have been shown to be required for both the sensitization and elicitation phase.[107] These evidence indicate that screening for IL-8 is a relatively robust way to study the skin sensitizing potential of compounds. Altogether, these efforts have built a foundation for scientific study of ACD. In this work, we show the importance of IRF3 in the ACD response, as well as a novel way to inhibit both sensitization and elicitation of ACD, by applying honokiol to the site of exposure.

1.18 References

(1) Mäkelä, P. H. Vaccines, Coming of Age after 200 Years. *FEMS Microbiol. Rev.* **2000**, *24* (1), 9–20. https://doi.org/10.1111/j.1574-6976.2000.tb00530.x.

(2) Burton, D. R. Antibodies, Viruses and Vaccines. *Nat. Rev. Immunol.* **2002**, *2* (9), 706–713. https://doi.org/10.1038/nri891.

(3) Plotkin, S. A.; Plotkin, S. L. The Development of Vaccines: How the Past Led to the Future. *Nat. Rev. Microbiol.* **2011**, *9* (12), 889–893. https://doi.org/10.1038/nrmicro2668.

(4) Rueckert, C.; Guzmán, C. A. Vaccines: From Empirical Development to Rational Design. *PLOS Pathog.* **2012**, *8* (11), e1003001. https://doi.org/10.1371/journal.ppat.1003001.

(5) Pulendran, B.; Ahmed, R. Immunological Mechanisms of Vaccination. *Nat. Immunol.* **2011**, *12* (6), 509–517. https://doi.org/10.1038/ni.2039.

(6) Lane, J. M. The Current and Future Landscape of Smallpox Vaccines. *Glob. Biosecurity* **2019**, *1* (1). https://doi.org/10.31646/gbio.2.

(7) Vetter, V.; Denizer, G.; Friedland, L. R.; Krishnan, J.; Shapiro, M. Understanding Modern-Day Vaccines: What You Need to Know. *Ann. Med.* **2018**, *50* (2), 110–120. https://doi.org/10.1080/07853890.2017.1407035.

(8) Silva, J. V. J.; Lopes, T. R. R.; Oliveira-Filho, E. F. de; Oliveira, R. A. S.; Durães-Carvalho, R.; Gil, L. H. V. G. Current Status, Challenges and Perspectives in the Development of Vaccines against Yellow Fever, Dengue, Zika and Chikungunya Viruses. *Acta Trop.* **2018**, *182*, 257–263. https://doi.org/10.1016/j.actatropica.2018.03.009.

(9) Bhurani, V.; Mohankrishnan, A.; Morrot, A.; Dalai, S. K. Developing Effective Vaccines: Cues from Natural Infection. *Int. Rev. Immunol.* **2018**, *37* (5), 249–265. https://doi.org/10.1080/08830185.2018.1471479.

(10) Murphy, K., Travers, P., Walport, M. and Janeway, C.,. *Janeway's Immunobiology*, New York: Garland Science.; 2008.

(11) Mancini, R. J.; Stutts, L.; Ryu, K. A.; Tom, J. K.; Esser-Kahn, A. P. Directing the Immune System with Chemical Compounds. *ACS Chem. Biol.* **2014**, *9* (5), 1075–1085. https://doi.org/10.1021/cb500079s.

(12) Caux, C.; Vanbervliet, B.; Massacrier, C.; Ait-Yahia, S.; Vaure, C.; Chemin, K.; Dieu-Nosjean, M.-C.; Vicari, A. Regulation of Dendritic Cell Recruitment by Chemokines. *Transplantation* **2002**, *73* (1 Suppl), S7-11. https://doi.org/10.1097/00007890-200201151-00005.

(13) Zhang, L.; Wang, C.-C. Inflammatory Response of Macrophages in Infection. *Hepatobiliary Pancreat. Dis. Int.* **2014**, *13* (2), 138–152. https://doi.org/10.1016/S1499-3872(14)60024-2.

(14) Gaudino, S. J.; Kumar, P. Cross-Talk Between Antigen Presenting Cells and T Cells Impacts Intestinal Homeostasis, Bacterial Infections, and Tumorigenesis. *Front. Immunol.* **2019**, *10*.

(15) Takeda, K.; Akira, S. TLR Signaling Pathways. *Semin. Immunol.* **2004**, *16* (1), 3–9. https://doi.org/10.1016/j.smim.2003.10.003.

(16) Kawasaki, T.; Kawai, T. Toll-Like Receptor Signaling Pathways. *Front. Immunol.* **2014**, *5*.

(17) El-Zayat, S. R.; Sibaii, H.; Mannaa, F. A. Toll-like Receptors Activation, Signaling, and Targeting: An Overview. *Bull. Natl. Res. Cent.* **2019**, *43* (1), 187. https://doi.org/10.1186/s42269-019-0227-2.

(18) Oeckinghaus, A.; Ghosh, S. The NF-KappaB Family of Transcription Factors and Its Regulation. *Cold Spring Harb. Perspect. Biol.* **2009**, *1* (4), a000034. https://doi.org/10.1101/cshperspect.a000034.

(19) Nguyen, H.; Hiscott, J.; Pitha, P. M. The Growing Family of Interferon Regulatory Factors. *Cytokine Growth Factor Rev.* **1997**, *8* (4), 293–312. https://doi.org/10.1016/S1359-6101(97)00019-1.

(20) Vallabhapurapu, S.; Karin, M. Regulation and Function of NF-KappaB Transcription Factors in the Immune System. *Annu. Rev. Immunol.* **2009**, *27*, 693–733. https://doi.org/10.1146/annurev.immunol.021908.132641.

(21) Basagoudanavar, S. H.; Thapa, R. J.; Nogusa, S.; Wang, J.; Beg, A. A.; Balachandran, S. Distinct Roles for the NF-Kappa B RelA Subunit during Antiviral Innate Immune Responses. *J. Virol.* **2011**, *85* (6), 2599–2610. https://doi.org/10.1128/JVI.02213-10.

(22) Gilmore, T. D. Introduction to NF-KB: Players, Pathways, Perspectives. *Oncogene* **2006**, *25* (51), 6680–6684. https://doi.org/10.1038/sj.onc.1209954.

(23) Liu, T.; Zhang, L.; Joo, D.; Sun, S.-C. NF-KB Signaling in Inflammation. *Signal Transduct. Target. Ther.* **2017**, *2* (1), 1–9. https://doi.org/10.1038/sigtrans.2017.23.

(24) A, H.; D, B. Circuitry of Nuclear Factor KappaB Signaling. *Immunol. Rev.* **2006**, *210*. https://doi.org/10.1111/j.0105-2896.2006.00375.x.

(25) *NF-kB Target Genes » NF-kB Transcription Factors | Boston University*. https://www.bu.edu/nf-kb/gene-resources/target-genes/ (accessed 2022-10-03).

(26) *Regulation of type I interferon responses - PMC*. https://www.ncbi.nlm.nih.gov/pmc/articles/PMC4084561/ (accessed 2022-10-03).

(27) Lee, A. J.; Ashkar, A. A. The Dual Nature of Type I and Type II Interferons. *Front. Immunol.* **2018**, *9*, 2061. https://doi.org/10.3389/fimmu.2018.02061.

(28) Raj, A.; van den Bogaard, P.; Rifkin, S. A.; van Oudenaarden, A.; Tyagi, S. Imaging Individual MRNA Molecules Using Multiple Singly Labeled Probes. *Nat. Methods* **2008**, *5* (10), 877–879. https://doi.org/10.1038/nmeth.1253.

(29) Germain, R. N. Maintaining System Homeostasis - the Third Law of Newtonian Immunology. *Nat. Immunol.* **2012**, *13* (10), 902–906. https://doi.org/10.1038/ni.2404.

(30) Satija, R.; Shalek, A. K. Heterogeneity in Immune Responses – From Populations to Single Cells. *Trends Immunol.* **2014**, *35* (5), 219–229. https://doi.org/10.1016/j.it.2014.03.004.

(31) Collin, M.; Bigley, V. Human Dendritic Cell Subsets: An Update. *Immunology* **2018**, *154* (1), 3–20. https://doi.org/10.1111/imm.12888.

(32) Gordon, S.; Taylor, P. R. Monocyte and Macrophage Heterogeneity. *Nat. Rev. Immunol.* **2005**, *5* (12), 953–964. https://doi.org/10.1038/nri1733.

(33) Lubeck, E.; Cai, L. Single Cell Systems Biology by Super-Resolution Imaging and Combinatorial Labeling. *Nat. Methods* **2012**, *9* (7), 743–748. https://doi.org/10.1038/nmeth.2069.

(34) Saliba, A.-E.; Westermann, A. J.; Gorski, S. A.; Vogel, J. Single-Cell RNA-Seq: Advances and Future Challenges. *Nucleic Acids Res.* **2014**, *42* (14), 8845–8860. https://doi.org/10.1093/nar/gku555.

(35) Shalek, A. K.; Satija, R.; Shuga, J.; Trombetta, J. J.; Gennert, D.; Lu, D.; Chen, P.; Gertner, R. S.; Gaublomme, J. T.; Yosef, N.; Schwartz, S.; Fowler, B.; Weaver, S.; Wang, J.; Wang, X.; Ding, R.; Raychowdhury, R.; Friedman, N.; Hacohen, N.; Park, H.; May, A. P.; Regev, A. Single-Cell RNA-Seq Reveals Dynamic Paracrine Control of Cellular Variation. *Nature* **2014**, *510* (7505), 363–369. https://doi.org/10.1038/nature13437.

(36) Marx, V. A Dream of Single-Cell Proteomics. *Nat. Methods* **2019**, *16* (9), 809–812. https://doi.org/10.1038/s41592-019-0540-6.

(37) *Heterogeneity in the Differentiation and Function of CD8+ T Cells | SpringerLink*. https://link.springer.com/article/10.1007/s00005-014-0293-y (accessed 2023-01-08).

(38) Banchereau, J.; Steinman, R. M. Dendritic Cells and the Control of Immunity. *Nature* **1998**, *392* (6673), 245–252. https://doi.org/10.1038/32588.

(39) Dzionek, A.; Sohma, Y.; Nagafune, J.; Cella, M.; Colonna, M.; Facchetti, F.; Günther, G.; Johnston, I.; Lanzavecchia, A.; Nagasaka, T.; Okada, T.; Vermi, W.; Winkels, G.; Yamamoto, T.; Zysk, M.; Yamaguchi, Y.; Schmitz, J. BDCA-2, a Novel Plasmacytoid Dendritic Cell–Specific Type II C-Type Lectin, Mediates Antigen Capture and Is a Potent Inhibitor of Interferon α/β Induction. *J. Exp. Med.* **2001**, *194* (12), 1823–1834.

(40) Bao, M.; Liu, Y.-J. Regulation of TLR7/9 Signaling in Plasmacytoid Dendritic Cells. *Protein Cell* **2013**, *4* (1), 40–52. https://doi.org/10.1007/s13238-012-2104-8.

(41) Haniffa, M.; Shin, A.; Bigley, V.; McGovern, N.; Teo, P.; See, P.; Wasan, P. S.; Wang, X.-N.; Malinarich, F.; Malleret, B.; Larbi, A.; Tan, P.; Zhao, H.; Poidinger, M.; Pagan, S.; Cookson, S.; Dickinson, R.; Dimmick, I.; Jarrett, R. F.; Renia, L.; Tam, J.; Song, C.; Connolly, J.; Chan, J. K. Y.; Gehring, A.; Bertoletti, A.; Collin, M.; Ginhoux, F. Human Tissues Contain CD141hi Cross-Presenting Dendritic Cells with Functional Homology to Mouse CD103+ Nonlymphoid Dendritic Cells. *Immunity* **2012**, *37* (1), 60–73. https://doi.org/10.1016/j.immuni.2012.04.012.

(42) Nizzoli, G.; Krietsch, J.; Weick, A.; Steinfelder, S.; Facciotti, F.; Gruarin, P.; Bianco, A.; Steckel, B.; Moro, M.; Crosti, M.; Romagnani, C.; Stölzel, K.; Torretta, S.; Pignataro, L.; Scheibenbogen, C.; Neddermann, P.; De Francesco, R.; Abrignani, S.; Geginat, J. Human CD1c+ Dendritic Cells Secrete High Levels of IL-12 and Potently Prime Cytotoxic T-Cell Responses. *Blood* **2013**, *122* (6), 932–942. https://doi.org/10.1182/blood-2013-04-495424.

(43) van der Aar, A. M. G.; Sylva-Steenland, R. M. R.; Bos, J. D.; Kapsenberg, M. L.; de Jong, E. C.; Teunissen, M. B. M. Loss of TLR2, TLR4, and TLR5 on Langerhans Cells Abolishes Bacterial Recognition. *J. Immunol. Baltim. Md 1950* **2007**, *178* (4), 1986–1990. https://doi.org/10.4049/jimmunol.178.4.1986.

(44) A Comparative Study of the T Cell Stimulatory and Polarizing Capacity of Human Primary Blood Dendritic Cell Subsets - PMC. https://www.ncbi.nlm.nih.gov/pmc/articles/PMC4761397/ (accessed 2022-10-14).

(45) Nizzoli, G.; Larghi, P.; Paroni, M.; Crosti, M. C.; Moro, M.; Neddermann, P.; Caprioli, F.; Pagani, M.; De Francesco, R.; Abrignani, S.; Geginat, J. IL-10 Promotes Homeostatic Proliferation of Human CD8(+) Memory T Cells and, When Produced by CD1c(+) DCs, Shapes

Naive CD8(+) T-Cell Priming. *Eur. J. Immunol.* **2016**, *46* (7), 1622–1632. https://doi.org/10.1002/eji.201546136.

(46) Di Blasio, S.; Wortel, I. M. N.; van Bladel, D. A. G.; de Vries, L. E.; Duiveman-de Boer, T.; Worah, K.; de Haas, N.; Buschow, S. I.; de Vries, I. J. M.; Figdor, C. G.; Hato, S. V. Human CD1c+ DCs Are Critical Cellular Mediators of Immune Responses Induced by Immunogenic Cell Death. *Oncoimmunology* **2016**, *5* (8), e1192739. https://doi.org/10.1080/2162402X.2016.1192739.

(47) Bakdash, G.; Buschow, S. I.; Gorris, M. A. J.; Halilovic, A.; Hato, S. V.; Sköld, A. E.; Schreibelt, G.; Sittig, S. P.; Torensma, R.; Duiveman-de Boer, T.; Schröder, C.; Smits, E. L.; Figdor, C. G.; de Vries, I. J. M. Expansion of a BDCA1+CD14+ Myeloid Cell Population in Melanoma Patients May Attenuate the Efficacy of Dendritic Cell Vaccines. *Cancer Res.* **2016**, *76* (15), 4332–4346. https://doi.org/10.1158/0008-5472.CAN-15-1695.

(48) Guilliams, M.; van de Laar, L. A Hitchhiker's Guide to Myeloid Cell Subsets: Practical Implementation of a Novel Mononuclear Phagocyte Classification System. *Front. Immunol.* **2015**, *6*, 406. https://doi.org/10.3389/fimmu.2015.00406.

(49) Van Eyndhoven, L. C.; Singh, A.; Tel, J. Decoding the Dynamics of Multilayered Stochastic Antiviral IFN-I Responses. *Trends Immunol.* **2021**, *42* (9), 824–839. https://doi.org/10.1016/j.it.2021.07.004.

(50) Leal, J. M.; Huang, J. Y.; Kohli, K.; Stoltzfus, C.; Lyons-Cohen, M. R.; Olin, B. E.; Gale, M.; Gerner, M. Y. Innate Cell Microenvironments in Lymph Nodes Shape the Generation of T Cell Responses during Type I Inflammation. *Sci. Immunol.* **2021**, *6* (56), eabb9435. https://doi.org/10.1126/sciimmunol.abb9435.

(51) Rodda, L. B.; Lu, E.; Bennett, M. L.; Sokol, C. L.; Wang, X.; Luther, S. A.; Barres, B. A.; Luster, A. D.; Ye, C. J.; Cyster, J. G. Single-Cell RNA Sequencing of Lymph Node Stromal Cells Reveals Niche-Associated Heterogeneity. *Immunity* **2018**, *48* (5), 1014-1028.e6. https://doi.org/10.1016/j.immuni.2018.04.006.

(52) Riedel, S. Edward Jenner and the History of Smallpox and Vaccination. *Proc. Bayl. Univ. Med. Cent.* **2005**, *18* (1), 21–25.

(53) *History of Smallpox | Smallpox | CDC*. https://www.cdc.gov/smallpox/history/history.html (accessed 2022-10-03).

(54) *A Brief History of Polio Vaccines | Science*. https://www.science.org/doi/full/10.1126/science.288.5471.1593 (accessed 2022-10-03).

(55) Baicus, A. History of Polio Vaccination. *World J. Virol.* **2012**, *1* (4), 108–114. https://doi.org/10.5501/wjv.v1.i4.108.

(56) Ada, G. Vaccines and Vaccination. *N. Engl. J. Med.* **2001**, *345* (14), 1042–1053. https://doi.org/10.1056/NEJMra011223.

(57) Dai, X.; Xiong, Y.; Li, N.; Jian, C.; Dai, X.; Xiong, Y.; Li, N.; Jian, C. *Vaccine Types*; IntechOpen, 2019. https://doi.org/10.5772/intechopen.84626.

(58) Minor, P. D. Live Attenuated Vaccines: Historical Successes and Current Challenges. *Virology* **2015**, *479–480*, 379–392. https://doi.org/10.1016/j.virol.2015.03.032.

(59) Reyes, M. A.; de Borrero, M. F.; Roa, J.; Bergonzoli, G.; Saravia, N. G. Measles Vaccine Failure after Documented Seroconversion. *Pediatr. Infect. Dis. J.* **1987**, *6* (9), 848–851. https://doi.org/10.1097/00006454-198709000-00012.

(60) *Subunit Vaccine Delivery*; Foged, C., Rades, T., Perrie, Y., Hook, S., Eds.; Advances in Delivery Science and Technology; Springer New York: New York, NY, 2015. https://doi.org/10.1007/978-1-4939-1417-3.

(61) Pashine, A.; Valiante, N. M.; Ulmer, J. B. Targeting the Innate Immune Response with Improved Vaccine Adjuvants. *Nat. Med.* **2005**, *11* (4 Suppl), S63-68. https://doi.org/10.1038/nm1210.

(62) Rabinovich, N. R.; McInnes, P.; Klein, D. L.; Hall, B. F. Vaccine Technologies: View to the Future. *Science* **1994**, *265* (5177), 1401–1404. https://doi.org/10.1126/science.7521064.

(63) Mbow, M. L.; De Gregorio, E.; Valiante, N. M.; Rappuoli, R. New Adjuvants for Human Vaccines. *Curr. Opin. Immunol.* **2010**, *22* (3), 411–416. https://doi.org/10.1016/j.coi.2010.04.004.

(64) Barclay, T.; Petrovsky, N. Vaccine Adjuvant Nanotechnologies. *Micro Nanotechnol. Vaccine Dev.* **2017**, 127–147. https://doi.org/10.1016/B978-0-323-39981-4.00007-5.

(65) Cao, X. Self-Regulation and Cross-Regulation of Pattern-Recognition Receptor Signalling in Health and Disease. *Nat. Rev. Immunol.* **2016**, *16* (1), 35–50. https://doi.org/10.1038/nri.2015.8.

(66) Tan, R. S. T.; Ho, B.; Leung, B. P.; Ding, J. L. TLR Cross-Talk Confers Specificity to Innate Immunity. *Int. Rev. Immunol.* **2014**, *33* (6), 443–453. https://doi.org/10.3109/08830185.2014.921164.

(67) Reed, S. G.; Orr, M. T.; Fox, C. B. Key Roles of Adjuvants in Modern Vaccines. *Nat. Med.* **2013**, *19* (12), 1597–1608. https://doi.org/10.1038/nm.3409.

(68) Toussi, D. N.; Massari, P. Immune Adjuvant Effect of Molecularly-Defined Toll-Like Receptor Ligands. *Vaccines* **2014**, *2* (2), 323–353. https://doi.org/10.3390/vaccines2020323.

(69) Fischetti, L.; Zhong, Z.; Pinder, C. L.; Tregoning, J. S.; Shattock, R. J. The Synergistic Effects of Combining TLR Ligand Based Adjuvants on the Cytokine Response Are Dependent upon P38/JNK Signalling. *Cytokine* **2017**, *99*, 287–296. https://doi.org/10.1016/j.cyto.2017.08.009.

(70) Goff, P. H.; Hayashi, T.; Martínez-Gil, L.; Corr, M.; Crain, B.; Yao, S.; Cottam, H. B.; Chan, M.; Ramos, I.; Eggink, D.; Heshmati, M.; Krammer, F.; Messer, K.; Pu, M.; Fernandez-Sesma, A.; Palese, P.; Carson, D. A. Synthetic Toll-Like Receptor 4 (TLR4) and TLR7 Ligands as Influenza Virus Vaccine Adjuvants Induce Rapid, Sustained, and Broadly Protective Responses. *J. Virol.* **2015**, *89* (6), 3221–3235. https://doi.org/10.1128/JVI.03337-14.

(71) Duggan, J. M.; You, D.; Cleaver, J. O.; Larson, D. T.; Garza, R. J.; Guzmán Pruneda, F. A.; Tuvim, M. J.; Zhang, J.; Dickey, B. F.; Evans, S. E. Synergistic Interactions of TLR2/6 and TLR9 Induce a High Level of Resistance to Lung Infection in Mice. *J. Immunol. Baltim. Md 1950* **2011**, *186* (10), 5916–5926. https://doi.org/10.4049/jimmunol.1002122.

(72) Ryu, K. A.; Slowinska, K.; Moore, T.; Esser-Kahn, A. Immune Response Modulation of Conjugated Agonists with Changing Linker Length. *ACS Chem. Biol.* **2016**, *11* (12), 3347–3352. https://doi.org/10.1021/acschembio.6b00895.

(73) Pavot, V.; Rochereau, N.; Rességuier, J.; Gutjahr, A.; Genin, C.; Tiraby, G.; Perouzel, E.; Lioux, T.; Vernejoul, F.; Verrier, B.; Paul, S. Cutting Edge: New Chimeric NOD2/TLR2 Adjuvant Drastically Increases Vaccine Immunogenicity. *J. Immunol. Baltim. Md 1950* **2014**, *193* (12), 5781–5785. https://doi.org/10.4049/jimmunol.1402184.

(74) Tom, J. K.; Dotsey, E. Y.; Wong, H. Y.; Stutts, L.; Moore, T.; Davies, D. H.; Felgner, P. L.; Esser-Kahn, A. P. Modulation of Innate Immune Responses via Covalently Linked TLR Agonists. *ACS Cent. Sci.* **2015**, *1* (8), 439–448. https://doi.org/10.1021/acscentsci.5b00274.

(75) Mogensen, T. H.; Paludan, S. R.; Kilian, M.; Ostergaard, L. Live Streptococcus Pneumoniae, Haemophilus Influenzae, and Neisseria Meningitidis Activate the Inflammatory Response through Toll-like Receptors 2, 4, and 9 in Species-Specific Patterns. *J. Leukoc. Biol.* **2006**, *80* (2), 267–277. https://doi.org/10.1189/jlb.1105626.

(76) Leleux, J.; Roy, K. Micro and Nanoparticle-Based Delivery Systems for Vaccine Immunotherapy: An Immunological and Materials Perspective. *Adv. Healthc. Mater.* **2013**, *2* (1), 72–94. https://doi.org/10.1002/adhm.201200268.

(77) Zwaveling, S.; Ferreira Mota, S. C.; Nouta, J.; Johnson, M.; Lipford, G. B.; Offringa, R.; van der Burg, S. H.; Melief, C. J. M. Established Human Papillomavirus Type 16-Expressing Tumors Are Effectively Eradicated Following Vaccination with Long Peptides. *J. Immunol. Baltim. Md 1950* **2002**, *169* (1), 350–358. https://doi.org/10.4049/jimmunol.169.1.350.

(78) Demento, S. L.; Siefert, A. L.; Bandyopadhyay, A.; Sharp, F. A.; Fahmy, T. M. Pathogen-Associated Molecular Patterns on Biomaterials: A Paradigm for Engineering New Vaccines. *Trends Biotechnol.* **2011**, *29* (6), 294–306. https://doi.org/10.1016/j.tibtech.2011.02.004.

(79) Oyewumi, M. O.; Kumar, A.; Cui, Z. Nano-Microparticles as Immune Adjuvants: Correlating Particle Sizes and the Resultant Immune Responses. *Expert Rev. Vaccines* **2010**, *9* (9), 1095–1107. https://doi.org/10.1586/erv.10.89.

(80) Song, X.; Zhao, Y.; Hou, S.; Xu, F.; Zhao, R.; He, J.; Cai, Z.; Li, Y.; Chen, Q. Dual Agents Loaded PLGA Nanoparticles: Systematic Study of Particle Size and Drug Entrapment Efficiency. *Eur. J. Pharm. Biopharm.* **2008**, *69* (2), 445–453. https://doi.org/10.1016/j.ejpb.2008.01.013.

(81) Makadia, H. K.; Siegel, S. J. Poly Lactic-Co-Glycolic Acid (PLGA) as Biodegradable Controlled Drug Delivery Carrier. *Polymers* **2011**, *3* (3), 1377–1397. https://doi.org/10.3390/polym3031377.

(82) Saroja, C.; Lakshmi, P.; Bhaskaran, S. Recent Trends in Vaccine Delivery Systems: A Review. *Int. J. Pharm. Investig.* **2011**, *1* (2), 64–74. https://doi.org/10.4103/2230-973X.82384.

(83) Waeckerle-Men, Y.; Allmen, E. U.; Gander, B.; Scandella, E.; Schlosser, E.; Schmidtke, G.; Merkle, H. P.; Groettrup, M. Encapsulation of Proteins and Peptides into Biodegradable Poly(D,L-Lactide-Co-Glycolide) Microspheres Prolongs and Enhances Antigen Presentation by Human Dendritic Cells. *Vaccine* **2006**, *24* (11), 1847–1857. https://doi.org/10.1016/j.vaccine.2005.10.032.

(84) Shen, H.; Ackerman, A. L.; Cody, V.; Giodini, A.; Hinson, E. R.; Cresswell, P.; Edelson, R. L.; Saltzman, W. M.; Hanlon, D. J. Enhanced and Prolonged Cross-Presentation Following Endosomal Escape of Exogenous Antigens Encapsulated in Biodegradable Nanoparticles. *Immunology* **2006**, *117* (1), 78–88. https://doi.org/10.1111/j.1365-2567.2005.02268.x.

(85) Moser, B. A.; Steinhardt, R. C.; Esser-Kahn, A. P. Surface Coating of Nanoparticles Reduces Background Inflammatory Activity While Increasing Particle Uptake and Delivery. *ACS Biomater. Sci. Eng.* **2017**, *3* (2), 206–213. https://doi.org/10.1021/acsbiomaterials.6b00473.

(86) Deak, P. E.; Studnitzer, B.; Ung, T.; Steinhardt, R.; Swartz, M.; Esser-Kahn, A. Isolating and Targeting a Highly Active, Stochastic Dendritic Cell Subpopulation for Improved Immune Responses. Rochester, NY April 25, 2022. https://doi.org/10.2139/ssrn.4093302.

(87) Schwendener, R. A. Liposomes as Vaccine Delivery Systems: A Review of the Recent Advances. *Ther. Adv. Vaccines* **2014**, *2* (6), 159–182. https://doi.org/10.1177/2051013614541440.

(88) Watson, D. S.; Endsley, A. N.; Huang, L. Design Considerations for Liposomal Vaccines: Influence of Formulation Parameters on Antibody and Cell-Mediated Immune Responses to Liposome Associated Antigens. *Vaccine* **2012**, *30* (13), 2256–2272. https://doi.org/10.1016/j.vaccine.2012.01.070.

(89) Torchilin, V. P. Recent Advances with Liposomes as Pharmaceutical Carriers. *Nat. Rev. Drug Discov.* **2005**, *4* (2), 145–160. https://doi.org/10.1038/nrd1632.

(90) Watson, D. S.; Platt, V. M.; Cao, L.; Venditto, V. J.; Szoka, F. C. Antibody Response to Polyhistidine-Tagged Peptide and Protein Antigens Attached to Liposomes via Lipid-Linked Nitrilotriacetic Acid in Mice. *Clin. Vaccine Immunol.* **2011**, *18* (2), 289–297. https://doi.org/10.1128/CVI.00425-10.

(91) Li, Y.; Hu, Y.; Jin, Y.; Zhang, G.; Wong, J.; Sun, L.-Q.; Wang, M. Prophylactic, Therapeutic and Immune Enhancement Effect of Liposome-Encapsulated PolyICLC on Highly Pathogenic H5N1 Influenza Infection. *J. Gene Med.* **2011**, *13* (1), 60–72. https://doi.org/10.1002/jgm.1536.

(92) Ali, O. A.; Verbeke, C.; Johnson, C.; Sands, R. W.; Lewin, S. A.; White, D.; Doherty, E.; Dranoff, G.; Mooney, D. J. Identification of Immune Factors Regulating Antitumor Immunity

Using Polymeric Vaccines with Multiple Adjuvants. *Cancer Res.* **2014**, *74* (6), 1670–1681. https://doi.org/10.1158/0008-5472.CAN-13-0777.

(93) Gutjahr, A.; Phelip, C.; Coolen, A.-L.; Monge, C.; Boisgard, A.-S.; Paul, S.; Verrier, B. Biodegradable Polymeric Nanoparticles-Based Vaccine Adjuvants for Lymph Nodes Targeting. *Vaccines* **2016**, *4* (4), E34. https://doi.org/10.3390/vaccines4040034.

(94) Madan-Lala, R.; Pradhan, P.; Roy, K. Combinatorial Delivery of Dual and Triple TLR Agonists via Polymeric Pathogen-like Particles Synergistically Enhances Innate and Adaptive Immune Responses. *Sci. Rep.* **2017**, *7* (1), 2530. https://doi.org/10.1038/s41598-017-02804-y.

(95) Kasturi, S. P.; Skountzou, I.; Albrecht, R. A.; Koutsonanos, D.; Hua, T.; Nakaya, H. I.; Ravindran, R.; Stewart, S.; Alam, M.; Kwissa, M.; Villinger, F.; Murthy, N.; Steel, J.; Jacob, J.; Hogan, R. J.; García-Sastre, A.; Compans, R.; Pulendran, B. Programming the Magnitude and Persistence of Antibody Responses with Innate Immunity. *Nature* **2011**, *470* (7335), 543–547. https://doi.org/10.1038/nature09737.

(96) Yang, K.; Whalen, B.; Tirabassi, R. S.; Selin, L.; Levchenko, T.; Torchilin, V. P.; Kislauskis, E. H.; Guberski, D. L. A DNA Vaccine Prime Followed By A Liposome-Encapsulated Protein Boost Confers Enhanced Mucosal Immune Responses And Protection. *J. Immunol. Baltim. Md 1950* **2008**, *180* (9), 6159–6167.

(97) Leroux-Roels, I.; Forgus, S.; De Boever, F.; Clement, F.; Demoitié, M.-A.; Mettens, P.; Moris, P.; Ledent, E.; Leroux-Roels, G.; Ofori-Anyinam, O.; M72 Study Group. Improved $CD4^+$ T Cell Responses to Mycobacterium Tuberculosis in PPD-Negative Adults by M72/AS01 as Compared to the M72/AS02 and Mtb72F/AS02 Tuberculosis Candidate Vaccine Formulations:

A Randomized Trial. *Vaccine* **2013**, *31* (17), 2196–2206. https://doi.org/10.1016/j.vaccine.2012.05.035.

(98) Leroux-Roels, I.; Koutsoukos, M.; Clement, F.; Steyaert, S.; Janssens, M.; Bourguignon, P.; Cohen, K.; Altfeld, M.; Vandepapelière, P.; Pedneault, L.; McNally, L.; Leroux-Roels, G.; Voss, G. Strong and Persistent CD4+ T-Cell Response in Healthy Adults Immunized with a Candidate HIV-1 Vaccine Containing Gp120, Nef and Tat Antigens Formulated in Three Adjuvant Systems. *Vaccine* **2010**, *28* (43), 7016–7024. https://doi.org/10.1016/j.vaccine.2010.08.035.

(99) Casella, C. R.; Mitchell, T. C. Putting Endotoxin to Work for Us: Monophosphoryl Lipid A as a Safe and Effective Vaccine Adjuvant. *Cell. Mol. Life Sci. CMLS* **2008**, *65* (20), 3231–3240. https://doi.org/10.1007/s00018-008-8228-6.

(100) Hyer, R.; McGuire, D. K.; Xing, B.; Jackson, S.; Janssen, R. Safety of a Two-Dose Investigational Hepatitis B Vaccine, HBsAg-1018, Using a Toll-like Receptor 9 Agonist Adjuvant in Adults. *Vaccine* **2018**, *36* (19), 2604–2611. https://doi.org/10.1016/j.vaccine.2018.03.067.

(101) Garçon, N.; Di Pasquale, A. From Discovery to Licensure, the Adjuvant System Story. *Hum. Vaccines Immunother.* **2016**, *13* (1), 19–33. https://doi.org/10.1080/21645515.2016.1225635.

(102) Kleinnijenhuis, J.; Oosting, M.; Joosten, L. A. B.; Netea, M. G.; Van Crevel, R. Innate Immune Recognition of Mycobacterium Tuberculosis. *Clin. Dev. Immunol.* **2011**, *2011*, 405310. https://doi.org/10.1155/2011/405310.

(103) Ko, E.-J.; Lee, Y.-T.; Lee, Y.; Kim, K.-H.; Kang, S.-M. Distinct Effects of Monophosphoryl Lipid A, Oligodeoxynucleotide CpG, and Combination Adjuvants on Modulating Innate and Adaptive Immune Responses to Influenza Vaccination. *Immune Netw.* **2017**, *17* (5), 326–342. https://doi.org/10.4110/in.2017.17.5.326.

(104) Seydoux, E.; Liang, H.; Cauwelaert, N. D.; Archer, M.; Rintala, N. D.; Kramer, R.; Carter, D.; Fox, C. B.; Orr, M. T. Effective Combination Adjuvants Engage Both TLR and Inflammasome Pathways To Promote Potent Adaptive Immune Responses. *J. Immunol.* **2018**, *201* (1), 98–112. https://doi.org/10.4049/jimmunol.1701604.

(105) Schmidt, S. T.; Khadke, S.; Korsholm, K. S.; Perrie, Y.; Rades, T.; Andersen, P.; Foged, C.; Christensen, D. The Administration Route Is Decisive for the Ability of the Vaccine Adjuvant CAF09 to Induce Antigen-Specific CD8(+) T-Cell Responses: The Immunological Consequences of the Biodistribution Profile. *J. Control. Release Off. J. Control. Release Soc.* **2016**, *239*, 107–117. https://doi.org/10.1016/j.jconrel.2016.08.034.

(106) Kaplan, D. H.; Igyarto, B. Y.; Gaspari, A. A. Early Immune Events in the Induction of Allergic Contact Dermatitis. **2012**, *12* (2), 114–124.

(107) Weber, F. C.; Nemeth, T.; Csepregi, J. Z.; Dudeck, A.; Roers, A.; Ozsvari, E.; Puskas, L.; Thilo, J.; Mocsai, A.; Martin, S. F. Neutrophils Are Required for Both the Sensitization and Elicitation Phase of Contact Hypersensitivity. **2015**, *212* (1), 15–22. https://doi.org/10.1084/jem.20130062.

(108) Kondo, S.; Pastore, S.; Shivji, G. M.; McKenzie, R. C.; Sauder, D. N. Characterization of Epidermal Cytokine Profiles in Sensitization and Elicitation Phases of Allergic Contact

Dermatitis as Well as Irritant Contact Dermatitis in Mouse Skin. *Lymphokine Cytokine Res* **1994**, *13* (6), 367–475.

(109) *FastStats*. https://www.cdc.gov/nchs/fastats/allergies.htm (accessed 2022-09-05).

(110) Diepgen, T. L.; Coenraads, P. J. The Epidemiology of Occupational Contact Dermatitis. *Int. Arch. Occup. Environ. Health* **1999**, *72* (8), 496–506. https://doi.org/10.1007/s004200050407.

(111) Thyssen, J. P.; Linneberg, A.; Menné, T.; Johansen, J. D. The Epidemiology of Contact Allergy in the General Population--Prevalence and Main Findings. *Contact Dermatitis* **2007**, *57* (5), 287–299. https://doi.org/10.1111/j.1600-0536.2007.01220.x.

(112) Alinaghi, F.; Bennike, N. H.; Egeberg, A.; Thyssen, J. P.; Johansen, J. D. Prevalence of Contact Allergy in the General Population: A Systematic Review and Meta-Analysis. *Contact Dermatitis* **2019**, *80* (2), 77–85. https://doi.org/10.1111/cod.13119.

(113) Buys, L. M. Treatment Options for Atopic Dermatitis. *Am. Fam. Physician* **2007**, *75* (4), 523–528.

(114) Vatti, R. R.; Ali, F.; Teuber, S.; Chang, C.; Gershwin, M. E. Hypersensitivity Reactions to Corticosteroids. *Clin Rev Allergy Immunol* **2014**, *47* (1), 36–37. https://doi.org/10.1007/s12016-013-8365-z.

(115) Braun, T. P.; Marks, D. L. The Regulation of Muscle Mass by Endogenous Glucocorticoids. *Front. Physiol.* **2015**. https://doi.org/10.3389/fphys.2015.00012.

(116) Picado, C.; Luengo, M. Corticosteroid-Induced Bone Loss. Prevention and Management. *Drug Saf.* **1996**, *15* (5), 347–359. https://doi.org/10.2165/00002018-199615050-00005.

(117) Phan, K.; Smith, S. D. Topical Corticosteroids and Risk of Diabetes Mellitus: Systematic Review and Meta-Analysis. *J Dermatolog Treat* **2021**, *32* (3). https://doi.org/10.1080/09546634.2019.1657224.

(118) *Contact dermatitis - Treatment*. nhs.uk. https://www.nhs.uk/conditions/contact-dermatitis/treatment/ (accessed 2022-09-05).

(119) Justiz Vaillant, A. A.; Vashisht, R.; Zito, P. M. Immediate Hypersensitivity Reactions. In *StatPearls*; StatPearls Publishing: Treasure Island (FL), 2022.

(120) Son, J. H.; Park, S. Y.; Cho, Y. S.; Chung, B. Y.; Kim, H. O.; Park, C. W. Immediate Hypersensitivity Reactions Induced by Triamcinolone in a Patient with Atopic Dermatitis. *J. Korean Med. Sci.* **2018**, *33* (12), e87. https://doi.org/10.3346/jkms.2018.33.e87.

(121) Koike, Y.; Sato, S.; Yanagida, N.; Asaumi, T.; Ogura, K.; Ohtani, K.; Imai, T.; Ebisawa, M. Predictors of Persistent Milk Allergy in Children: A Retrospective Cohort Study. *Int. Arch. Allergy Immunol.* **2018**, *175* (3), 177–180. https://doi.org/10.1159/000486311.

(122) Abbas, M.; Moussa, M.; Akel, H. Type I Hypersensitivity Reaction. In *StatPearls*; StatPearls Publishing: Treasure Island (FL), 2022.

(123) Bhattacharya, S. The Facts about Penicillin Allergy: A Review. *J. Adv. Pharm. Technol. Res.* **2010**, *1* (1), 11–17.

(124) Bajwa, S. F.; Mohammed, R. H. A. Type II Hypersensitivity Reaction. In *StatPearls*; StatPearls Publishing: Treasure Island (FL), 2022.

(125) Usman, N.; Annamaraju, P. Type III Hypersensitivity Reaction. In *StatPearls*; StatPearls Publishing: Treasure Island (FL), 2022.

(126) Ghazavi, M. K.; Johnston, G. A. Insulin Allergy. *Clin. Dermatol.* **2011**, *29* (3), 300–305. https://doi.org/10.1016/j.clindermatol.2010.11.009.

(127) Marwa, K.; Kondamudi, N. P. Type IV Hypersensitivity Reaction. In *StatPearls*; StatPearls Publishing: Treasure Island (FL), 2022.

(128) Justiz Vaillant, A. A.; Zulfiqar, H.; Ramphul, K. Delayed Hypersensitivity Reactions. In *StatPearls*; StatPearls Publishing: Treasure Island (FL), 2022.

(129) Bennett, C. L.; van Rijn, E.; Jung, S.; Inaba, K.; Steinman, R. M.; Kapsenberg, M. L.; Clausen, B. E. Inducible Ablation of Mouse Langerhans Cells Diminishes but Fails to Abrogate Contact Hypersensitivity. *J. Cell Biol.* **2005**, *169* (4), 569–576. https://doi.org/10.1083/jcb.200501071.

(130) *Type IV Hypersensitivity - an overview | ScienceDirect Topics*. https://www.sciencedirect.com/topics/medicine-and-dentistry/type-iv-hypersensitivity (accessed 2022-09-14).

(131) Kim, S.-M.; Studnitzer, B.; Esser-Kahn, A. Heat Shock Protein 90's Mechanistic Role in Contact Hypersensitivity. *J Immunol* **2022**. https://doi.org/10.4049/jimmunol.2101023.

(132) St. Mazard, P.; Rosieres, A.; Krasteva, M.; Berard, F.; Dubois, B.; Kaiserlian, D.; Nicolas, J.-F. Allergic Contact Dermatitis. *Eur J Dermatol* **2004**, *14*, 284–295.

(133) *Contact dermatitis - Symptoms and causes*. Mayo Clinic. https://www.mayoclinic.org/diseases-conditions/contact-dermatitis/symptoms-causes/syc-20352742 (accessed 2022-09-05).

(134) Martin, S. F. T Lymphocyte-Mediated Immune Responses to Chemical Haptens and Metal Ions: Implications for Allergic and Autoimmune Disease. *Int. Arch. Allergy Immunol.* **2004**, *134* (3), 186–198. https://doi.org/10.1159/000078765.

(135) Basketter, D. A. Chemistry of Contact Allergens and Irritants. *Am. J. Contact Dermat.* **1998**, *9* (2), 119–124. https://doi.org/10.1016/S1046-199X(98)90008-2.

(136) Groot, A. C. D.; Frosch, P. J. Patch Test Concentrations and Vehicles for Testing Contact Allergens. 22.

(137) Heydorn, S.; Menné, T.; Andersen, K. E.; Bruze, M.; Svedman, C.; White, I. R.; Basketter, D. A. Citral a Fragrance Allergen and Irritant. *Contact Dermatitis* **2003**, *49* (1), 32–36. https://doi.org/10.1111/j.0105-1873.2003.00144.x.

(138) *Cinnamic Aldehyde | Allergic Contact Dermatitis Database*. https://www.contactdermatitisinstitute.com/cinnamic-aldehyde.php (accessed 2022-09-14).

(139) Kuper, C. F.; Stierum, R. H.; Boorsma, A.; Schijf, M. A.; Prinsen, M.; Bruijntjes, J. P.; Bloksma, N.; Arts, J. H. E. The Contact Allergen Dinitrochlorobenzene (DNCB) and Respiratory Allergy in the Th2-Prone Brown Norway Rat. *Toxicology* **2008**, *246* (2–3), 213–221. https://doi.org/10.1016/j.tox.2008.01.013.

(140) Dotson, G. S.; Maier, A.; Siegel, P. D.; Anderson, S. E.; Green, B. J.; Stefaniak, A. B.; Codispoti, C. D.; Kimber, I. Setting Occupational Exposure Limits for Chemical Allergens—Understanding the Challenges. *J. Occup. Environ. Hyg.* **2015**, *12* (sup1), S82–S98. https://doi.org/10.1080/15459624.2015.1072277.

(141) Friedmann, P. S. The Immunology of Allergic Contact Dermatitis: The DNCB Story. *Adv. Dermatol.* **1990**, *5*, 175-195;discussion 196.

(142) Uter, W.; Pfahlberg, A.; Gefeller, O.; Geier, J.; Schnuch, A. Risk Factors for Contact Allergy to Nickel - Results of a Multifactorial Analysis. *Contact Dermatitis* **2003**, *48* (1), 33–38. https://doi.org/10.1034/j.1600-0536.46.s4.29_102.x.

(143) McGovern, T. W.; LaWarre, S. Botanical Briefs: The Scourge of India— Parthenium Hysterophorus L. 3.

(144) Thyssen, J. P.; Ross-Hansen, K.; Menné, T.; Johansen, J. D. Patch Test Reactivity to Metal Allergens Following Regulatory Interventions: A 33-Year Retrospective Study. *Contact Dermatitis* **2010**, *63* (2), 102–106. https://doi.org/10.1111/j.1600-0536.2010.01751.x.

(145) Pickard, C.; Smith, A. M.; Cooper, H.; Strickland, I.; Jackson, J.; Healy, E.; Friedmann, P. S. Investigation of Mechanisms Underlying the T-Cell Response to the Hapten 2,4-Dinitrochlorobenzene. *J. Invest. Dermatol.* **2007**, *127* (3), 630–637. https://doi.org/10.1038/sj.jid.5700581.

(146) Gefen, T.; Vaya, J.; Khatib, S.; Rapoport, I.; Lupo, M.; Barnea, E.; Admon, A.; Heller, E. D.; Aizenshtein, E.; Pitcovski, J. The Effect of Haptens on Protein-Carrier Immunogenicity. *Immunology* **2015**, *144* (1), 116–126. https://doi.org/10.1111/imm.12356.

(147) Landsteiner, K.; Jacobs, J. STUDIES ON THE SENSITIZATION OF ANIMALS WITH SIMPLE CHEMICAL COMPOUNDS. II. *J. Exp. Med.* **1936**, *64* (4), 625–639.

(148) Gerberick, G. F.; Ryan, C. A.; Dearman, R.; Kimber, I. Local Lymph Node Assay (LLNA) for Detection of Sensitization Capacity of Chemicals. *Methods* **2007**, *41* (1), 54–60. https://doi.org/10.1016/j.ymeth.2006.07.006.

(149) Kimber, I.; Dearman, R. J.; Scholes, E. W.; Basketter, D. A. The Local Lymph Node Assay: Developments and Applications. *Toxicology* **1994**, *93* (1), 13–31. https://doi.org/10.1016/0300-483x(94)90193-7.

(150) Kimber, I.; Dearman, R. J.; Basketter, D. A.; Ryan, C. A.; Gerberick, G. F. The Local Lymph Node Assay: Past, Present and Future. *Contact Dermatitis* **2002**, *47* (6), 315–328. https://doi.org/10.1034/j.1600-0536.2002.470601.x.

(151) Noonan, F. P.; Halliday, W. J. Studies of Contact Hypersensitivity and Tolerance in Vivo and in Vitro. I. Basic Characteristics of the Reactions and Confirmation of an Immune Response in Tolerant Mice. *Int. Arch. Allergy Appl. Immunol.* **1978**, *56* (6), 523–532.

(152) Röse, L.; Schneider, C.; Stock, C.; Zollner, T. M.; Döcke, W.-D. Extended DNFB-Induced Contact Hypersensitivity Models Display Characteristics of Chronic Inflammatory Dermatoses. *Exp. Dermatol.* **2012**, *21* (1), 25–31. https://doi.org/10.1111/j.1600-0625.2011.01395.x.

(153) Gerberick, G. F.; Ryan, C. A.; Kimber, I.; Dearman, R. J.; Lea, L. J.; Basketter, D. A. Local Lymph Node Assay: Validation Assessment for Regulatory Purposes. *Am. J. Contact Dermat. Off. J. Am. Contact Dermat. Soc.* **2000**, *11* (1), 3–18. https://doi.org/10.1053/ajcd.2000.0003.

(154) Tuschl, H.; Kovac, R. Langerhans Cells and Immature Dendritic Cells as Model Systems for Screening of Skin Sensitizers. *Toxicol. Vitro Int. J. Publ. Assoc. BIBRA* **2001**, *15* (4–5), 327–331. https://doi.org/10.1016/s0887-2333(01)00030-3.

(155) Gerberick, G. F.; Vassallo, J. D.; Bailey, R. E.; Chaney, J. G.; Morrall, S. W.; Lepoittevin, J.-P. Development of a Peptide Reactivity Assay for Screening Contact Allergens. *Toxicol. Sci. Off. J. Soc. Toxicol.* **2004**, *81* (2), 332–343. https://doi.org/10.1093/toxsci/kfh213.

(156) Gerberick, G. F.; Vassallo, J. D.; Foertsch, L. M.; Price, B. B.; Chaney, J. G.; Lepoittevin, J.-P. Quantification of Chemical Peptide Reactivity for Screening Contact Allergens: A Classification Tree Model Approach. *Toxicol. Sci. Off. J. Soc. Toxicol.* **2007**, *97* (2), 417–427. https://doi.org/10.1093/toxsci/kfm064.

(157) Lambrechts, N.; Verstraelen, S.; Lodewyckx, H.; Felicio, A.; Hooyberghs, J.; Witters, H.; Van Tendeloo, V.; Van Cauwenberge, P.; Nelisson, I.; Van Den Heuvel, R.; Schoeters, G. THP-1 Monocytes but Not Macrophages as a Potential Alternative for CD34+ Dendritic Cells to Identify Chemical Skin Sensitizers. **2009**, *236* (2), 221–230. https://doi.org/10.1016/j.taap.2009.01.026.

(158) Yoshida, Y.; Sakaguchi, H.; Ito, Y.; Okuda, M.; Suzuki, H. Evaluation of the Skin Sensitization Potential of Chemicals Using Expression of Co-Stimulatory Molecules, CD54 and CD86, on the Naive THP-1 Cell Line. *Toxicol. Vitro Int. J. Publ. Assoc. BIBRA* **2003**, *17* (2), 221–228. https://doi.org/10.1016/s0887-2333(03)00006-7.

(159) Ashikaga, T.; Yoshida, Y.; Hirota, M.; Yoneyama, K.; Itagaki, H.; Sakaguchi, H.; Miyazawa, M.; Ito, Y.; Suzuki, H.; Toyoda, H. Development of an in Vitro Skin Sensitization Test Using Human Cell Lines: The Human Cell Line Activation Test (h-CLAT). I. Optimization

of the h-CLAT Protocol. *Toxicol. Vitro Int. J. Publ. Assoc. BIBRA* **2006**, *20* (5), 767–773. https://doi.org/10.1016/j.tiv.2005.10.012.

(160) Sakaguchi, H.; Miyazawa, M.; Yoshida, Y.; Ito, Y.; Suzuki, H. Prediction of Preservative Sensitization Potential Using Surface Marker CD86 and/or CD54 Expression on Human Cell Line, THP-1. *Arch. Dermatol. Res.* **2007**, *298* (9), 427–437. https://doi.org/10.1007/s00403-006-0714-9.

(161) Espagnolle, N.; Balguerie, A.; Arnaud, E.; Sensebé, L.; Varin, A. CD54-Mediated Interaction with Pro-Inflammatory Macrophages Increases the Immunosuppressive Function of Human Mesenchymal Stromal Cells. *Stem Cell Rep.* **2017**, *8* (4), 961–976. https://doi.org/10.1016/j.stemcr.2017.02.008.

(162) Sakaguchi, H.; Ashikaga, T.; Miyazawa, M.; Yoshida, Y.; Ito, Y.; Yoneyama, K.; Hirota, M.; Itagaki, H.; Toyoda, H.; Suzuki, H. Development of an in Vitro Skin Sensitization Test Using Human Cell Lines; Human Cell Line Activation Test (h-CLAT). II. An Inter-Laboratory Study of the h-CLAT. *Toxicol. Vitro Int. J. Publ. Assoc. BIBRA* **2006**, *20* (5), 774–784. https://doi.org/10.1016/j.tiv.2005.10.014.

(163) Nuriya, S.; Yagita, H.; Okumura, K.; Azuma, M. The Differential Role of CD86 and CD80 Co-Stimulatory Molecules in the Induction and the Effector Phases of Contact Hypersensitivity. *Int. Immunol.* **1996**, *8* (6), 917–926. https://doi.org/10.1093/intimm/8.6.917.

(164) Bauch, C.; Kolle, S. N.; Ramirez, T.; Eltze, T.; Fabian, E.; Mehling, A.; Teubner, W.; van Ravenzwaay, B.; Landsiedel, R. Putting the Parts Together: Combining in Vitro Methods to Test for Skin Sensitizing Potentials. *Regul. Toxicol. Pharmacol. RTP* **2012**, *63* (3), 489–504. https://doi.org/10.1016/j.yrtph.2012.05.013.

(165) Mitjans, M.; Galbiati, V.; Lucchi, L.; Viviani, B.; Marinovich, M.; Galli, C. L.; Corsini, E. Use of IL-8 Release and P38 MAPK Activation in THP-1 Cells to Identify Allergens and to Assess Their Potency in Vitro. *Toxicol. Vitro Int. J. Publ. Assoc. BIBRA* **2010**, *24* (6), 1803–1809. https://doi.org/10.1016/j.tiv.2010.06.001.

(166) Mitjans, M.; Viviani, B.; Lucchi, L.; Galli, C. L.; Marinovich, M.; Corsini, E. Role of P38 MAPK in the Selective Release of IL-8 Induced by Chemical Allergen in Naive THp-1 Cells. *Toxicol. Vitro Int. J. Publ. Assoc. BIBRA* **2008**, *22* (2), 386–395. https://doi.org/10.1016/j.tiv.2007.10.005.

(167) Mukaida, N.; Okamoto, S.; Ishikawa, Y.; Matsushima, K. Molecular Mechanism of Interleukin-8 Gene Expression. *J. Leukoc. Biol.* **1994**, *56* (5), 554–558.

(168) Goebeler, M.; Trautmann, A.; Voss, A.; Bröcker, E.-B.; Toksoy, A.; Gillitzer, R. Differential and Sequential Expression of Multiple Chemokines during Elicitation of Allergic Contact Hypersensitivity. *Am. J. Pathol.* **2001**, *158* (2), 431–440.

Chapter 2: Isolating and targeting a highly active, stochastic dendritic cell subpopulation for improved immune responses

2.1 Summary

Dendritic cell (DC) activation via pathogen-associated molecular patterns (PAMPs) is critical for antigen presentation and development of adaptive immune responses, but the stochastic distribution of DC responses to PAMP signaling, especially during the initial stages of immune activation, is poorly understood. In this study, we isolate a unique DC subpopulation via preferential phagocytosis of microparticles (MPs) and characterize this subpopulation of "first responders" (FRs). We present results that show these cells (1) can be isolated and studied via both increased accumulation of the micron-sized particles and combinations of cell surface markers, (2) show increased responses to PAMPs, (3) facilitate adaptive immune responses by providing the initial paracrine signaling, and (4) can be selectively targeted by vaccines to modulate both antibody and T cell responses *in vivo*. This study presents insights into a temporally controlled, distinctive cell population that influences downstream immune responses. Furthermore, it demonstrates potential for improving vaccine designs via FR targeting.

2.2 Introduction

The complexity and robustness of immune responses rely on heterogeneity in the differentiation and functional responses of immune cell subsets. For dendritic cells (DCs), functional heterogeneity is critical for initiating adaptive immune responses: if only a fraction of a DC population reacts to a given stimulus at a given time, this allows the remainder to respond at later times or to other stimuli. Within immune cells, heterogeneity exists broadly—helping generate effector and memory subsets and antibody affinity maturation.[1] In addition to

phenotype, heterogeneity also exists in the functional responses of immune cell subsets, including cytotoxic T cells, Th1 cells, and neutrophils.[2,3,4] Stochastic distributions of responses are especially important for early activation in myeloid cells. Xue et al. characterized a small (<5%) population within macrophages that can, in certain conditions, generate >70% of the early inflammatory cytokine tumor necrosis factor alpha (TNF-α).[5] A similar stochastically arising and small population of high interferon β (IFN-β)-secreting cells was observed in a population of murine bone-marrow-derived DCs (BMDCs).[6] Recently, a population of plasmacytoid DCs (pDCs) with similarly high IFNα release at early time points, referred to as "first responders" (FRs), were identified via single-cell mRNA sequencing.[7] In this study, we hypothesized a set of cells that behaved and responded with a similar phenotype, might exist in conventional DC (cDC) populations.

DCs have been extensively studied due to their importance in antigen presentation and facilitating adaptive immune responses.[8] DCs have been divided into four subtypes based on transcriptional and surface markers: (1) pDCs, (2) type 1 DCs (cDC1s), (3) cDC2s, and (4) monocyte-derived DCs (mo-DCs).[9] For our study, we focused on cDCs due to their importance in effective vaccinations.[10] Recent advances in single-cell immune profiles highlighted the inherent heterogeneity of DC populations.[11] This heterogeneity suggests that DCs exist in a spectrum of phenotypes and that the four distinct categories do not capture the heterogeneity and possibly the full functionality of DCs. For example, DC functionality varies by tissue location, even within the same lymphoid structure.[12,13] For DCs, a major question is whether heterogeneity arises from predetermined conditions (e.g., environmental or genetic factors) or from stochastic processes. Stochastic processes have been demonstrated in DC response kinetics, including changes in receptors, responses to stimuli, and speed of response, indicating that many elements

of heterogeneity rely not on predetermined subtypes but on stochastic, emergent properties of these subtypes.[14,15]

We are especially interested in DCs that have strong cytokine responses to pathogen-associated molecular patterns (PAMPs). This strong cytokine response, a FR phenotype described in pDCs, plays an outsized role in initiating global activation of a wider population of heterogeneous antigen-presenting cells (APCs).[16,17,7] To date, however, study on the function of these types of phenotypic cells has been limited due to the lack of methods to identify FR behavior. While circulating pDCs are important for viral responses, cDCs are the predominant category of DC involved in vaccine responses. We sought FR phenotypes in cDCs to determine three main questions: (1) can live cDC FRs be identified and separated from a heterogeneous distribution of cDCs? (2) Is FR behavior a stochastic feature of cDCs as opposed to a consistent behavior within a predetermined subtype? (3) Can FRs in a population be specifically targeted to modulate and improve adaptive immune responses?

We developed a method to identify and isolate FRs from cDCs by exploiting their unique affinity to phagocytose microparticles (MPs). Next, we present evidence that FRs are a distinct, temporally modulated, stochastic DC subpopulation that contribute disproportionately to the bulk stimulation of innate immune cells after Toll-like receptor 4 (TLR4) stimulation. We report that the vast majority of FRs are $CD11b^+$ DCs, suggesting that they are cDC2s. While less than 5% of the total $CD11b^+$ DC population, they secrete the majority of initial TNF-α upon TLR stimulation. We further characterize the kinetics and unique expression profile of FR responsiveness using RNA-Sequencing (RNA-seq). From this, we also discovered two distinctive cell surface markers, DAP12 and PRG2, for identifying FRs within a population of cDCs. Finally, we demonstrate a liposomal-based method to target FRs that can either block or

improve adaptive immune responses. Together, these data show that a stochastic and transient DC state can be targeted to modulate immunity, which is highly relevant to improving immunotherapy.

2.3 Results

2.3.1 Isolation and phenotyping of first responders (FRs), a unique dendritic cell subpopulation with enhanced microparticle (MP) uptake

Since FRs are a rare cell population, we conjectured that the FR state had not been isolated previously due to the low percentage of cells, their transience, and accompanying difficulty in identifying distinguishing cell-surface markers that persist, potentially, only for a few hours. Therefore, our first objective was to develop a method to reliably isolate FRs from a heterogeneous population of DCs. Prior literature indicated that the hallmark of the FR subpopulation is an early and increased inflammatory cytokine secretion to TLR signaling, so we hypothesized that FRs may have increased sensitivity to TLR agonist stimulation.[6] Alternatively, we hypothesized that because DCs specialize in the phagocytosis of micron-sized pathogens like bacteria, FRs may have an increased or early rate of phagocytosis of micron-sized particles—bare or bearing TLRs. If either hypothesis proved true, we could then reliably isolate FRs using MP uptake.[18]

To explore these hypotheses, we utilized a TLR-conjugated MP system, which we previously validated, to attempt to isolate FRs from other DCs.[19] We synthesized 2-μm-diameter, fluorescein isothiocyanate (FITC)-labeled MPs and coated them with a siloxane copolymer to reduce non-specific immune reactivity. We conjugated one of 5 different TLR agonists (TLR2, -4, -5, -7, and -9) to the MPs. We hypothesized that if FRs have either increased TLR sensitivity or MP phagocytosis, then we could incubate the MPs with DCs for short time

periods and use particle uptake to isolate FRs using fluorescence-activated cell sorting (FACS) from the remaining APCs which we refer to as non-FRs.

We noticed an exceptionally large statistical anomaly in these experiments—a small percentage of DCs had a disproportionally MP^{hi} population that deviated greatly from a normal (Poisson) distribution. Specifically, when spleen-derived DCs (sDCs) or BMDCs were incubated with unconjugated 2-μm MPs (MP^{blank}) at a 1:1 cell-to-MP ratio for only 15 min, we observed a clear minority (3%–5%) population with high MP uptake (MP^{hi}) (Figure 2.1A). Interestingly, when sDCs or BMDCs were incubated with unconjugated 250-nm nanoparticles (NPs), there was not a specific subpopulation with high uptake but rather a larger (20%) population with moderate uptake (Figure 2.1A). To further confirm this, we incubated granulocyte-macrophage colony-stimulating factor (GM-CSF)-derived BMDCs or a homogeneous cell line, which we did not expect to exhibit stochastic behavior (RAW cells), with MP^{blank} or NP^{blank} at a 1:1 cell-to-MP ratio for 15 min and then analyzed the cells using ImageStream (ISX) analysis).[20] We counted the particles phagocytosed in the MP^{hi} population and compared it with the total particle uptake. We observed that the MP^{hi} contained almost 80% of the MP^{blank} for BMDCs but <40% for RAW 264.7 macrophages (RAW cells) (Figure 2.1B). Furthermore, the distribution of MP uptake in BMDCs deviated from a Poisson distribution, but not in RAW cells.[1] This indicates that there is a subpopulation of DCs with increased MP uptake that occurs at 3%–5% of all DCs, like the distribution of FR populations in pDCs and BMDCs. We next asked whether adding a TLR agonist to the particle surface would activate DCs or alter MP uptake. We incubated lipopolysaccharide (LPS)-conjugated MPs (MP^{TLR4}) to BMDCs and confirmed that the MP^{hi} DC population phagocytosed similar numbers of MPs as the MP^{blank} groups but also activated NF-κB (Figure 2.1C). Using the various agonist-conjugated MPs, we sought to quantitatively validate

our qualitative observations that MP^{hi} DC populations accumulate a disproportionally high number of MPs and that this effect does not change with the addition of TLR agonists. Using ISX, we determined that (1) BMDCs treated with MPs have increased and statistically unlikely numbers of cells with >3 MPs, (2) this increased accumulation is only seen with MP:cell ratios of 1 or less (3) the skewed increase in MP uptake in the MP^{hi} population is independent of TLR activity (Figure S1).[21] It is important to note that while we anticipated the cells on the far end of the stochastic distribution to contain more MPs than the homogeneous control cells (RAW cells), DC MP^{hi} populations (both BMDCs and sDCs) contained a disproportionally large percentage of MPs, suggesting an effect that is not random but biological in nature (Figure S2F). Furthermore, this population is also observed in human moDCs, indicating that the MP^{hi} subpopulation is not mouse specific (Figure S2).

We questioned whether this increased uptake was due to how our BMDCs were cultured. *Helft et al*. observed that BMDCs differentiated using GM-CSF were widely heterogeneous, displaying typical "DC" markers such as CD135(FLT-3) or more macrophage-like markers of CD115 (CSF1R).[22] To validate that (1) our BMDC cultures generate DC-like phenotypes instead of macrophage-like phenotypes and (2) FRs are not skewed toward one subpopulation of BMDCs, we cultured BMDCs in either GM-CSF or FLT-3L, incubated them 1:1 with MP^{blank}, and analyzed them via flow for macrophage and DC markers (Figure S2G, S2H).[23] Gating on the MP^{hi} (FR) population saw no change in BMDC distribution, with the majority of cells being $CD115/CD135^{-}$ and $CD11b^{+}$. We believe this phenotype is an immature DC phenotype, as this compartment is decreased in DCs from murine spleens (Figure S2G, S2H).[22] We only observe differences between $CCR7^{+}$ DCs in the MP^{hi} group and especially in sDCs, indicating that FRs are more activated, especially in more mature sDCs.[24]

After confirming that this increase in MP uptake is not a flaw in our cell culture, we next sought to determine whether immune cells other than DCs could preferentially accumulate MPs in a similar fashion. We dosed murine splenocytes with MP^{TLR4} and determined that MP^{hi} cells are exclusively overrepresented in DCs, particularly $SIRP\alpha^{+}$ $CD11b^{+}$, markers that suggest a cDC2 lineage (Figure 2.1D, 2.1E, and S2).[25] While DCs represent only ~4% of all splenocytes, DCs constituted almost 50% of all MP^{hi} cells, nearly all of which were $CD11b^{+}$ (Figure 2.1D–G). It is important to note that while FRs were mainly $CD11b^{+}$, they still only account for <5% of all $CD11b^{+}$ cells (Figure 2.1G). Therefore, any conclusions drawn concerning FRs are not expected to be broadly applicable to $CD11b^{+}$ or cDC2s in general.

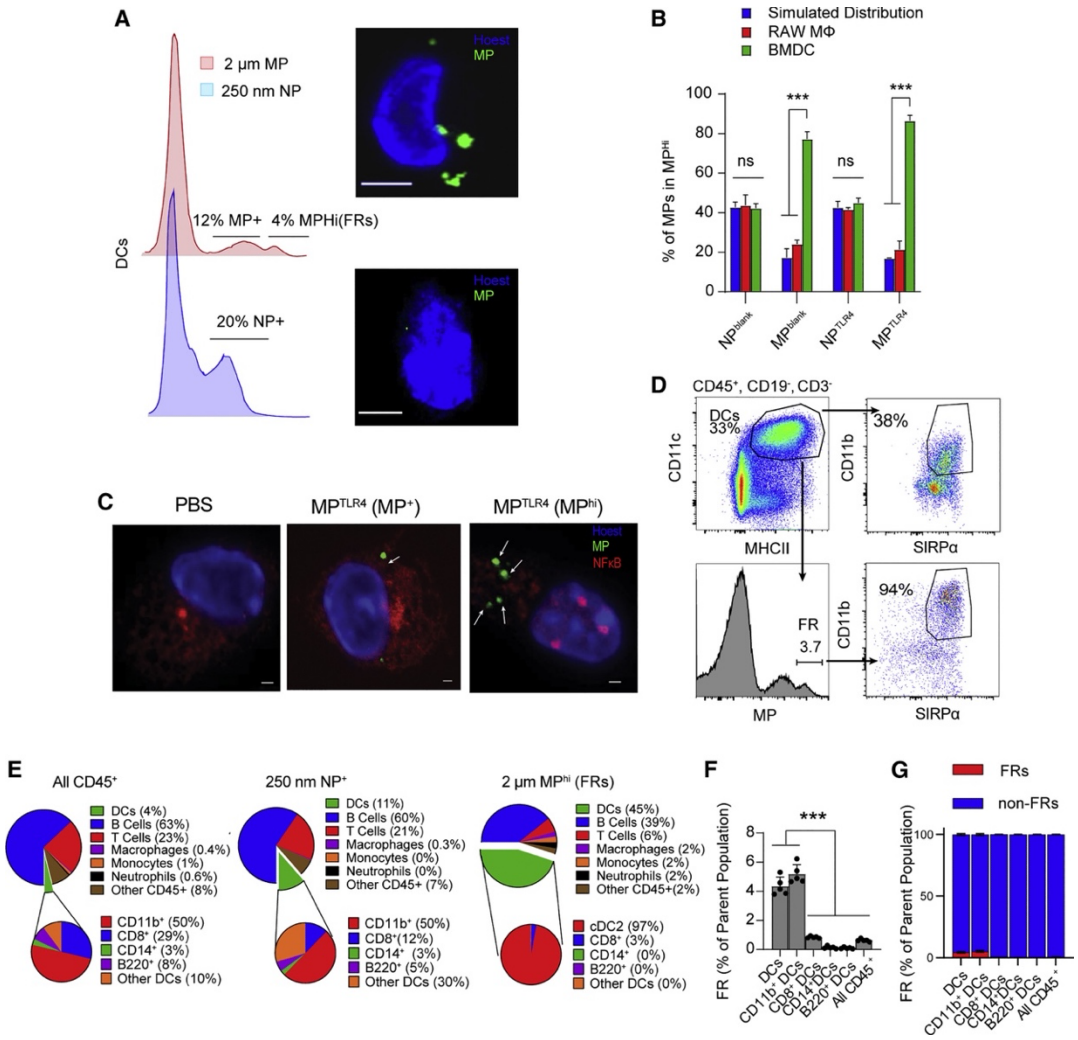

Figure 2.1: Isolation and phenotyping of first responders (FRs), a unique dendritic cell subpopulation with enhanced microparticle (MP) uptake. (A) Representative flow cytometry histograms of mouse spleen DCs treated with 2-μm MPblank (red, top) or 250-nm unconjugated NPs (blue, bottom) for 15 min. Areas of MPhi, MP+, or NP+ are highlighted with a representative image taken using ImageStream Analysis for MPhi (top) or NP+ (bottom). Note that areas with skewed increased (MPhi) uptake are only seen with 2-μm MP. Scale bar: 5 μm. (B) MPs, but not NPs, disproportionally accumulate in FR population. 1 million BMDCs or a control RAW cell line were incubated with 1 million MPs either unconjugated (blank) or conjugated with LPS (TLR4) for 15 min. Cells were then analyzed with ISX, and the total number of MPs uptaken in the top 5% of MP signal (the FR population) was calculated. This was compared with a simulated distribution using the average particle uptake from the BMDC experiment and the Poisson distribution function (blue bars).(C) Representative confocal microscopy images showing that FRs accumulate high levels of MP signal and are immunologically active. BMDCs were stained for NF-κB after 15-min treatment with PBS (left) or MPTLR4 (middle and right). Representative cellular image of MPhi (right) and MP+ (middle) are shown. Blue channel (DAPI), green channel (FITC MPTLR4), and red channel (NF-κB). Scale bar: 1 μm.(D) Representative flow plots showing an increase in CD11b+ DC population for the FR population. Freshly isolated mouse splenocytes were gated on live, single CD45+ cells, then gated to remove

Figure 2.1 (continued): CD19/B220+ cells and CD3+ cells. DCs were gated from the remaining cells (CD11c+, MHC class IIhi). DCs were further gated on SIRPα and CD11b+ (CD11b+ DCs) and/or MP uptake for FRs.(E) Representative pie charts show (left) the distribution of cells in splenocytes, (middle) the distribution of NP+ cells, and (right) the distribution of MPhi (FRs) subpopulations after 15-min incubation.(F) FR distribution as percentage of each parent cell type, showing FRs are approximately 5% of DCs and CD11b+ DC populations.(G) Data from (F) shown in another manner to illustrate low FR percentage.(E)–(G) were performed with N = 5 mice, while (A)–(D) were performed in biological triplicates. Error bars indicate ± SD. ∗∗∗p < 10−4 by one-way ANOVA with Tukey's posttest.

2.3.2 MP^{hi} DCs exhibit FR characteristics of increased TLR activation and TNF-α release

After phenotyping the MP^{hi} DCs and determining that they are a distinct and reliable subpopulation of DCs, we evaluated their cytokine profiles to test whether MP^{hi} DCs demonstrate a similar inflammatory profile as previous reports of FRs. FRs were previously identified by their increased and early release of inflammatory cytokines such as TNF-α and IFN-β in response to TLR stimulation) rather than their affinity for MP uptake; thus, it was critical to confirm that MP^{hi} DCs show similar release profiles of TNF-α, IFN-β, or both.[17,5,7] We observed that MP^{hi} BMDCs have significantly increased TNF-α expression when examined via ISX analysis of intracellular cytokine staining after 4 h incubation with MP^{TLR4}, supporting our hypothesis that MP^{hi} DCs are FRs (Figure 2.2A and S2). We sought to further quantify TNF-α release to corroborate prior reports that "super-secreting" cells released the majority of the TNF-α using FACS-isolated DCs and brefeldin A (BrefA)-treated BMDCs.[17] We observed that FRs from BMDCs, when treated with MP^{TLR4}, release a disproportionate amount of TNF-α compared with either non-FRs treated in the same dish (30 times greater) or FR-like cells (i.e., RAW cells with the top 5% of MP signal, only <4 times greater) (Figure 2.2B-2C). Despite being only 5% of the cells, FRs in the MP^{TLR4} group accounted for over 60% of the total TNF-α released. For simplicity, we will exclusively use FR to describe MP^{hi} DCs from this point forward.

We next asked whether this increased activation of FRs was due to the increased TLR activation of DCs that accumulate most of the particles or whether FRs are inherently more responsive to TLR activation. To test this, we decoupled the enhanced uptake and TLR activation of FRs by incubating sDCs with MP^{Blank} together with either PBS or LPS for 1 h using BrefA to inhibit cytokine release, and measured intracellular TNF-α expression (Figures 2.2D, S2H, and S2I for gating strategy). The data indicate that FR cells are significantly more likely to be TNF-α^+ for all treatment groups, including PBS and no incubation (Figure 2.2E). This result indicates that FRs have a pre-existing cytokine reservoir even in the absence of TLR signaling, suggesting that they not only generate more TNF-α but also are ready to respond before encountering a PAMP. We also confirmed that FRs do not have increased TLR expression relative to non-FRs, indicating that this increase in TLR signaling was not due to overstimulation of TLR pathways (Figure S3). Next, we performed a similar experiment to observe intracellular generation of IFN-β, which was previously seen to be overexpressed in BMDC FR-type cells.[6] There is a similar increase in IFN-β expressing FRs at 1 h (Figure 2.2F). This increase in IFN-β was co-expressed with TNF-α (Figure 2.2G). Overall, these data indicate that FRs engage standard TLR signaling pathways to generate early inflammatory signals.

After observing the high TNF-α levels produced by FRs, we sought to determine whether FRs could induce pro-inflammatory responses in an *in vitro* population of naive DCs and whether FRs are a temporal stochastic subpopulation or a predetermined subset of DCs. To test these questions, we activated BMDCs with MP^{TLR4} for 15 min and separated the FRs versus non-FRs via FACS. We isolated cells via FACS, added them to fresh BMDCs after incubating for various time points, and then measured TNF-α and CD40 expression (Figure 2.2H, 2.2I, and S3).[26] We observed high levels of TNF-α production in BMDCs only when FRs were added

at 0.25 h (Figure 2.2H). From this, we concluded that the FRs promote bulk *in vitro* activation of BMDCs but only at early timescales. Interestingly, only background expression of TNF-α was observed at 1 or 2 h, indicating that the FR response was short lived, implying that FRs might be highly temporal in its stochasticity. Non-FRs alone were not sufficient to stimulate an *in vitro* immune response, although non-FR ability to simulate BMDCs returned after 3 h (Figure 2.2H, S3). Similar results to Figure 2.2H were obtained when BMDCs were plated in a transwell membrane culture (Figure 2.2I, S3), indicating that soluble factors are driving the inflammatory signaling response.

Considering that TNF-α secretion (1) appeared to be more rapid in FRs versus non-FRs and (2) changed over time, we sought to examine cytokine production kinetics and the cyclic nature of FR activation. We performed an extended version of the ICS staining experiment in Figure 2.2E, varying incubation times in BrefA (Figure 2.2J). We observed that the TNF-α^+ cells in the FR DC population remained higher than non-FR DCs for all time points. However, the ratio of TNF-α^+ cells changed throughout the course of the experiment, increasing in the FRs at 15 min and then increasing in the non-FRs thereafter (Figure S3). This result is consistent with our previous findings that FRs have an increased amount of TNF-α initially followed by increases in surrounding non-FR cells.

To investigate the temporal state of FRs, we performed a staggered MP uptake experiment using two different colors of MPs. We hypothesized that if DCs periodically cycled through the FR state, then any currently active FRs would uptake particles. Therefore, introducing particles of different colors at timed intervals would reveal if DCs altered their MP uptake. If the same cells take up particles, then we would expect cells to contain both colored particles at given intervals and support our hypothesis that unstimulated DCs natively switch

between FR and non-FR states at a regular interval. The relative uptake ratios of FITC/Cy5 particles were determined via flow cytometry (Figure 2.2J-2.2K). We observed that there is a distinct population of cells that take up a combination of FITC and Cy5 MPs (dual) but that this number decreases until about t = 60 min. The results indicate that DCs cycle their particle uptake between 45 and 60 min.

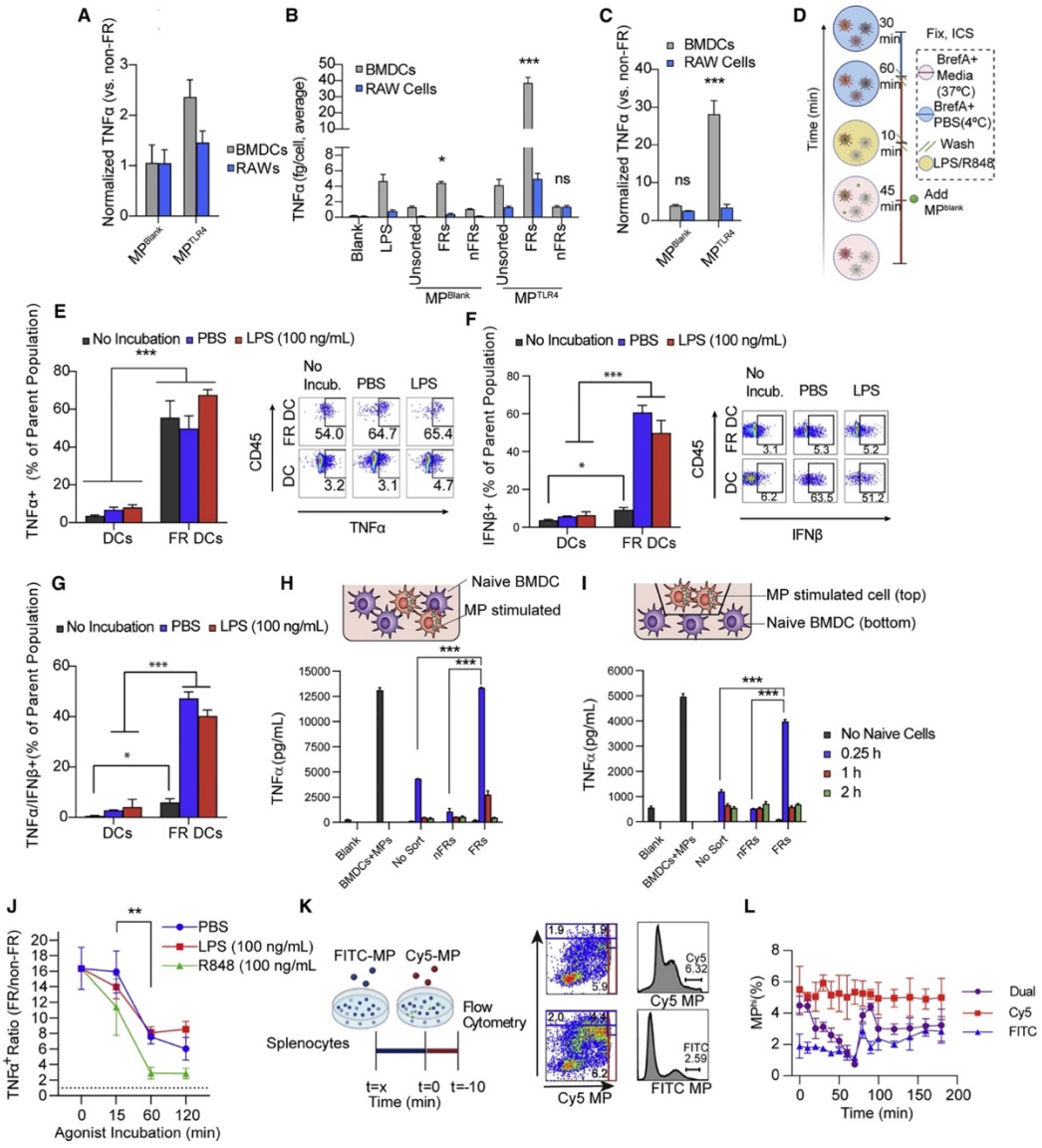

Figure 2.2: FR populations have an outsized and temporally controlled role in DC activation *in vitro* (A) MP^{TLR4} was added to 100,000 BMDCs preincubated with brefeldin A (brefA). After 4 h, the TNF-α levels were analyzed via ISX. (B) BMDCs preincubated with BrefA were stimulated at a 1:1 ratio with MP^{TLR4} or blank MPs for 15 min. The

Figure 2.2 (continued): FRs and non-FRs were sorted and resuspended at 1 million cells/mL for non-FRs and controls or 50,000 cells per mL for FRs in media with no BrefA, releasing cytokines. (C) Ratios of FR/non-FR TNF-α release from (B). (D) Experimental schematic of (E). (E) FRs show increased TLR response to free agonist and regenerate TNF-α in the absence of simulation. Splenocytes were incubated in BrefA, then MP^{Blank}, washed quickly, and incubated with 100 ng/mL LPS or PBS (no agonist addition). Representative flow plots are shown to the right. (F) In a similar experiment to (E), spleen DCs were analyzed for ICS expression of IFN-β. (G) Cells from (F) were analyzed for percentage of double-positive TNF-α and IFN-β. (H) FRs play an outsized role in stimulation of a naive DC population. FRs and non-FR populations were isolated via FACS after MP^{TLR4} incubation and incubated in media for 0, 1, or 2 h. 100,000 FRs, 1 million non-FRs, or unsorted BMDCs were added to 1 million naive BMDCs. After 16 h, TNF-α release was measured via ELISA of the supernatant. (I) A similar experiment to (H), but the naive BMDCs were plated on the bottom section of a transwell assay and the MP-stimulated FRs, non-FRs, and unsorted BMDCs were plated on top of the membrane. (J) Kinetic analysis of FR release of TNF-α. Similar to (E), splenocytes were incubated with 100 ng/mL LPS or 100 ng/mL R848 or PBS but for varying time points. The TNF-α^+ ratio was calculated by dividing the percentage of TNF-α^+ in FR DCs by the percentage of TNF-α^+ in all DCs. A significant drop was seen in all three treatment groups between 15 and 60 min. (K) Schematic of two-color MP uptake experiment to determine kinetics of FR cycling (left). Representative gating strategy (right). (L) Data for two-color MP uptake experiment. Briefly, FITC-labeled MP^{Blank} were incubated with splenocytes (1:5 MP:cell) for varying time points, then 15 min prior to flow analysis, cells were incubated with Cy5-labeled MP^{Blank}. Significant increase in dual MP uptake around 1 h indicates FR turnover. All experiments were performed in biological replicates (N = 5 for E–G and J, N = 3 for all others). Error bars indicate ± SD; $^{*}p < 0.05$, $^{**}p < 0.01$, $^{***}p < 10^{-4}$ by two-way ANOVA with Tukey's posttest (with multiple comparisons for J).

2.3.3 FRs have a unique temporal transcription profile

Given the relevance of FRs, we sought to further characterize FR activity via whole-transcriptome sequencing. We added MP^{TLR4} to BMDCs, washed, and sorted them after 0.25, 0.5, 1, 2, or 4 h. We noticed that at 15 min, transcription levels for several inflammatory cytokines, such as TNF-α, IFN-β, CXCL1, and IL-1β, were highly upregulated in FRs but not in non-FRs (Figure 2.3A, S1). In later time points, these cytokine mRNA levels decreased for FRs but increased for non-FRs, corroborating our cytokine release data from Figure 2.2. For example, TNF-α mRNA levels dropped to below baseline after 1 h for FRs but peaked for non-FRs at 1 h (Figure 2.3A). This further supported the previous observations that FRs have a burst release of

inflammatory paracrine signaling cytokines immediately following TLR engagement, which then stimulate neighboring cells at later time points.

We further analyzed the non-FR expression of genes related to IFN-β and TNF-α to further confirm our hypothesis that FRs' early release of inflammatory cytokines coordinates local innate immune activation. We saw increases compared with unstimulated BMDCs in STAT1, IRF5, IRF7, IRF8, and IRF9 in FRs, especially at 1 h post stimulation, each of which is important for IFN-β and TNF-α signaling (Figure 2.3B).[27,28,29,30] We saw very little transcription factor upregulation in FRs, as they are expected to already return to baseline after 0.25 h; however, we did observe an increase in IRF7 at all time points other than 0.25 h. Using gene set enrichment analysis (GSEA), we also observed a larger increase in the "response to IFN-β" and "response to TNF-α" gene sets for non-FRs compared with FRs (Figure 2.3C). In addition to cytokine genes, we analyzed genes that govern antigen presentation. We observed upregulation for major histocompatibility complex (MHC) class I and MHC class II genes in the FRs compared with the non-FRs, corroborating our flow cytometry data (Figure 2.3D and S3). Likewise, the MHC co-stimulatory molecule CD86 is upregulated 32-fold over untreated cells at 0.25 h. This is particularly significant as the 0.25 h MP incubation is unlikely sufficient time for *de novo* gene expression.

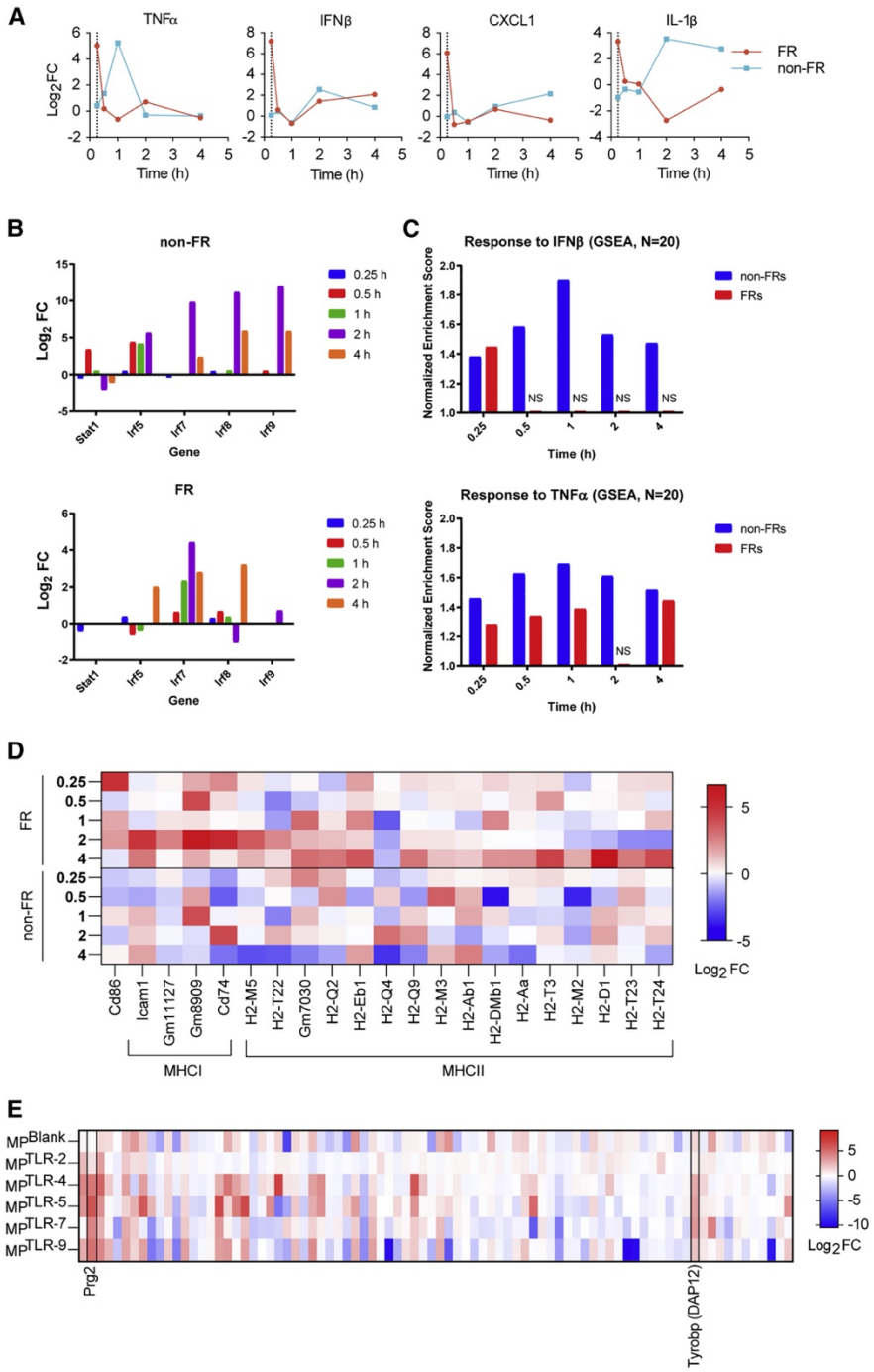

Figure 2.3: FRs possess a distinct mRNA profile. (A) BMDCs were incubated with MP^{TLR4} 1:1 for 15 min, washed, and immediately sorted into FRs (top 5% of MP signal) and non-FRs (bottom 90% of MP signal). The mRNA from these cells was isolated immediately after sorting (0.25 h) or incubated at 37°C for 0.5, 1, 2, or 4 h and isolated. Genes were aligned and 2-fold upregulation calculated by comparing with a non-treated BMDC control. Time course fold change of the following cytokines was plotted from left to right: TNF-α, INF-β, CXCL1, and IL-1β. (B) Log2 fold change of several IFNβ-related genes at varying time points for (top) non-FRs and (bottom) FRs. Genes with false discovery rate of $p < 0.05$ by Wilcoxon test were included. (C) Gene set enrichment analysis (GSEA) data

Figure 2.3 (continued): for (top) response to IFN-β and (bottom) response to TNF-α are shown for non-FRs and FRs at varying time points. Only enrichment with a false discovery rate (FDR) of <0.05 was included. (D) Heatmap of log2 fold change in the mRNA for genes with known antigen presentation function. Genes with an FDR of $p < 0.05$ by Wilcoxon test and at least 2-fold differential expression were included. (E) BMDCs were incubated with varying MP formulations for 16 h with brefA treatment, washed, and sorted into FRs and non-FRs as in (A)–(E), and mRNA was immediately isolated, transformed into cDNA, and sequenced, and genes were aligned. A list of upregulated mRNA genes in FRs that correspond to surface receptors is shown in a heatmap. All experiments were performed in biological triplicates with significant upregulation determined only if $p < 0.05$ (see STAR methods for further details).

2.3.4 FRs express unique and identifiable surface proteins

Our secondary objective of this study is to target FRs for immune modulation, so we also analyzed mRNA data for upregulated surface proteins in FRs. We looked for the genes that were most consistently upregulated among these dosing conditions (2-fold increase in expression and $p < 0.05$) when comparing the transcriptional profiles of the FRs with the non-FRs. which provided two promising candidates, DAP12 and PRG2 (Figure 2.3E). We validated that DAP12 and PRG2 showed increased expression on FRs compared with non-FRs for both BMDCs and sDCs via flow cytometry (Figure 2.4A, 2.4B, 2.4G, 2.4H, and S4, S5 for gating strategy). DAP12 is a protein reported for association with natural killer cells while PRG2 is reported in association with eosinophils. [31,32,33] To our knowledge, there are no established phenotypes that co-express these markers, and we observed a very small (<1%) percentage of all $CD45^+$ cells that co-express both PRG2 and DAP12 at any level in splenocytes, lymphocytes, or skin cells (Figure 2.4C, S4, and S5). Similarly, $DAP12^+/PRG2^+$ cells were represented by most cell populations at <1% (Figure S5). Meanwhile, we found that $DAP12^+$ and $PRG2^+$ cells were increased in the DC and $CD11b^+$ DCs, and even though most $DAP12^+/PRG2^+$ cells were B cells, they were overrepresented by $CD11b^+$ DCs (Figure 2.4C, 2.4D, S4, and S5). Most importantly, we

observed a significant increase in DAP12 and PRG2 mean fluorescence intensity (MFI), and DAP12/PRG2^{+} cells, and a significant increase in DAP12 and PRG2 signals overlapping with the DC FR populations (Figure 2.4E–4G and S5). To further confirm that the DAP12/PRG2+ DC population would identify the same cells as the MP method of identifying FRs, we performed an ICS experiment similar to Figure 2.2E to determine if DAP12/PRG2+ DCs have the same phenotype of increased cytokine responses to TLR signals as FRs—matching our experiments and previous literature (Figure 2.4H). We observed significantly increased TNF-α responses for DAP12/PRG2+ DCs from all groups but the highest responses from TLR-treated groups (Figure 2.4I).

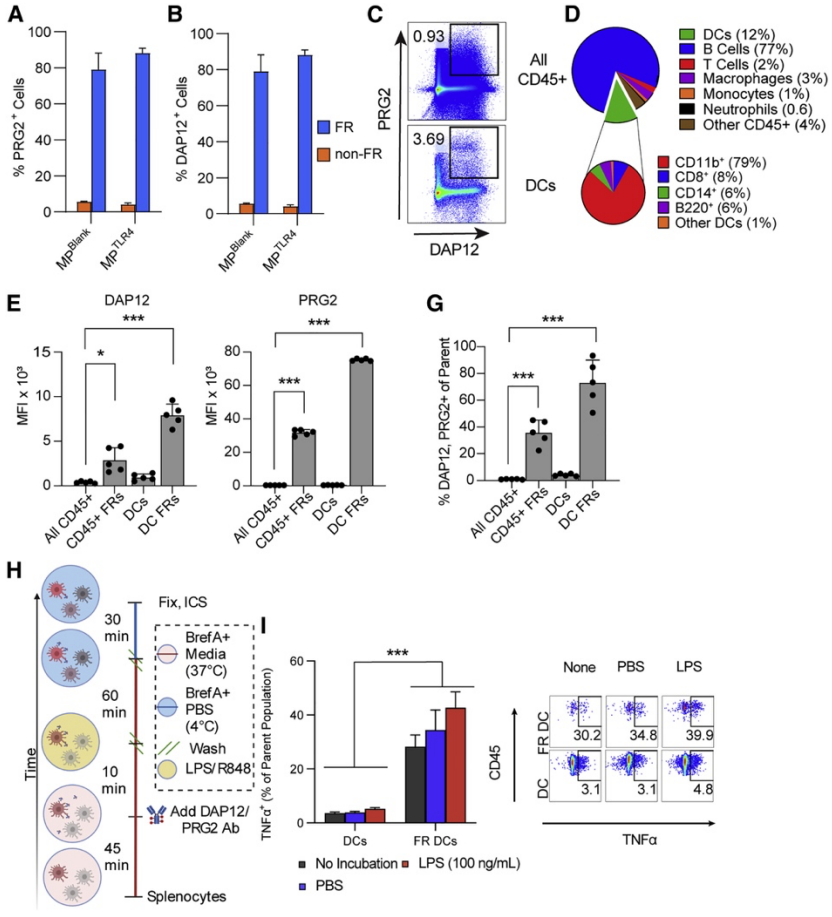

Figure 2.4: Confirmation of distinctive FR-related cell surface markers. (A and B) Murine splenocytes were incubated with MP^{TLR} formulations for 15 min, then stained for CD11c and either (A) PRG2 or (B) DAP12 and

Figure 2.4 (continued): analyzed via flow cytometry. Percentage of $PRG2^+$ or $DAP12^+$ $CD11c^+$ cells were calculated for FR and non-FR compartments. (C–G) Murine splenocytes were incubated with MP^{TLR4}, washed, stained, fixed, and analyzed via Aurora spectral flow cytometry. (C) Representative flow plot of splenocytes depicting $PRG2^+$ and $DAP12^+$ population for all $CD45^+$ cells (top) and DCs only (bottom). (D) Distribution of $PRG2^+$ and $DAP12^+$ cells in various immune subsets and DC subsets (expanded slide). (E–G) DAP12 MFI, (E) PRG2 MFI, (F) and percentage of (G) $DAP12^+$ and $PRG2^+$ of selected cell populations. (H) Experimental schematic of (I). (I) $DAP12/PRG2^+$ DCs have increased TNF-α secretion in response to TLR agonists similar to MP-identified FRs. Similar to Figure 2.2E, splenocytes were incubated with BrefA and stained for DAP12 and PRG2, washed once, then incubated with PBS or 100 ng/mL LPS. The percentage of $TNF\text{-}\alpha^+$ cells were compared between treatment groups with or without DAP12/PRG2 gating. See representative gates on the right. MFI, mean fluorescence intensity. Experiments performed in (A)–(C) were performed in biological triplicates. (D–I) N = 5, and error bars indicate ± SD. Significance was determined by two-way ANOVA with Tukey's multiple comparisons post hoc tests $^*p < 0.05$, $^{**}p < 0.01$, $^{***}p < 1 \times 10^{-4}$, and NS, not significant.

2.3.5 Selective targeting of FRs via DAP12 and PRG2 targeted liposomal formulations

After confirming that unique markers could identify FRs, we sought to develop a method to target DC FRs. To accomplish all these goals, we used a multivalent liposome containing ligands for DAP12 and PRG2. To bind DAP12, we identified a selective nonamer peptide (GFLSKSLVF).[34] To bind PRG2, we identified heparin, which has moderate affinity.[35] To test if these targeting elements would target FRs, we used a well-characterized liposomal system to insert both DAP12- and heparin-conjugated lipids into 200-nm DSPC liposomes. We synthesized and purified lipid-conjugated versions of the DAP12 and heparin polymer and determined optimal ligand loading (Figure S6).[36]

We co-incubated a fluorescently labeled version of the heparin/DAP12 liposome (referred to as FR-targeted liposomes [FR-TLs]) or non-targeted liposomes (non-TLs) with splenocytes for 15 min and analyzed the cells with flow cytometry. Upon analysis, we observed a significant increase in liposome MFI for FR-TLs compared with non-TLs for both DC FRs (as identified via MP uptake) and DC $DAP12/PRG2^+$ cells (Figure 2.5A, 2.5B, and S4 for gating strategy). This result showed that FR-TLs have enhanced localization to FRs (Figure 2.5A and

2.5B). The same trend was seen in cells extracted from mouse lymph nodes and skin (Figure 2.5B). We observed that >50% of DC FRs or PRG2$^+$ DAP12$^+$ DCs were FR-TL$^+$, while <5% of DCs were non-TL$^+$ (Figure 5C and 5D). We further confirmed the FR-TL selectivity for FRs via confocal microscopy and via an antibody-blocking experiment (Figure 2.5E, 2.5F, and S6L).

To further probe how reliably FR-TLs home to FRs *in vivo*, we performed a biodistribution experiment directly comparing FR-TLs with non-TLs. We hypothesized that if FRs are predominantly CD11b$^+$ DCs, then FR-TLs would accumulate in lymphoid organs (spleen and lymph nodes near injection site).[37] We observed that FR-TLs had significantly more accumulation in spleen and lymph nodes as well as the liver than non-TLs, which accumulate in the kidneys (Figure 2.5G and 2.5H). This indicates that FR-TLs are accumulating in organs more likely to have CD11b$^+$ DCs, like the spleen and lymph nodes, and supports targeting of FR cells. Although DCs do exist in the liver and kidneys, we believe the accumulation in the liver to be a non-specific effect of targeted liposomes and first-pass metabolism.[38] These data indicate that we can reliably target FR cells with the heparin/DAP12 peptide liposome formulation (FR-TLs).

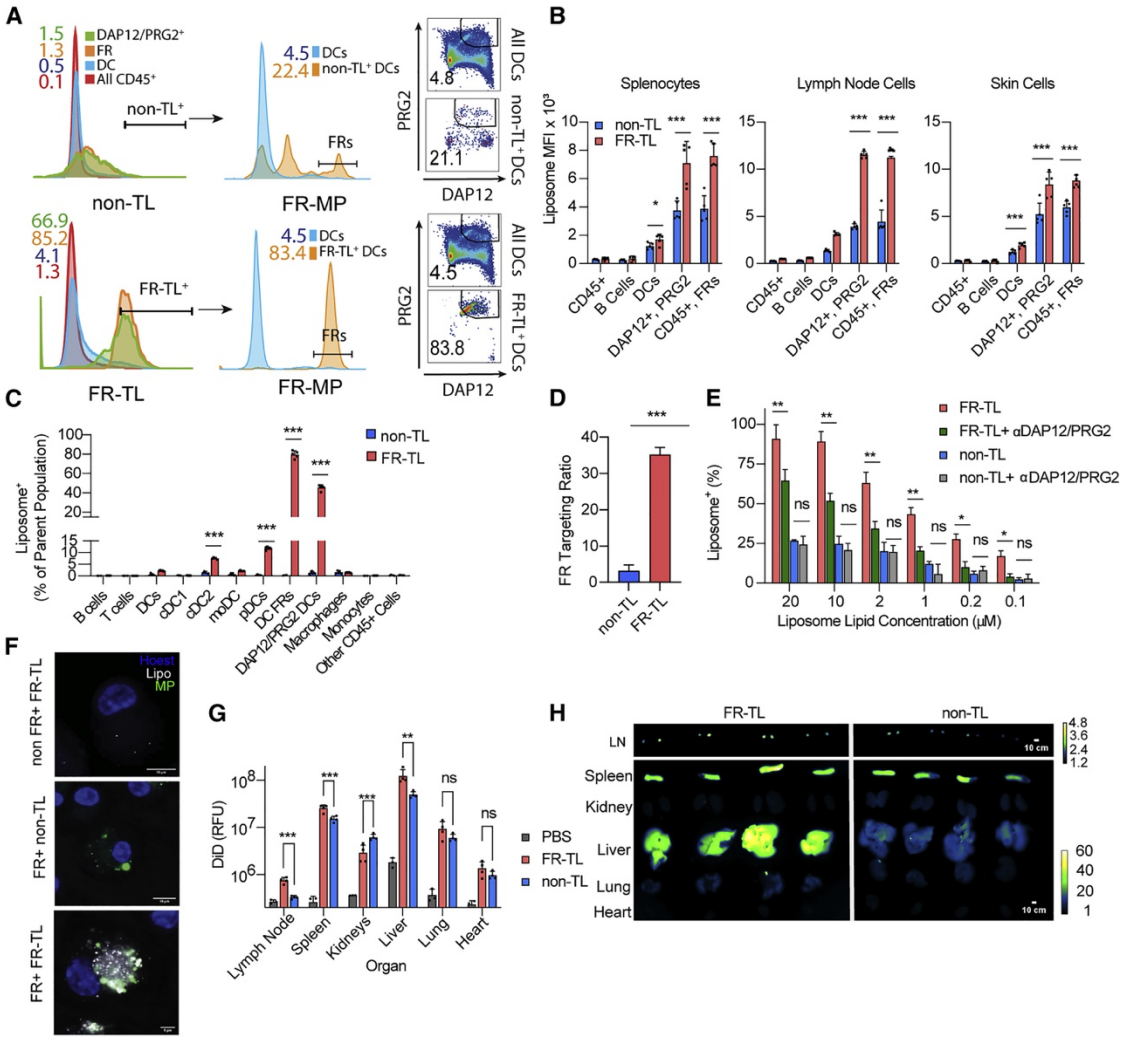

Figure 2.5: FR-targeted liposomes (FR-TLs) selectively target FR populations. (A–D) 1 mol % DAP12 peptide and 10 mol % heparin-lipid loaded, DiD-labeled (0.01 mol %) 200-nm diameter liposomes (FR-TLs) or blank DiD-labeled 200-nm liposomes (non-TLs) were incubated with splenocytes and lymphocytes of disaggregated mouse skin cells at 2-μM total lipid concentration for 15 min, then incubated with MPTLR4 at a 1:1 MP-to-cell ratio for 15 min. (A) Representative flow histograms showing FR-TLs specifically target DAP12/PRG2+ FR DC population. (left). Representative histogram of liposome signal for FR-TL (bottom) or non-TL (top) for all CD45+ cells (red), DCs (blue), FRs (orange), or DAP12/PRG2+ cells (green). Colored numbers indicate liposome+ population of each group. (Middle) Representative histogram of MP signal of cells in non-TL+ (top) or FR-TL+ (bottom) DC populations with an FR gate for all DCs (blue) or liposome+ populations (orange). (Right) Similar to middle plot, liposome+ (top panel) or all DC (bottom panel) populations were plotted for DAP12/PRG2 expression. (B) MFI liposome values for splenocytes, lymphocytes, and skin cells, respectively, treated with non-TLs or FR-TLs for selected cell populations. (C) Liposome+ percentage of various cell populations for splenocytes. (D) Calculation of FR-targeting ratio for non-TL and FR-TL in splenocytes. Targeting ratio was calculated by dividing the percentage of FRs in the liposome+ DC population by the percentage of FRs in the whole DC population. (E) Blocking PRG2

Figure 2.5 (continued): and DAP12 reduces FR-TL specificity. BMDCs were treated with or without a 1:100 dilution of anti-DAP12 and anti-PRG2 antibodies, incubated with FR-TL or non-TL for 30 mins, then incubated with MPBlank for 15 min. (F) Representative confocal images of BMDCs incubated with liposomes at 10-μM total lipid concentration and MPTLR4. Top: non-FRs (with no MP signal) with targeted liposome (FR-TL), middle: FRs incubated with 10-μM non-TL, and bottom: FRs + 10-μM FR-TLs. Scale bars: 10 μm. (G) Biodistribution of FR-TLs *in vivo*. Mice (N = 4) were injected with FR-TLs or non-TLs intraperitoneally (i.p.). One h later, mice were sacrificed, and popliteal lymph nodes, spleens, liver, kidneys, heart, and lung were analyzed via IVIS Spectrum *In Vivo* Imager. Normalized image fluorescence intensity for each organ is graphed. (H) Fluorescence image of mouse organs treated with FR-TL (left) and non-TL (right) used to generate data in (I). Scale bar: 10 cm. All experiments were performed with 4–5 biological replicates. Error bars indicate ± SD. Significance was determined by two-way ANOVA with Tukey's multiple comparisons post hoc tests. $*p < 0.05$, $**p < 0.01$, $***p < 1 \times 10{-}4$, and NS, not significant.

2.3.6 *In vivo* validation of FR ablation and FRs are important for generating antigen-specific responses via BMDC adoptive transfer

After demonstrating that FRs can be reliably targeted via liposomes (FR-TLs), we sought to evaluate how targeting FRs would alter adaptive immune responses. Our hypothesis is that since FRs have disproportionate influence over initial immune responses, modulating their immune signaling will drastically affect downstream adaptive responses (Figure 2.6A). To test this hypothesis, we performed an ablation experiment—to decrease the activity of FRs and therefore decrease the overall adaptive responses. We designed an experiment to temporarily suppress the FR responses by delivering BrefA in FR-TLs—preventing FRs from signaling via paracrine signaling –.[39,40] We loaded BrefA at 1 mg/mL into 200 nm liposomes (BrefA FR-TL or BrefA non-TL) and validated that these liposomes suppress BMDC activation *in vitro* (Figure S6). After validation, we injected these BrefA formulations into mice. BrefA FR-TLs resulted in a significant decrease in anti-ovalbumin (OVA) immunoglobulin G (IgG) and CD8/$OVA^{257–264}Tetramer^{+}$ and CD4/$OVA^{323–339}Tetramer^{+}$ cells, similar to levels seen in PBS control groups (Figure 2.6B, 2.6C, and S7 for gating strategy). These data indicate that by selectively inhibiting the FR population *in vivo*, the adaptive immune responses can be selectively diminished. In

contrast, we hypothesized that FR-TLs could also be used to enhance responses to adjuvants. To test this, we loaded OVA (1 mg/mL) and CpG (a TLR 9 agonist, 200 μg/mL) into FR-TLs (CpG FR-TLs) or non-TLs (CpG non-TLs) (Figure S6).[41] On day 14, there was a nearly 10-fold increase in anti-OVA IgG of CpG FR-TLs compared with CpG non-TLs (Figure 2.6D). Interestingly, when the mice serum cytokine levels were measured at 1 h post injection, we did not observe an increase in TNF-α levels, suggesting that targeting FRs maintained a largely local response and did not have far-reaching activation (Figure S7).

To test if these responses were independent of the adjuvant, we repeated the previous experiment using R848 (R848 FR-TLs), a TLR 7 agonist (Figure S6).[42] Similarly, R848 FR-TLs significantly improved anti-OVA IgG levels and CD8/OVA$^{257–264}$Tetramer^{+} and CD4/OVA$^{323–339}$Tetramer^{+} cells on day 21 (Figures 2.6E and 2.6F). This increase seems to be a result of an increase in CD45^{+} cells into the lymph nodes, not an increase in T cells; however, there is an increase in long-lived T cell subsets of central memory T cells (T_{CM}s) and effector memory T cells (T_{EM}s) in the R848 FR-TL group when compared with non-TL R848 controls, indicating that FR targeting increases overall long-lasting T cell responses (Figure S7). Further analysis of the splenocytes from these mice via ICS demonstrates significant antigen-specific increases in IFN-γ expressing CD4^{+} and CD8^{+} T cells, indicating an increase in Th1 responses (Figure S7).

Finally, we wanted to determine if the Th1 antigen-specific responses elicited by FR targeting could be translated into an OVA-expressing tumor model (EGF7.OVA).[43] There was a significant reduction in tumor volume for both liposomal formulations when compared with PBS controls beginning at day 14, but there was a further decrease in tumor volume for the FR-TLs compared with the non-TLs, which continued for the remainder of the study (Figure 2.6G; $p < 0.05$). On day 30, all mice except for the R848 FR-TL group had to be sacrificed due to

tumor size (Figure S7). Taken together, these experiments indicate that FR targeting can be used to modulate adaptive immune responses *in vivo*.

In addition to our *in vivo* FR targeting experiments, we performed an adoptive transfer of FRs to further demonstrate that FRs are critical for adaptive immune responses. We adoptively transferred MP^{TLR4}-treated BMDCs sorted into FRs or non-FRs into C57BL/6 mice in combination with the antigen OVA. The MP^{TLR4}/OVA-treated unsorted BMDCs generated anti-OVA responses when adoptively transferred, but the same level of T cell and antibody responses were observed in the FR groups, despite containing one tenth of the cells/OVA mix, while non-FRs had minimal responses (Figures 2.6H and S7). From these data, we conclude that FR signaling is important for generation of robust adaptive immune responses.

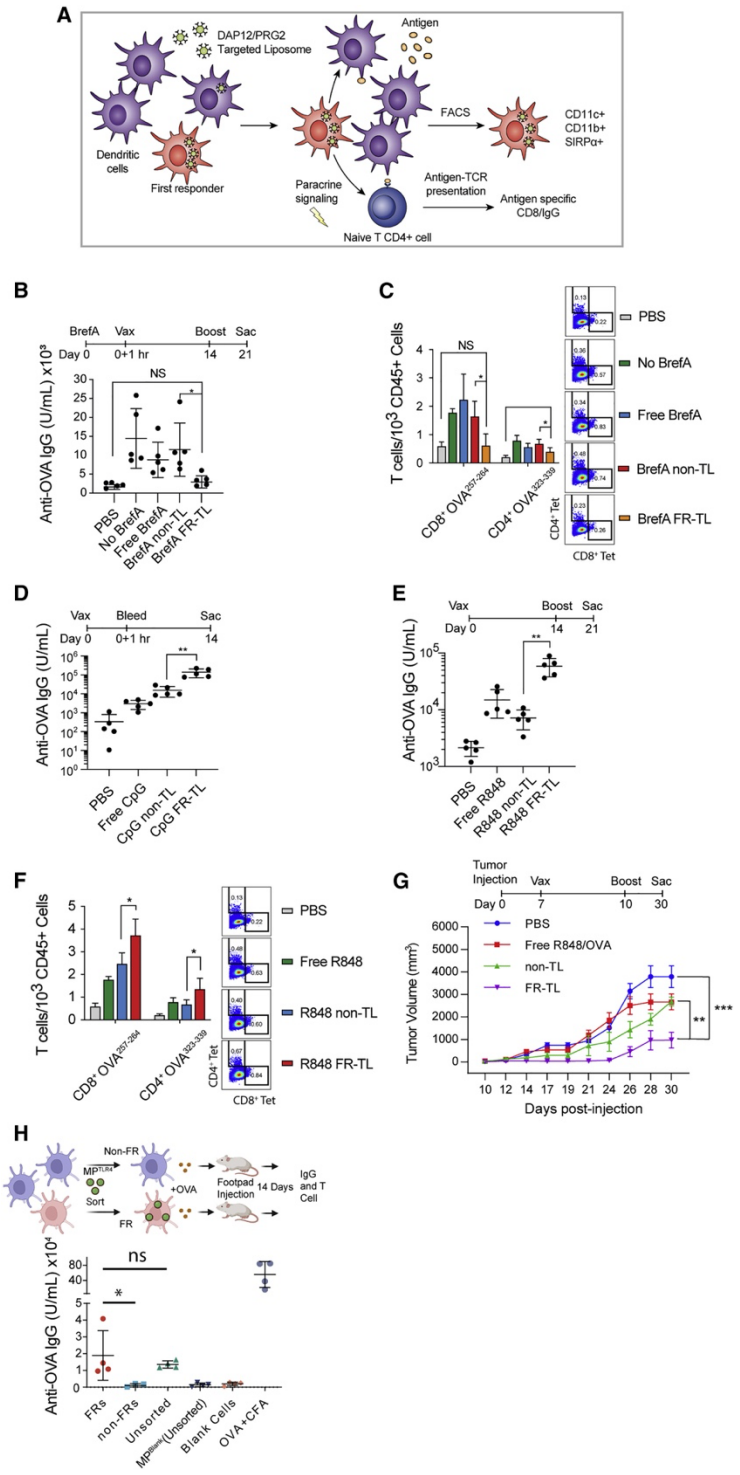

Figure 2.6: *In vivo* validation of FR targeting in vaccination models. (A) Schematic of hypothesized FR immune interactions. (B) Blocking FR paracrine signaling reduces adaptive immune response. C57BL/6 mice were injected with Bref A formulations, and then 1 h later, all mice except the PBS group were injected with 100-µg OVA and 10-µg CpG on day 1. On day 14, both injections were repeated. Mice were sacrificed on day 21, and their IgG titers analyzed. (C) Lymph nodes from experiment in (B) were stained for T cell surface markers and with tetramers for

Figure 2.6 (continued): the major OVA MHC I epitope (OVA 257–264) and the major MHC II epitope (OVA 323–339) and analyzed via flow. Representative flow plots of CD3+ and CD45+ T cells gated into Tetramer+ populations are shown to the right. (D) Targeting FRs with adjuvants increases adaptive responses. CpG and OVA were loaded into liposomes either targeted with DAP12/Heparin (CpG FR-TL) or blank liposomes (CpG non-TL), injected into C57BL/6 mice, and compared with a PBS control (no OVA) or free CpG/OVA equivalent (100-μg OVA and 10-μg CpG per mouse). 14 days later, anti-OVA IgG titers were measured. (E) R848 (10 μg per mouse) replaced CpG in a repeat of experiment from Figure 2.6B. Mice were injected on days 1 and 14 and then sacrificed, and anti-OVA IgG titers were measured on day 21. (F) Aurora analysis similar to (C) of lymph nodes of mice from (E). Representative flow plots of CD3+ and CD45+ T cells gated into Tetramer+ populations are shown to the right. (B–F) N = 5, error bars indicate ± SD, and all injections were i.p. (H) FR targeting reduces tumor burden in an EGF7.OVA tumor model. C57BL/6 mice (N = 10) were injected with 2 × 105 EGF7.OVA tumor cells in the left flank subcutaneously (s.c.) on day 1, and tumors were measured 3× per week. On days 7 and 10, mice were injected i.p. with the same R848/OVA formulations from (E). Tumors were tracked until day 30. Significance between groups was determined via area under the curve (AUC) calculation. (G) FRs are important for triggering adaptive immune responses *in vivo*. (Top) Schematic of FR adoptive transfer experiment. BMDCs were incubated 1:1 with MPTLR4 for 30 min, washed, and sorted into FR or non-FR populations. Both hind leg footpads of a C57BL/6 (N = 4) mouse were injected with either 100,000 FRs, 1 million non-FRs, 1 million unsorted MPTLR4-incubated BMDCs, untreated BMDCs, CFA (positive control), or PBS (negative control). All samples except PBS contained OVA (10 μg per footpad). (Bottom) Graph shows anti-OVA IgG titers 14 days post injection. Error bars indicate ± SEM. Significance for (A)–(E) and (G) were determined by two-way ANOVA with Tukey's post test. Statistical significance for (F) of AUC differences in tumor curves was assessed by using one-way ANOVA and Tukey's multiple comparison test. $*p < 0.05$, $**p < 0.01$, $***p < 1 \times 10{-}4$, and NS, not significant.

2.4 Discussion and Conclusion

In this study, we provide evidence of a transcriptionally distinct cellular subpopulation of DCs that could be identified via MP uptake. We present evidence that this DC subpopulation is a manifestation of the literature-defined FR subpopulation. Consistent with literature, we observe FRs having increased TLR response and inflammatory cytokine release and an outsized role in disseminating global APC activation via paracrine signaling. We present evidence that this state is temporally regulated, with cells potentially maintaining a high activation state for a brief period before returning to a non-FR state. This strongly supports our hypothesis that FRs are in fact a stochastic, cyclical state rather than a predetermined substate. We further identify several

proteins that are transcriptionally upregulated during the FR state. We note two, DAP12 and PRG2, that provided an effective targeting method both *in vitro* and *in vivo* to distinguish FR DCs. The FR-targeting strategy showed promise to improve immune responses for *in vivo* vaccination with OVA.

While the improved identification of the FR population could improve both our scientific understanding of how innate immune cells respond to pathogens and a wide range of therapeutic potential for FR targeting, we wish to acknowledge several experimental elements in this study that will require further expansion before the FR state can be fully characterized. Our kinetic analysis of FR activation was limited due to the restriction of FRs in our early experiments requiring uptake of a MP for analysis. While we have identified upregulated surface proteins in our mRNA analysis, our initial isolation protocols were limited by the ligands both for *in vivo* and *in vitro* analyses. Heparin can have varying immunological effects, and, due to its heterogeneous structure and low binding affinity to PRG2, it may have other effects that are difficult to decouple from FR targeting.[44] Furthermore, we do not know the functional importance that PRG2 and DAP12 might have on the FR state. Further research might help identify proteins more directly involved in FR state regulation and control and provide context to previous research on DAP12 and PRG2. For example, DAP12 is associated with natural killer (NK) cells and glial cells and associates with another protein, TREM2, which has recently been implicated as an immune regulator in brain cancer.[45] There may be a connection between TREM2, DAP12, and immune regulation that will require further research. Despite these limitations, we present these data as an important first evaluation and application of FRs so that others might explore their role in innate and adaptive immune function.

While the data are compelling to show that FRs do exist and contribute to immune signaling, there were limitations to our methods. This study focused on mouse cells rather than human, and while we did observe some evidence that FRs exist in humans, this requires further evaluation. We primarily relied upon *in vitro* methods to first detect FRs using MP uptake. We also did not evaluate the spatial locations of FR DCs *in vivo*, which could provide mechanistic insights into FR development. An additional crucial remaining question is why do DCs appear to cycle in activation states? For now, we offer an explanatory conjecture that this cycling may be due to the large metabolic strain placed on DCs during activation, requiring DCs to "share the load".[46,47] DCs release many cytokines by exosomes, which require synthesis of these cytokines prior to activation, in order to have rapid responses to pathogens.[48] We offer a yet untested conjecture that DCs might cycle through this state of increased responsiveness to reduce overall metabolic load on individual cells while relying on the high sensitivity of immune cells to cytokine signaling. This sort of cooperativity has a precedent in other APCs; macrophages exist in at least two distinct metabolic states, M1 and the less active M2, which have been suggested to divide up the metabolic strain between M1 and M2.[49] Furthermore, previous work has shown that DCs that have been previously activated can transmit their activation to naive cells, suggesting a similar paracrine signaling cascade.[50] Another alternative hypothesis is that the heterogeneity of activation responses is a result of local niches within lymphoid organs. Gerner et al. showed that initial DC response to vaccines seemed to be highly dependent upon location within the lymph node sinus. [51] As most experiments in this study were on disassociated cellular suspensions, it is unclear how critical spatial location is for FRs.

While further research is required to confirm these ideas, this work suggests a new insight into DC activation and propagation of immune signals. Identifying and communicating

with FR states has clear implications for therapies where targeted immune activation is desired, including vaccines and immunotherapies. Targeting FRs can potentially help improve therapeutics where innate immune activation is required. Finally, we show the potential for both understanding and improving immune responses by targeting a distinguishable cellular subpopulation from a stochastic distribution. This study shows the importance of stochastic states in immune activation and provides potential for studying stochastic DC responses to stimuli in the context of their physiological niche and in near real time. This could help analyze the role of heterogenous DC populations on overall immune responses.

2.5 Materials and Methods

Cell line:

RAW 264.7 Cells were cultured at 1 million cells per mL in DMEM + Penicillin/Streptomycin+ 10% HIFBS and split every 2–3 days. BMDCs were cultured according to a previously published protocol. Cells were used between 5-7 days after isolation. Splenocytes were cultured in RPMI +10% HIFBS + Penicillin/Streptomycin +2 μM β-mecaptoethanol. Splenocytes used in this study were freshly extracted, allowed to sit for 3 h in media and immediately used.

Animal models:

6 week C57BL/6 female mice were purchased from Jackson Laboratory and housed and treated according to our approved IACUC protocol.

Method details:

Silica-silane coated polystyrene microparticle (MP) synthesis:

PS MPs were synthesized and coated with a silica coating using a procedure from Moser et al.[19] Briefly, uniform, spherical, 2 μm diameter polystyrene microparticles were synthesized via controlled styrene polymerization. 2 g of polyvinylpyrrolidone, MW 40,000 and styrene (20 g), washed with NaOH and dried with MgSO4, was dissolved in EtOH (250 mL) and purged with nitrogen. AIBN (0.2 g) was added, the mixture stirred at 70°C and 200 rpm for 24 h. Mixture was purified by centrifugation (5000 RPM for 5 min, followed by washing 3X in 30 mL of EtOH to remove residual monomer, initiator, and stabilizer). The surfaces of MPs were modified with reactive thiol groups via Pickering emulsion reaction. A mixture of cyclohexane (45 mL), n-hexanol (10.8 mL), endotoxin free water (2 mL) and Triton X-114 (10.8 mL) were placed in a round-bottom flask and sonicated for 20 min. Particles (0.2 g) were added and the suspension was sonicated for 40 min. Tetraethyl-orthosilicate (TEOS) (400 μL) was added dropwise followed by 14 M aqueous ammonia (1.2 mL). The resulting solution was stirred for 30 min RT. Subsequently, 3-Mercaptosilane (200 μL) was added dropwise and stirred for 6 h. TEOS-mercaptosilane copolymer coated particles were then pelleted at 3,400 rpm for 30 min and washed 3× with EtOH. Particles were dried at 70°C and stored at 4°C.

TLR agonist surface functionalization:

Thiol bearing MPs were functionalized with MPLA and Pam_2 using thiol-maleimide chemistry. First MPs (5 mg) were swelled in ACN (500 uL) for 30 mins under sonication, then 1 mg of FITC in 500 uL of ACN was added for a final concentration of 1 mg/mL for 30 mins. MPs were then centrifuged for 1 min (5000 rcf), supernatant removed and washed 3x with PBS. For MPs conjugated with agonists to TLR2, 5, 7 and 9: FITC labeled MPs were dissolved in 500 uL of PBS, then 5 mg of Bismaleimide-PEG_3 was added and allowed to sonicate for 30 min, then washed 3x in PBS. During this LTA, FLA, 2BXY or CpG-SH (0.1 mg/mL) was incubated for

5 mins with Traut's reagent (1 mg/mL) in 500 uL of PBS. After washing, maleimide bearing MPs were incubated with thiol functionalized with either Traut's + LTA, FLA, 2BXY or CpG-SH (500 uL) and sonicated for 30 mins, then washed 10 times, 3x with PBS, 4x with PBS with 0.1 Tween 20, and 3x with PBS. For TLR4 MPs, 1 mg of LPS was dissolved in 400 uL of DMF and 10 ug of p maleimidophenyl isocyanate added and allowed to stir overnight under argon. Then PBS (400 uL) was added followed by 2,2'-(ethylenedioxy)diethanethiol (4 mg) and allowed to stir for 12 h. 100 uL of this mixture was added to the MP with 400 uL of PBS for 30 mins and similarly washed. After conjugation, all MPs were diluted in PBS + 0.05 %wt Tween20 at 20, 50 and 100X and then number of MPs in 10 uL counted using flow cytometry to determine a concentration. MP solutions were diluted to a concentration of 1 million MPs per uL of PBS and stored at 4°C until use.

Particle concentration determination via flow cytometry:

The concentration of particle was determined using flow cytometry (NovoCyte flow cytometer, ACEA Biosciences, Inc). MPs were rehydrated in 500 μL of PBS, then diluted down in PBS +0.01 %wt Tween20 by 50, 100 and 200-fold. 10 μL of these dilutions were analyzed via flow cytometry in triplicate, gating on FITC signal to remove noise. The MP concentration in the stock was then calculated using linear regression from the three dilutions. MP stocks were then diluted down with PBS to a final concentration of 1 million MPs/μL.

Synthesis and purification of DAP12 targeting peptide lipid:

Synthesis was performed using a Liberty Blue™ automated peptide synthesizer. Rink amide resin (100–200 mesh, 0.55 mmol/g, 0.05 mg) was weighed out into a solid-phase peptide synthesizer reaction vessel. The peptide (FVLSKSLFG) was constructed with standard Fmoc

protected peptides (0.2 M in DMF) from the C terminus to the N terminus. Then a Fmoc-EG2-COOH was conjugated followed by three lysines, EG8 linker, a Fmoc-Lys(Fmoc)-OH and palmitic acid. Deprotection was performed using 20% piperidine in DMF. Coupling was performed after activation with diisopropylcarbodiimide (DIC) (0.5 M in DMF) in the presence of ethyl cyanohydroxyiminoacetate (1 M in DMF). All other couplings were done at 90°C for 5 min. All reactions and subsequent washes were performed in DMF. After the synthesis was completed, the resin was transferred into a Bio-Rad Poly-Prep chromatography column.

Global deprotection was achieved by agitating the resin in trifluoroacetic acid (TFA)/3,6-dioxa-1,8-octanedithiol (DODT)/triisopropylsilane (TIPS)/H2O (8.5:0.5:0.5:0.5) for 2 h. The peptide was precipitated by adding the cleavage cocktail filtrate to 30 mL diethyl ether in a 50 mL centrifuge tube pre-cooled to −78°C. The precipitate was collected by centrifuge (4000 xG for 5 min). The precipitate was dissolved in 50% CH_3CN in 0.1%TFA) and filtered through a 0.45 μm syringe filter. Purification was performed using reversed-phase HPLC C8 column (gradient elution with 30–90% CH_3CN/0.1% TFA over 20 min). Pure fractions were pooled and the peptide was recovered through lyophilization and redissolved in MeOH. LC-MS (m/z) 2754.84 [M + H]

Bone marrow derived DCs:

GM-CSF murine bone marrow cells were collected from 6-week-old female C57BL/6 mice. Red blood cells were lysed with RBC Lysis Buffer(BioLegend). BM cells were plated per well in deep petri dishes (VWR) at a concentration of 10^6/mL. Cells were cultured at 37°C and 5% CO2 in culture media: RPMI 1640 (Life Technologies), 10% HIFBS (Gibco), GM-CSF (20 ng/mL; recombinant Mouse GM-CSF (carrier-free) from BioLegend), 2 mM l-glutamine (Life Technologies), 1% antibiotic- antimycotic (Life Technologies). Media was replenished on day 3.

Cells were used on day 5. For FLT-3L matured BMDCs, a similar procedure was used but replacing GM-CSF with 100 ng/mL of FLT-3L.

Splenocyte/Lymph Node/Footpad extraction:

Splenocyte/Lymph Node/Footpad were dissected into 1 mm sized portions and placed in disassociation media (0.5 mg/mL collagenase D, 0.1 mg/mL DNAse I in RPMI) for 30 mins at room temp, then incubated at 37°C for 30 mins, then passed through a 70 um filter. Footpads were incubated for 2 h rather than 30 mins. Splenocytes were treated with RBC lysis buffer (Invitrogen) prior to final wash.

Flow cytometry:

Flow cytometry in this study was performed on a ACEA NovoCyte Flow cytometer (6 channels, 2 laser). 1 million cells per sample were treated with liposomes/MPs/antibodies, washed and placed in HBSS+ 2% HIFBS +0.1 mM EDTA. Samples were gated on FCS and SCC for live and single cells. Samples were compensated based on sample with single stains and calculated using FlowJo.

Aurora spectral flow analysis:

A 5 laser Aurora spectral flow cytometer was used for phenotyping DCs and T cells. Single stained compensation controls were run first and then unmixed using the Aurora spectral flow software. Data was further analyzed in FlowJo.

Cell sorting:

BMDCs, Splenocytes or RAWs were sorted on an Aria Fusion 5–18, AriaIIIu 4–15 or AriaII 4–15 cell sorter. For sorting, cells were sometimes treated with or without Brefeldin A, then

incubated with MPs for 15 mins, washed with ice cold PBS, scrapped, washed again and diluted to 20 million cells per mL in RPMI on ice. Cells were gated on live and single cells by FSC and SCC and sorted into FR (top 5% of FITC signal from MPs) and non-FR (bottom 90% of FITC signal from MPs). Cells were then immediately placed on ice, spun down at 4°C and placed in cell culture media for subsequent experiments. For kinetic experiments, unsorted cell controls were also run through sorter but only gated on live and single cells. All FACS occurred at 4°C.

Cytokine Bead Array:

A Mouse Inflammation CBA kit was purchased from BD Biosciences and used according to the manufacturer's instructions.

First responder cytokine analysis:

BMDCs were incubated at a 1:1 ratio with MP^{TLR} for 15 min and the FRs and non-FRs were isolated via FACS. The cells were washed and resuspended at 1 million cells/mL in culture media (10% HIFBS in RPMI). The cells were incubated at 37°C and 5% CO2 for 1 h. The supernatant was collected and the cytokines were profiled using a mouse inflammation CBA kit (BD Biosciences).

First responder kinetic analysis:

Sorted BMDC FRs or non-FRs cells (BMDCs incubated 1:1 with MP-TLR4 for 15 mins, then sorted) were incubated at 100k cells in 200 uL in cell culture media (10% HIFBS in RPMI) and incubated at 37°C and 5% CO2 for varying time points. Then naïve BMDCs (1 million in 1 mL) were mixed with FRs or non-FRs separated by a 1 um transwell insert or without for 16 hrs. Cell supernatants were tested via CBA for cytokine secretion and cells were tested via flow cytometry

for CD80(PerCP-Cy5.5 rat anti-mouse CD80, 1:100) and CD40 (APC rat anti-mouse CD40, 1:200), incubated for 1 h at 4°C then washed 3X with PBS, then tested via flow cytometry.

First responder ICS analysis:

FRs were analyzed for TNF-α ICS by taking 1 million splenocytes, preincubating them with BrefA for 45 mins and incubating with either MP^{blank} at a 1:1 cell:MP ratio or PBS in splenocyte cell culture media for 15 min, quickly washed and incubated with for varying times with 100 ng/mL R848 or LPS + BrefA. Cells were washed with ice cold staining buffer (2% HIFBS+ 0.2 mM EDTA in PBS), stained for 30 mins on ice for cell surface markers, washed again, and then treated with Cytofix/CytoPerm Kit (BD biosciences) according to manufacturer's instructions to stain for intracellular TNF-α. Cells were analyzed via spectral flow cytometry.

Two color MP uptake FR assay:

Splenocytes were incubated with Cy5 or FITC colored MPs to observe kinetics of FR turnover. Splenocytes were incubated with FITC labeled MP^{TLR4} at a 1:2 ratio of MP:cells for varying times. All samples were then incubated with a Cy5 labeled unconjugated MP for 10 min, immediately washed in ice cold PBS, stained for CD11c and MHCII and fixed in 2% PFA then analyzed via flow cytometry, gated into FITC or Cy5 MP^{hi} or dual MP^{+} uptake (dual MP) populations, see Figure 2.2I for representative gate. Note that the "0" timepoint indicates both colored MPs were simultaneously. Cells were gated on CD11c+ DCs only.

Anti-OVA ELISA:

Mouse anti-OVA IgG were measured using a commercially available kit from Alpha Diagnostic International according to the manufacturer's instructions.

Statistics:

Unless otherwise noted, all statistics were performed using a student's t test with significance $p < 0.05$. For multiple comparisons, a two-way ANOVA was used. All comparisons were performed in Prism GraphPad 7 software. Poisson distribution was used to calculate the standard distribution of discrete particles where Probability of Number of MP uptaken = P, κ = Number of particles uptaken per cell, λ = average number of MPs per cell for each experiment. $P=\lambda\kappa e-\lambda k!$

Human moDC culture:

Frozen PBMC (BuyPBMCs) were purchased commercially and the vial of 10 million cells was warmed at 37°C. Then, PBMCs from the cryo-vial were transferred into the new tube contains warmed media (RPMI 1640). Then the cells were centrifuged at 400xG for 10 min. The supernatant was discarded, resuspended, and centrifuged. $CD14^{+}CD16^{-}$ monocytes were isolated by using the positive selection kit from StemCell Technologies(EasySep™ Human Monocyte Isolation Kit) Isolated Monocytes were resuspended at a density of 1×10^6 cells/mL in culture media (RPMI 1640 containing 10% serum 1% pen/strep 2 mM L-glutamine) supplemented with 500 U/mL IL-4 and 500 U/mL GM-CSF. The cell culture was plated in 6-well tissue culture plates and incubated for 6 days. One day 3, half of fresh media supplemented with cytokines were added.

Microscopy:

BMDCs, Splenocytes, BMDCs or RAWs were analyzed with a SP5 two photon confocal microscope. 100k cells were allowed to attach to the bottom of a 96 well plate in their respective cell culture media. The next day, cells were washed with HBSS then either incubated with DiD containing liposomes for 15 mins, washed and incubated with MPs for 15 mins or incubated with

MPs for 15 mins, washed and then incubated with antibodies. Cells were washed and placed in fluorobrite media (Gibco) with 10% HIFBS +1:2000 dilution of Hoescht 33342 then analyzed by microscopy using relevant wavelengths/filters. Wide field images were taken using 20X lens. Single images were taken using a 60x lens.

Quantification of images were performed in Fuji ImageJ. Wide field images of >100 cells were isolated based on nuclear stain. Gates were drawn on individual cells, FRs identified by cells with top 5% of RFU signal in FITC channel and liposome RFU calculated. Three images each from three separate wells were analyzed for a total of 9 images and >900 total cells.

Synthesis and purification of heparin sulfate lipid:

This procedure was adapted from a paper by Kim et al.rapid[36]300 mg Heparin Sulfate (18 kDa) was dissolved in water (10 mL) and mixed with DPPE (60 mg) dissolved in IPA (10 mL). 138 mg EDC and 69 mg of NHS were added. The mixture was stirred constantly at 65°C for 20 hrs. After reaction, the mixture was evaporated under reduced pressure to remove excess IPA, lyophilized, redissolved in 5 mL of water, filtered and dialyzed against water in a 3500 Da cutoff dialysis cassette for 48 hrs. Then the purified Heparin-lipid was analyzed via LC-MS, confirming between 2-5 conjugation of DPPE per heparin chain, lyophilized again and redissolved at 10 mg/mL in MeOH.

Liposome synthesis:

Liposomes were synthesized via membrane extrusion method using a setup from Avanti polar lipids and 200 nm extrusion filters. DSPC, PEG2000 PE, Cholesterol, and/or DiD, Heparin-lipid, DAP12 peptide lipid and any TLR agonists/ Brefeldin A were combined in 1 mL methanol added, dried via lyophilization, and rehydrated in PBS to make a 10 mM total lipid, 200 uL

solutions. OVA was added during rehydration. Solutions were gently rotated at 67°C and passed through a 70°C 200 nm filter 5 times. The liposome solution was dialyzed against PBS with a 3,500 Da filter for 24 hrs.

LC-MS analysis of liposome loading:

Liposomes loaded with DiD, DAP12 peptide, Heparin, brefeldin A, CpG, R848, OVA or any combinations of these were tested for loading via LC-MS analysis. Stock solutions of liposomes were diluted down to 1 mM total lipid and then 5 uL of this solution was injected on a C8 analytical HPLC column with a gradient of 10–90% ACN in 20 mins and the effluent observed by an Agilent 6135BAR LCMS XT mass spectrometer and a diode array detector at 220 nm. Signal from various compounds in liposome formulations were compared to standard curves at 220 nm.

Dynamic light scattering analysis of liposomes:

Hydrodynamic diameter of liposomes was confirmed using a Wyatt Möbius DLS/ELS at 100 uM total liposome concentration.

SEM of functionalized particles:

Scanning electron microscopy (SEM) and energy-dispersive spectroscopy (EDS) of the particles was performed using an FEI Quanta 3D FEG dual beam (SEM/FIB) equipped with Inca EDS (Oxford Instruments). High-resolution images were taken with an FEI Magellan 400 XHR SEM particle samples were dried under vacuum for 24 h, mounted on carbon tape, and sputter coated (South Bay Technologies) with approximately 2–4 nm of Au/Pd 60:40 or Ir.

RAW blue NF-κB assay:

RAW-Blue NF-κB cells (Invivogen) were passaged and plated in a 96 well plate at 100k cells/well in 180 µL DMEM containing 10% HIFBS. Cells were incubated at 37°C and 5% CO_2 for 24 h. 100 ul of cells were incubated with varying ratios of MPs at 37°C and 5% CO2 for 18 h. After 18 h, 20 µL of the cell supernatant was placed in 180 µL freshly prepared QuantiBlue (Invivogen) solution and incubated at 37°C/5% CO2 for up to 2 h. The plate was analyzed every hour using a Multiskan FC plate reader (Thermo Scientific) and absorbance was measured at 620 nm *BCA Assay*- This was performed according to manufacturer's instruction (Thermo Fischer) with some modifications. 100 million beads were incubated with BCA solution and reacted for 30 mins at 60°C then analyzed every hour using a Multiskan FC plate reader (Thermo Scientific) and absorbance was measured at 562 nm and compared to a standard curve of modified MPLA or Pam_2 after subtracting a background of maleimide modified MP.

Image stream MP uptake analysis for TNF-α expression:

1 million BMDCs, RAWs or Splenocytes were incubated with 1 million MPs in 1 mL of cell culture media (DMEM supplanted with 10% HIFBS) for 1 hour. After 1 h, protein export was inhibited using a GolgiPlug Kit (BD Biosciences) with Brefeldin A according to manufacturer's instructions for 16 h at 37°C under 5% CO_2. Cells were then washed and fixed and permeabilized with a BD Cytofix/Cytoperm Plus Kit (BD Biosciences). Cells were stained with a solution of anti- TNF-α (1:500 dilution) and their nuclei stained using Hoechst Solution (2 µM final concentration) in permeabilization buffer for 1 hr. Cells were washed 3x in PBS with 2% HIFBS, concentrated into a 20 µL volume and analyzed with ImageStream Flow Cytometry. Each MP condition was performed in triplicate, analyzing >100,000 cells per run. MPs were identified using the "Particle Count" wizard in the IDEAS software and compared to TNF-α intensity per cell.

Image stream MP uptake analysis for NF-κB expression:

1 million BMDCs, RAWs or Splenocytes were incubated with 1 million MPs in 1 mL of cell culture media (DMEM supplanted with 10% HIFBS) for 15 min. Immediately cells were fixed using ice cold Cytofixation Buffer (BD Biosciences) for 15 min. Cells were then fixed in PBS +0.04% triton X for 3 min, immediately spun down (400 RCF, 5 min), supernatant removed and washed with CytoPerm Buffer (BD Biosciences) 2 times (200 µL per wash). Cells were then stained with Rabbit anti-NF-κB p65 (1:500 dilution) for 1 h on ice, washed 3x, then stained with a secondary goat anti-rabbit AF647 (1:1000 dilution) for 1 h on ice, washed, concentrated into a 20 µL volume of PBS with 2% HIFBS and analyzed with ImageStream flow cytometry. Each MP condition was performed in triplicate, analyzing >100,000 cells per run. MPs were identified using the "Particle Count" wizard in the IDEAS software and compared to NF-κB nuclear colocalization using the "Colocalization" wizard in the IDEAS software.

Imagestream data analysis:

ImageStream data was analyzed in the IDEAS software (Amnis) for nuclear colocalization and particle counting using built-in analysis wizards. Single cell data was then exported into Graphpad Prism 6 software for further analysis. Cell data was divided into the following categories: 0 MP, 1 MP, 2 MP, 3 MP, 4 MP or 5 MP or >5 MPs. "Simulated Distributions" were calculated by using the Poisson distribution and the average MP uptake from the triplicate BMDC uptake experiments to determine the breakdown of cells with 0,1,2,3…etc. MPs. The number of cells in each category was rounded to the nearest whole number and assumed that the cells in the 95th percentile for number of MP uptake matched the "FR" population. The total number of MPs from this population was calculated and compared to the total number of MPs uptaken by the cell population.

Adoptive transfer of BMDCs:

FRs and non-FRs treated with MP-TLR4 like previous section were treated with DiL dye (1 ug/mL) and OVA (100 ug/mL) in 1 million cells in 1 mL cell culture media for 30 mins. Treated cells were then washed with PBS then concentrated at 1 million cells into 30 uL of HBSS and then immediately injected into C57BL/6 mouse footpads, one injection per footpad, two per mouse. 1 h post injection, blood was taken for CBA analysis. 14 days later, mice were sacrificed, popliteal lymph nodes from both sides of the mouse were removed, disaggregated, stained and analyzed via Aurora spectral flow analysis. 4 mice were treated per group: (1) mice injected with untreated BMDCs (2) mice injected with BMDCs treated with 5 uL CFA+100 ug OVA, (3) mice injected with unsorted BMDCs treated with MP^{blank} (4) mice injected with unsorted BMDCs treated with MP^{TLR4} (5) mice injected with FR sorted BMDCs treated with MP^{TLR4} and (6) mice injected with non-FRs sorted BMDCs treated with MP^{TLR4}.

mRNA whole transcriptome analysis:

For 16 h sequencing: BMDCs were incubated at a 1:1 ratio with MP^{TLR-X} (x = blank, 2, 4, 5, 7, 9) for 16 h. The FRs and non-FRs were isolated via FACS. RNA was extracted using a Direct-zol RNA-Microprep kit (Zymo), prepped using SMARTer® Stranded Total RNA-Seq Kit v2 (Takara), and sequenced on a NextSeq550 (Illumina). RNA-Seq reads were mapped to GRCm38 mouse reference genome using STAR version 2.7.0b.[52] The resulting files from the alignment step above were taken to evaluate transcriptional expression using subread::featureCounts with gencode transcript annotation M19.[53] The obtained count table was normalized and log fold change in expression was generated using the edgeR package.[54] Using the Cell Surface Protein Atlas's database for mouse cell surface protein, we identified proteins that were most frequently upregulated in the most MP^{TLR-X} dosing conditions that met both the following criteria: 2-fold

upregulation and pval <.05.[55] For time series sequencing: BMDCs were incubated at 1:1 ratio with MP^{TLR-4} for 15 min. The FRs and non-FRs were isolated via FACS, washed, and resuspended in media. At 0, 0.5, 1, 2, 4 h, the RNA was extracted using a Direct-zol RNA-Microprep kit (Zymo). Sequencing was performed by the University of Chicago Genomics Core, and BasePairTech's DESEQ2 pipeline was used to align the reads to the mm10 genome, and compute the differential expression and Gene Set Enrichment Analysis. Using the Mouse Genomic Informatics database to acquire lists of genes with 1) immune function 2) antigen presentation the immune response of the FRs and non-FRs were profiled by analyzing the differential expression, using only genes with 2-fold differential expression change and pval < .05 for at least one of the timepoints.[56]

Brefeldin A *In vivo* experiment:

6 week, C57BL/6 female mice, 5 mice per experimental group were injected with liposomes containing Brefeldin A (BrefA) or free BrefA or PBS control. Mice were injected with 100 ug of Brefeldin A (either free or loaded equivalent) i.p. and then 1 h later mice were injected i.p. with 10 ug R848 and 100 ug OVA in PBS. 14 days later this injection procedure was repeated. On day 21, mice were sac'd, blood tested for anti-OVA IgG and lymph and spleen analyzed. Groups: (1) PBS injected mice only (2) No BrefA- mice injected with PBS in lieu of brefeldin A and then injected 1 h later with R848/OVA. (3) Free BrefA- Mice injected with 100 ug of Free Brefeldin A then 1 h later R848/OVA (4) BrefA NTL- mice injected with brefeldin A loaded into a blank non-targeted 200 nm liposome and injected with a 100 ug brefeldin A equivalent dose then injected with R848/OVA 1 h later. (5) BrefA FR-TL- same are previous group but with FR targeting elements.

CpG loaded liposome *in vivo* experiment:

6 week, C57BL/6 female mice, 5 mice per experimental group were injected with liposomes containing CpG or free CpG or PBS control. Mice were injected with 10 ug of CpG (either free or loaded equivalent) with 100 ug OVA i.p. On day 14, mice were sac'd, blood tested for anti-OVA IgG and lymph and spleen analyzed.

R848 loaded liposome *in vivo* experiment:

6 week, C57BL/6 female mice, 5 mice per experimental group were injected with liposomes containing R848 or free R848 or PBS control. Mice were injected with 10 ug of R848 (either free or loaded equivalent) with 100 ug OVA i.p. On day 14, this procedure was repeated. On day 21, mice were sacrificed, blood tested for anti-OVA IgG and lymph and spleen analyzed.

Intracellular Staining (ICS):

Fresh suspensions of mouse splenocytes were incubated with OVA peptides for 30 min in ICS media (RPMI, 10% FBS, Penicillin/Streptomycin, 1x Non-Essential Amino Acids, 1 um β-mercaptoethanol, 1 mM HEPES and 1 mM sodium pyruvate. Then splenocytes were incubated for 12 h with monensin (1 ug/mL), washed, fixed and stained for intracellular and extracellular antigens (CD4, CD8, INF-γ and IL-4) according to the manufacture's instruction for BD Cytofix/Cytoperm Kit.

E.G7 OVA Tumor Model:

C57BL/6 female mice were injected with 5×10^5 E.G7 OVA expressing cells in PBS in the left flank. Mice were shaved to observe tumor growth. On day 7 and day 10, mice were injected with liposome formulation or free R848/OVA (10 ug/100 ug per mouse) i.p. Tumor volume was tracked via calipers 3 times per week and volume calculated by the formula Volume= (1/2) (length*(width)^2).[57]

Quantification and statistical analysis:

Statistical details of experiments, number of repeats performed, and statistical tests used can be found in the figure legends. All statistics were calculated using GraphPad Prism v9. Normally distributed samples were compared using ANOVA for multiple comparison and Student t-tests for two independent samples. For nonparametrically distributed samples ANOVA Mann-Whitney U-Test for two independent samples or Wilcoxon test for dependent samples. Kaplan-Meier curves for the survival function were compared via log rank test. $p < 0.05$ was considered significant.

2.6 References

(1) Reiner, S. L.; Adams, W. C. Lymphocyte Fate Specification as a Deterministic but Highly Plastic Process. *Nat. Rev. Immunol.* **2014**, *14* (10), 699–704. https://doi.org/10.1038/nri3734.

(2) Lafouresse, F.; Jugele, R.; Müller, S.; Doineau, M.; Duplan-Eche, V.; Espinosa, E.; Puisségur, M.-P.; Gadat, S.; Valitutti, S. Stochastic Asymmetric Repartition of Lytic Machinery in Dividing CD8+ T Cells Generates Heterogeneous Killing Behavior. *eLife* **2021**, *10*, e62691. https://doi.org/10.7554/eLife.62691.

(3) Long, M.; Adler, A. J. Cutting Edge: Paracrine, but Not Autocrine, IL-2 Signaling Is Sustained during Early Antiviral CD4 T Cell Response. *J. Immunol. Baltim. Md 1950* **2006**, *177* (7), 4257–4261.

(4) Filep, J. G.; Ariel, A. Neutrophil Heterogeneity and Fate in Inflamed Tissues: Implications for the Resolution of Inflammation. *Am. J. Physiol.-Cell Physiol.* **2020**, *319* (3), C510–C532. https://doi.org/10.1152/ajpcell.00181.2020.

(5) *Analysis of single-cell cytokine secretion reveals a role for paracrine signaling in coordinating macrophage responses to TLR4 stimulation | Science Signaling*. https://www.science.org/doi/10.1126/scisignal.aaa2155 (accessed 2022-12-08).

(6) Shalek, A. K.; Satija, R.; Shuga, J.; Trombetta, J. J.; Gennert, D.; Lu, D.; Chen, P.; Gertner, R. S.; Gaublomme, J. T.; Yosef, N.; Schwartz, S.; Fowler, B.; Weaver, S.; Wang, J.; Wang, X.; Ding, R.; Raychowdhury, R.; Friedman, N.; Hacohen, N.; Park, H.; May, A. P.; Regev, A. Single-Cell RNA-Seq Reveals Dynamic Paracrine Control of Cellular Variation. *Nature* **2014**, *510* (7505), 363–369. https://doi.org/10.1038/nature13437.

(7) Van Eyndhoven, L. C.; Singh, A.; Tel, J. Decoding the Dynamics of Multilayered Stochastic Antiviral IFN-I Responses. *Trends Immunol.* **2021**, *42* (9), 824–839. https://doi.org/10.1016/j.it.2021.07.004.

(8) Banchereau, J.; Steinman, R. M. Dendritic Cells and the Control of Immunity. *Nature* **1998**, *392* (6673), 245–252. https://doi.org/10.1038/32588.

(9) Collin, M.; Bigley, V. Human Dendritic Cell Subsets: An Update. *Immunology* **2018**, *154* (1), 3–20. https://doi.org/10.1111/imm.12888.

(10) *Frontiers | Dendritic Cell-Targeted Vaccines*. https://www.frontiersin.org/articles/10.3389/fimmu.2014.00255/full (accessed 2022-12-08).

(11) Villar, J.; Segura, E. Decoding the Heterogeneity of Human Dendritic Cell Subsets. *Trends Immunol.* **2020**, *41* (12), 1062–1071. https://doi.org/10.1016/j.it.2020.10.002.

(12) Rodda, L. B.; Lu, E.; Bennett, M. L.; Sokol, C. L.; Wang, X.; Luther, S. A.; Barres, B. A.; Luster, A. D.; Ye, C. J.; Cyster, J. G. Single-Cell RNA Sequencing of Lymph Node Stromal

Cells Reveals Niche-Associated Heterogeneity. *Immunity* **2018**, *48* (5), 1014-1028.e6. https://doi.org/10.1016/j.immuni.2018.04.006.

(13) Leal, J. M.; Huang, J. Y.; Kohli, K.; Stoltzfus, C.; Lyons-Cohen, M. R.; Olin, B. E.; Gale, M.; Gerner, M. Y. Innate Cell Microenvironments in Lymph Nodes Shape the Generation of T Cell Responses during Type I Inflammation. *Sci. Immunol.* **2021**, *6* (56), eabb9435. https://doi.org/10.1126/sciimmunol.abb9435.

(14) *Dendritic cell chemotaxis in 3D under defined chemokine gradients reveals differential response to ligands CCL21 and CCL19 | PNAS.* https://www.pnas.org/doi/full/10.1073/pnas.1014920108 (accessed 2022-12-08).

(15) Brown, C. C.; Gudjonson, H.; Pritykin, Y.; Deep, D.; Lavallée, V.-P.; Mendoza, A.; Fromme, R.; Mazutis, L.; Ariyan, C.; Leslie, C.; Pe'er, D.; Rudensky, A. Y. Transcriptional Basis of Mouse and Human Dendritic Cell Heterogeneity. *Cell* **2019**, *179* (4), 846-863.e24. https://doi.org/10.1016/j.cell.2019.09.035.

(16) *Single-cell analysis shows that paracrine signaling by first responder cells shapes the interferon-β response to viral infection | Science Signaling*. https://www.science.org/doi/10.1126/scisignal.2005728 (accessed 2022-12-08).

(17) Wimmers, F.; Subedi, N.; van Buuringen, N.; Heister, D.; Vivié, J.; Beeren-Reinieren, I.; Woestenenk, R.; Dolstra, H.; Piruska, A.; Jacobs, J. F. M.; van Oudenaarden, A.; Figdor, C. G.; Huck, W. T. S.; de Vries, I. J. M.; Tel, J. Single-Cell Analysis Reveals That Stochasticity and Paracrine Signaling Control Interferon-Alpha Production by Plasmacytoid Dendritic Cells. *Nat. Commun.* **2018**, *9* (1), 3317. https://doi.org/10.1038/s41467-018-05784-3.

(18) Baranov, M. V.; Kumar, M.; Sacanna, S.; Thutupalli, S.; van den Bogaart, G. Modulation of Immune Responses by Particle Size and Shape. *Front. Immunol.* **2021**, *11*.

(19) Moser, B. A.; Steinhardt, R. C.; Esser-Kahn, A. P. Surface Coating of Nanoparticles Reduces Background Inflammatory Activity While Increasing Particle Uptake and Delivery. *ACS Biomater. Sci. Eng.* **2017**, *3* (2), 206–213. https://doi.org/10.1021/acsbiomaterials.6b00473.

(20) Yi, H.-J.; Lu, G.-X. Adherent and Non-Adherent Dendritic Cells Are Equivalently Qualified in GM-CSF, IL-4 and TNF-α Culture System. *Cell. Immunol.* **2012**, *277* (1), 44–48. https://doi.org/10.1016/j.cellimm.2012.05.014.

(21) Meraz, I. M.; Melendez, B.; Gu, J.; Wong, S. T. C.; Liu, X.; Andersson, H. A.; Serda, R. E. Activation of the Inflammasome and Enhanced Migration of Microparticle-Stimulated Dendritic Cells to the Draining Lymph Node. *Mol. Pharm.* **2012**, *9* (7), 2049–2062. https://doi.org/10.1021/mp3001292.

(22) Helft, J.; Böttcher, J.; Chakravarty, P.; Zelenay, S.; Huotari, J.; Schraml, B. U.; Goubau, D.; Reis e Sousa, C. GM-CSF Mouse Bone Marrow Cultures Comprise a Heterogeneous Population of CD11c+MHCII+ Macrophages and Dendritic Cells. *Immunity* **2015**, *42* (6), 1197–1211. https://doi.org/10.1016/j.immuni.2015.05.018.

(23) Brasel, K.; De Smedt, T.; Smith, J. L.; Maliszewski, C. R. Generation of Murine Dendritic Cells from Flt3-Ligand–Supplemented Bone Marrow Cultures. *Blood* **2000**, *96* (9), 3029–3039. https://doi.org/10.1182/blood.V96.9.3029.

(24) Clatworthy, M. R.; Aronin, C. E. P.; Mathews, R. J.; Morgan, N. Y.; Smith, K. G. C.; Germain, R. N. Immune Complexes Stimulate CCR7-Dependent Dendritic Cell Migration to Lymph Nodes. *Nat. Med.* **2014**, *20* (12), 1458–1463. https://doi.org/10.1038/nm.3709.

(25) Hochrein, H.; O'Keeffe, M. Dendritic Cell Subsets and Toll-Like Receptors. In *Toll-Like Receptors (TLRs) and Innate Immunity*; Bauer, S., Hartmann, G., Eds.; Handbook of Experimental Pharmacology; Springer: Berlin, Heidelberg, 2008; pp 153–179. https://doi.org/10.1007/978-3-540-72167-3_8.

(26) Elgueta, R.; Benson, M. J.; De Vries, V. C.; Wasiuk, A.; Guo, Y.; Noelle, R. J. Molecular Mechanism and Function of CD40/CD40L Engagement in the Immune System. *Immunol. Rev.* **2009**, *229* (1), 152–172. https://doi.org/10.1111/j.1600-065X.2009.00782.x.

(27) Barchet, W.; Cella, M.; Odermatt, B.; Asselin-Paturel, C.; Colonna, M.; Kalinke, U. Virus-Induced Interferon α Production by a Dendritic Cell Subset in the Absence of Feedback Signaling In Vivo. *J. Exp. Med.* **2002**, *195* (4), 507–516. https://doi.org/10.1084/jem.20011666.

(28) Honda, K.; Taniguchi, T. IRFs: Master Regulators of Signalling by Toll-like Receptors and Cytosolic Pattern-Recognition Receptors. *Nat. Rev. Immunol.* **2006**, *6* (9), 644–658. https://doi.org/10.1038/nri1900.

(29) Krausgruber, T.; Saliba, D.; Ryzhakov, G.; Lanfrancotti, A.; Blazek, K.; Udalova, I. A. IRF5 Is Required for Late-Phase TNF Secretion by Human Dendritic Cells. *Blood* **2010**, *115* (22), 4421–4430. https://doi.org/10.1182/blood-2010-01-263020.

(30) Kui, L.; Chan, G. C.; Lee, P. P. W. TSG-6 Downregulates IFN-Alpha and TNF-Alpha Expression by Suppressing IRF7 Phosphorylation in Human Plasmacytoid Dendritic Cells. *Mediators Inflamm.* **2017**, *2017*, e7462945. https://doi.org/10.1155/2017/7462945.

(31) *A Dap12-Mediated Pathway Regulates Expression of Cc Chemokine Receptor 7 and Maturation of Human Dendritic Cells | Journal of Experimental Medicine | Rockefeller*

University Press. https://rupress.org/jem/article/194/8/1111/115/A-Dap12-Mediated-Pathway-Regulates-Expression-of (accessed 2023-01-05).

(32) *TMEM176A and TMEM176B Are Candidate Regulators of Inhibition of Dendritic Cell Maturation and Function after Chronic Spinal Cord Injury | Journal of Neurotrauma*. https://www.liebertpub.com/doi/10.1089/neu.2019.6498 (accessed 2023-01-05).

(33) Ogasawara, H.; Furuno, M.; Edamura, K.; Noguchi, M. Peptides of Major Basic Protein and Eosinophil Cationic Protein Activate Human Mast Cells. *Biochem. Biophys. Rep.* **2020**, *21*, 100719. https://doi.org/10.1016/j.bbrep.2019.100719.

(34) Shen, Z. T.; Sigalov, A. B. Rationally Designed Ligand-Independent Peptide Inhibitors of TREM-1 Ameliorate Collagen-Induced Arthritis. *J. Cell. Mol. Med.* **2017**, *21* (10), 2524–2534. https://doi.org/10.1111/jcmm.13173.

(35) Weiler, J. M.; Gleich, G. J. Eosinophil Granule Major Basic Protein Regulates Generation of Classical and Alternative-Amplification Pathway C3 Convertases in Vitro. *J. Immunol. Baltim. Md 1950* **1988**, *140* (5), 1605–1610.

(36) *Rapid and Versatile Cell Aggregate Formation Using Lipid-Conjugated Heparin | ACS Applied Materials & Interfaces*. https://pubs.acs.org/doi/full/10.1021/acsami.8b07731 (accessed 2022-12-08).

(37) Castell-Rodríguez, A.; Piñón-Zárate, G.; Herrera-Enríquez, M.; Jarquín-Yáñez, K.; Medina-Solares, I.; Castell-Rodríguez, A.; Piñón-Zárate, G.; Herrera-Enríquez, M.; Jarquín-Yáñez, K.; Medina-Solares, I. *Dendritic Cells: Location, Function, and Clinical Implications*; IntechOpen, 2017. https://doi.org/10.5772/intechopen.68352.

(38) Feng, J.; Iyer, A.; Seo, Y.; Broaddus, C.; Liu, B.; VanBrocklin, H.; He, J. Effects of Size and Targeting Ligand on Biodistribution of Liposome Nanoparticles in Tumor Mice. *J. Nucl. Med.* **2013**, *54* (supplement 2), 1339–1339.

(39) *Cutting Edge: Re-evaluating the In Vivo Cytokine Responses of CD8+ T Cells during Primary and Secondary Viral Infections1 | The Journal of Immunology | American Association of Immunologists*. https://journals.aai.org/jimmunol/article/174/10/5936/36586/Cutting-Edge-Re-evaluating-the-In-Vivo-Cytokine (accessed 2023-01-05).

(40) Wohn, C.; Ober-Blöbaum, J. L.; Haak, S.; Pantelyushin, S.; Cheong, C.; Zahner, S. P.; Onderwater, S.; Kant, M.; Weighardt, H.; Holzmann, B.; Reizis, B.; Becher, B.; Prens, E. P.; Clausen, B. E. Langerinneg Conventional Dendritic Cells Produce IL-23 to Drive Psoriatic Plaque Formation in Mice. *Proc. Natl. Acad. Sci.* **2013**, *110* (26), 10723–10728. https://doi.org/10.1073/pnas.1307569110.

(41) *Sterically Stabilized Cationic Liposomes Improve the Uptake and Immunostimulatory Activity of CpG Oligonucleotides1 | The Journal of Immunology | American Association of Immunologists*. https://journals.aai.org/jimmunol/article/167/6/3324/34030/Sterically-Stabilized-Cationic-Liposomes-Improve (accessed 2023-01-05).

(42) Rodell, C. B.; Arlauckas, S. P.; Cuccarese, M. F.; Garris, C. S.; Li, R.; Ahmed, M. S.; Kohler, R. H.; Pittet, M. J.; Weissleder, R. TLR7/8-Agonist-Loaded Nanoparticles Promote the Polarization of Tumour-Associated Macrophages to Enhance Cancer Immunotherapy. *Nat. Biomed. Eng.* **2018**, *2* (8), 578–588. https://doi.org/10.1038/s41551-018-0236-8.

(43) Predina, J.; Eruslanov, E.; Judy, B.; Kapoor, V.; Cheng, G.; Wang, L.-C.; Sun, J.; Moon, E. K.; Fridlender, Z. G.; Albelda, S.; Singhal, S. Changes in the Local Tumor Microenvironment

in Recurrent Cancers May Explain the Failure of Vaccines after Surgery. *Proc. Natl. Acad. Sci.* **2013**, *110* (5), E415–E424. https://doi.org/10.1073/pnas.1211850110.

(44) Korhan, P.; Yılmaz, Y.; Bağırsakçı, E.; Güneş, A.; Topel, H.; Carr, B. I.; Atabey, N. Pleiotropic Effects of Heparins: From Clinical Applications to Molecular Mechanisms in Hepatocellular Carcinoma. *Can. J. Gastroenterol. Hepatol.* **2018**, *2018*, e7568742. https://doi.org/10.1155/2018/7568742.

(45) Molgora, M.; Esaulova, E.; Vermi, W.; Hou, J.; Chen, Y.; Luo, J.; Brioschi, S.; Bugatti, M.; Omodei, A. S.; Ricci, B.; Fronick, C.; Panda, S. K.; Takeuchi, Y.; Gubin, M. M.; Faccio, R.; Cella, M.; Gilfillan, S.; Unanue, E. R.; Artyomov, M. N.; Schreiber, R. D.; Colonna, M. TREM2 Modulation Remodels the Tumor Myeloid Landscape Enhancing Anti-PD-1 Immunotherapy. *Cell* **2020**, *182* (4), 886-900.e17. https://doi.org/10.1016/j.cell.2020.07.013.

(46) *Dendritic cell metabolism | Nature Reviews Immunology*. https://www.nature.com/articles/nri3771 (accessed 2023-01-05).

(47) Wculek, S. K.; Khouili, S. C.; Priego, E.; Heras-Murillo, I.; Sancho, D. Metabolic Control of Dendritic Cell Functions: Digesting Information. *Front. Immunol.* **2019**, *10*.

(48) Obregon, C.; Rothen-Rutishauser, B.; Gerber, P.; Gehr, P.; Nicod, L. P. Active Uptake of Dendritic Cell-Derived Exovesicles by Epithelial Cells Induces the Release of Inflammatory Mediators through a TNF-α-Mediated Pathway. *Am. J. Pathol.* **2009**, *175* (2), 696–705. https://doi.org/10.2353/ajpath.2009.080716.

(49) Pearce, E. L.; Pearce, E. J. Metabolic Pathways in Immune Cell Activation and Quiescence. *Immunity* **2013**, *38* (4), 633–643. https://doi.org/10.1016/j.immuni.2013.04.005.

(50) Johansson, U.; Walther-Jallow, L.; Smed-Sörensen, A.; Spetz, A.-L. Triggering of Dendritic Cell Responses after Exposure to Activated, but Not Resting, Apoptotic PBMCs1. *J. Immunol.* **2007**, *179* (3), 1711–1720. https://doi.org/10.4049/jimmunol.179.3.1711.

(51) Thomson, M.; Tringali, A.; Dumonceau, J.-M.; Tavares, M.; Tabbers, M. M.; Furlano, R.; Spaander, M.; Hassan, C.; Tzvinikos, C.; Ijsselstijn, H.; Viala, J.; Dall'Oglio, L.; Benninga, M.; Orel, R.; Vandenplas, Y.; Keil, R.; Romano, C.; Brownstone, E.; Hlava, Š.; Gerner, P.; Dolak, W.; Landi, R.; Huber, W. D.; Everett, S.; Vecsei, A.; Aabakken, L.; Amil-Dias, J.; Zambelli, A. Paediatric Gastrointestinal Endoscopy: European Society for Paediatric Gastroenterology Hepatology and Nutrition and European Society of Gastrointestinal Endoscopy Guidelines. *J. Pediatr. Gastroenterol. Nutr.* **2017**, *64* (1), 133. https://doi.org/10.1097/MPG.0000000000001408.

(52) Dobin, A.; Davis, C.A.; Schlesinger, F.; Drenkow, J.; Zaleski, C.; Jha, S.; Batut, P.; Chaisson, M.; Gingeras, T. R. STAR: Ultrafast Universal RNA-Seq Aligner, Bioinformatics, 29, 1, (2013), 15–21, Https://Doi.Org/10.1093/Bioinformatics/Bts635.

(53) Liao, Y.; Smyth, G. K.; Shi, W. The Subread Aligner: Fast, Accurate and Scalable Read Mapping by Seed-and-Vote. *Nucleic Acids Res.* **2013**, *41* (10), e108. https://doi.org/10.1093/nar/gkt214.

(54) Robinson, M. D.; McCarthy, D. J.; Smyth, G. K. EdgeR: A Bioconductor Package for Differential Expression Analysis of Digital Gene Expression Data. *Bioinformatics* **2010**, *26* (1), 139–140. https://doi.org/10.1093/bioinformatics/btp616.

(55) Bausch-Fluck D, Hofmann A, Bock T, Frei AP, Cerciello F, et al. A Mass Spectrometric-Derived Cell Surface Protein Atlas. *PLoS* **2015**, No. One 10: e0121314.

(56) Bult, C. J.; Blake, J. A.; Smith, C. L.; Kadin, J. A.; Richardson, J. E.; the Mouse Genome Database Group. Mouse Genome Database (MGD) 2019. *Nucleic Acids Res.* **2019**, *47* (D1), D801–D806. https://doi.org/10.1093/nar/gky1056.

(57) Jensen, M. M.; Jørgensen, J. T.; Binderup, T.; Kjær, A. Tumor Volume in Subcutaneous Mouse Xenografts Measured by MicroCT Is More Accurate and Reproducible than Determined by 18F-FDG-MicroPET or External Caliper. *BMC Med. Imaging* **2008**, *8* (1), 16. https://doi.org/10.1186/1471-2342-8-16.

Chapter 3: Characterizing the FR Response to Synergistic TLR Activation

3.1 Summary

Vaccines have been the most impactful public health innovation in history, helping to eradicate numerous diseases, such as diphtheria and polio. The most successful vaccines rely on synergistic immune responses to elicit a robust, long-term protective response. First Responding dendritic cells (FRs) have powerful cytokine responses to TLR signaling. We demonstrate that we can enhance the FR cytokine response for TNF-α, IL-6, and IL12-p70 after synergistic stimulation with a MP-TLR4_7 microparticle. Additionally, we reduce bulk population cytokines using a brefeldin loaded liposome that selectively targets FRs, ablating their signaling function. We would like to improve this brefeldin-liposome targeting system, so it can be used *in vivo* to remove inflammatory side effects of vaccines while maintaining a strong antibody response. Lastly, we sequenced the transcriptional profile of FRs 16 h after MP-TLR4_7 stimulation and observed synergistic upregulation of multiple cell adhesion genes, indicating that the FRs increase their antigen presentation after this synergistic stimulation – a key step in generating antibody specific responses. These results will improve vaccine development by enhancing immune signals produced by cells that already have robust inflammation signaling capabilities.

3.2 Introduction

Vaccines have been the most impactful public health innovation in history, helping to eradicate numerous diseases, such as diphtheria and polio, and reducing infection for many other diseases. One of the best vaccines ever developed is the yellow fever vaccine. The yellow fever

vaccine is lauded as such an effective vaccine, because with just one dose, it protects an individual against yellow fever for life with minimal side effects.[1] The yellow fever vaccine is so effective, because it activates numerous pattern recognition receptors (PRRs), such as TLR2, TLR7, TLR9, etc. in a synergistic manner, resulting in a balanced Th1/Th2 response and strong antibody production.[2,3] As a result, researchers are interested in understanding synergies in the immune system to confer stronger protection with vaccines

To study immune synergies, researchers have used multiple pathogen-associated molecular patterns (PAMPs) to elicit stronger immune responses. From these studies, we have learned that combinatorial activation of two TLRs can result in a synergy. When properly activated, some of the TLR combinations that result in synergy are TLR4/7, TLR2/9, and TLR2/4.[4,5,6] Chemical conjugation of synergistic agonists or attachment of such agonists to a nanoparticle have further increased responses, as the spatial linking of the agonists more closely resembles the spatial orientation of these PAMPs in a pathogen.[7,8,9,10,11,12] Our lab has developed a microparticle that is not only the size and surface charge of a pathogen, but also has reactive handles by which PAMPs can be attached.[13] By using this microparticle, we can isolate first-responding dendritic cells.[14] We hypothesized that by attaching synergistic TLR agonists to this pathogen mimetic particle combinations, we can improve immune responses.

Dendritic cells (DCs), named for the dendrites that extend from the cell, are key immune cells, as they link the innate and adaptive immune system. They have an important role in recognizing PAMPs, presenting antigen, via MHCs and facilitating adaptive immune responses.[15] Dendritic cells are broken down into four main subsets based on transcriptional and surface markers: plasmacytoid DCs (pDC), type 1 classical DCs (cDC1), type 2 classical DCs (cDC2), and monocyte-derived DCs (mo-DCs), with each subset having a nuanced integral role

in the immune system.[16] Even within subsets, DC populations have heterogeneous responses to immune stimulation. For example, in bone marrow derived DCs, a stochastically arising and small population of high IFN-β secreting cells was observed; and in pDCs, a similar stochastic response for IFN-α release was identified via single-cell mRNA sequencing.[17,18] These studies suggest that DCs exist in a range of phenotypes and functionalities that is not captured by the subclasses of DCs. More importantly, it seems that a small percent of DCs have strong cytokine responses to initial immune stimulation. We hypothesize that by targeting these hyper-active cells with synergistic stimulation, we can enhance the overall immune response to vaccines using this microparticle formulation.

In this chapter, we present 1) that synergistic microparticle (MP) stimulation of FRs results in increased cytokine expression *in vitro*, 2) that ablating FR signaling reduces overall cytokine production *in vitro* and 3) that MP-TLR4_7 stimulation synergistically increases intercellular adhesion genes in FRs. Using this knowledge, we hope to engineer vaccines that can leverage the signaling of FRs to maximize antibody responses, as well as honing our ability to reduce inflammatory side effects of vaccines without altering their efficacy.

3.3 Results and Discussion

3.3.1 FRs have synergistic response to MP-TLR4_7 system *in vitro*

Since FRs release strong, initial bursts of cytokines after agonist stimulation, we wanted to study the kinetics and magnitude of their cytokine responses using a synergistic TLR system to see if we could enhance this early-stage cytokine response. To assess the FR cytokine response, we attached TLR4 and/or TLR7 agonist to 1 um polystyrene pathogen mimetic particles (MPs). These MPs are non-immunogenic and deliver agonist to FRs.[13] We incubated the MP-TLRs with naïve BMDCs and observed the magnitude and kinetics of cytokine

expression of FRs and nFRs via ICS. We observed that FRs stimulated with MP-TLR4_7 have a higher percent of TNF-α + cells compared to FRs stimulated with MP-TLR4 or MP-TLR7 at 1 h (Figure 3.1A). Similarly, FRs stimulated with MP-TLR4_7 display synergistic TNF-α MFI expression compared to FRs stimulated with MP-TLR4 or MP-TLR7 (Figure 3.1B) at 1 h. These results indicate that FRs have a synergistic, initial TNF-α burst in response to MP-TLR4_7 stimulation. It is important to note that in this early 1 h time point, nFRs have a baseline TNF-α MFI value. To better understand TNF-α expression kinetics of FRs, we repeated the same experiment but incubated the MPs with naïve BMDCs for 6 h instead of 1 h. At 6 h. we observed that the majority of FRs are TNF-α + after MP-TLR4, MP-TLR-7, and MP-TLR4_7 stimulation (Figure 3.1C). Even though FRs are mostly TNF-α + at 6 h, FRs that were stimulated with MP-TLR4_7 still have a significantly higher TNF-α MFI than FRs stimulated with MP-TLR4 or MP-TLR7 (Figure 3.1D). These data indicate 6 h is enough time for FRs to generate TNF-α respond to the MP-TLR-agonist stimulation, and that response is increased after synergistic MP-TLR stimulation. Similar to the 1 h timepoint, at 6 h, the nFRs still have baseline TNF-α MFI, indicating that they are not undergoing an inflammatory response. To assess how the FR and nFR response changes when the BMDCs are stimulated with soluble TLR agonist and MPs, we added MPs and MPLA (TLR 4 agonist) and/or R848 (TLR 7 agonist) as indicated for 1 h and 6 h, and we observed that the FRs still had a higher TNF-α than nFRs (Figure 3.1E). At 1 h, FRs the relative TNF-α MFI for after MPLA + R848 stimulation is only 50 % greater than that of the nFRs, but at 6 h, the relative TNF-α MFI is 3.5 times greater than nFRs, indicating significantly higher TNF-α production for FRs between 1 and 6 hours than nFRs. In addition to observing TNF-α MFI's, we also ran ICS at 6 h for two additional pro-inflammatory cytokines, IL-12 and IL-6 (Figure 3.1F, 3.1G). For both IL-12 and IL-6, FRs have much higher

MFIs than nFRs. For IL-12, the MFI for MP-TLR4_7 stimulation is synergistic for FRs; however, for IL-6, the FRs had a similar MFI for MP-TLR4_7 simulation as for MP-TLR7. These data indicate that FRs have much stronger cytokine responses, and even synergistic ones to the MP-TLR4_7 system for TNF-α and IL-12, highlighting their role as key cytokine signalers in an immune response.

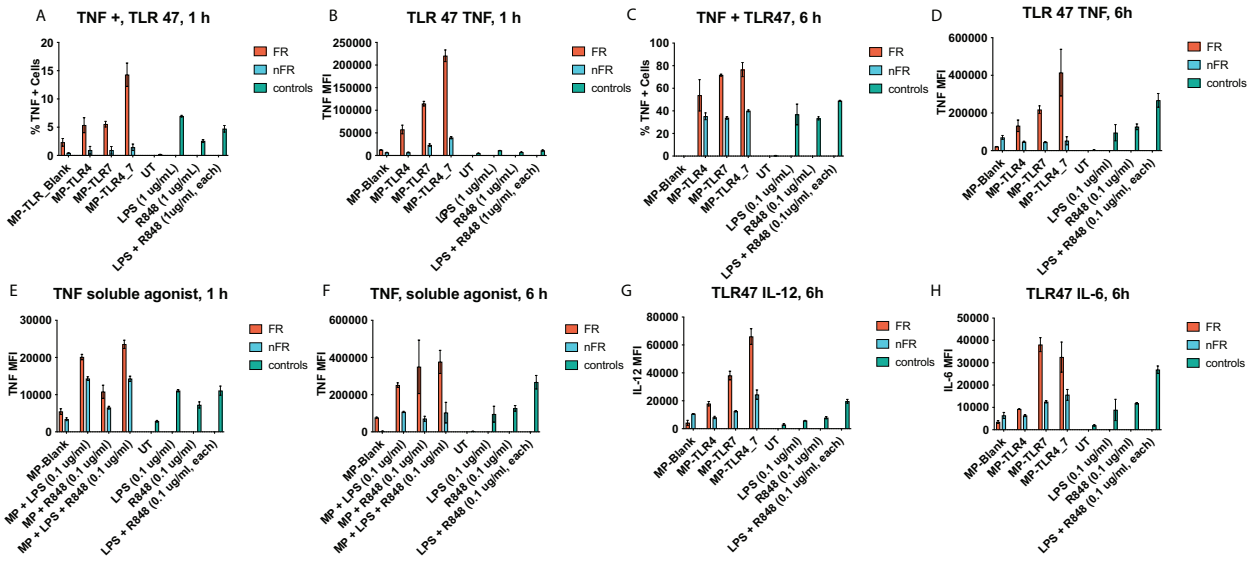

Figure 3.1. Kinetics of cytokine expression of FR and nFR response to MP-TLR stimulation using intracellular cytokine staining. A) % TNF-α+ FRs and nFRs 1 h after MP stimulation B) TNF-α MFI of FRs and nFRs after MP stimulation at 1 h. C) % TNF-α+ FRs and nFRs 6 h after MP stimulation D) TNF-α MFI of FRs and nFRs after MP stimulation at 6 h. E) BMDCs co-incubated with MP and soluble TLR agonist. TNF-α MFI measured after 1 h. F) BMDCs co-incubated with MP and soluble TLR agonist. TNF-α MFI measured after 6 h. G) IL-12 MFI at 6 h after MP-TLR stimulation H) IL-6 MFI after MP-TLR stimulation

3.3.2 Brefeldin loaded FR targeting liposomes reduce cytokine secretion *in vitro*

Given that the FRs have a strong initial burst of cytokine production, we want to be able to reduce population wide inflammation signals in BMDCs by ablating this FR signaling. By reducing pro-inflammatory cytokine signals, we aim to translate this *in vitro* FR targeting technology to an *in vivo* vaccine model to the reduce the inflammatory side effects of the vaccine while maintaining a strong antibody response. To attempt to reduce this cytokine signaling, we

loaded brefeldin A (BFA), an inhibitor of cytokine signaling, at 1 % of total lipid into a previously developed liposome system that selectively colocalizes with FR cells.[14] We will refer to this targeting system as a BFA-TL system. We added this BFA-TL to naïve BMDCs along with soluble agonist for 24 h. For IL-6 and TNF-α, there is no difference in cytokine expression for non-BFA treated BMDCs and 1% BFA-TL treated BMDCs (Figure 3.2A, B). However, for IL-12p70, a pro-inflammatory cytokine, we observe a decrease in cytokine release for BMDCs treated with BFA-TL for MPLA + R848 compared to non-BFA treated samples (Figure 3.2C). Additionally, we witness a similar decrease for BMDCs treated with BFA-TL IL-10, an anti-inflammatory cytokine for MPLA + R848 (Figure 3.2D). Based on this data, there is some reduction of IL-12p70 (pro-inflammatory) and IL-10 (anti-inflammatory) after addition of BFA-TL, but there is no reduction of pro-inflammatory cytokines IL-6 and TNF-α; thus, we cannot determine whether the BFA-TLs are reducing inflammation signals *in vitro*.

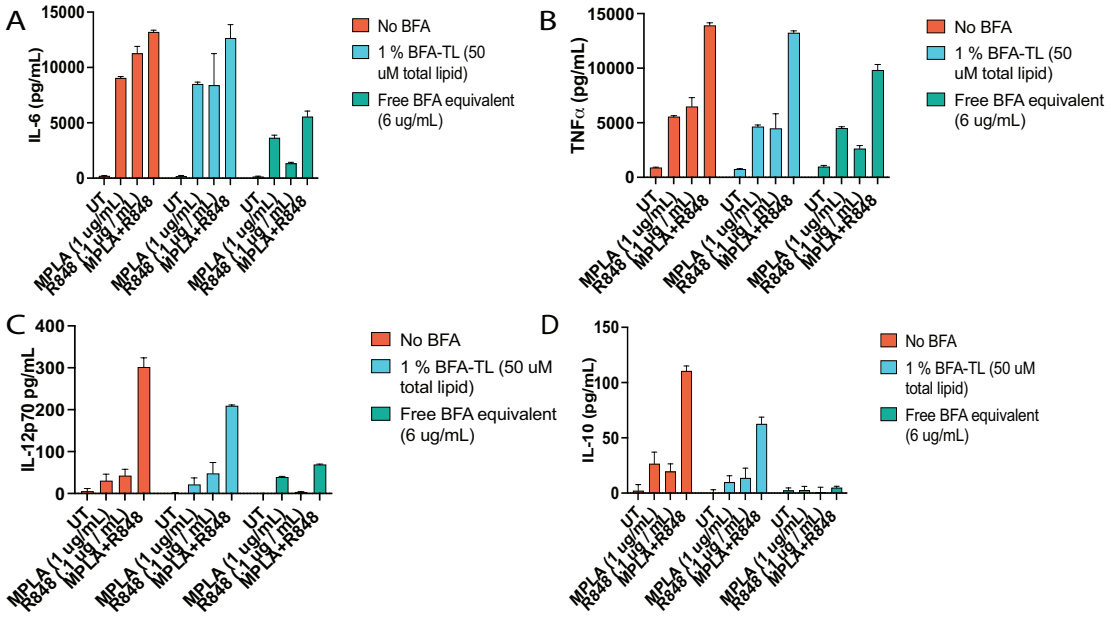

Figure 3.2: Cytokine profile of BMDCs after addition of soluble agonist and brefeldin loaded liposomes that target FRs (BFA-TL). The loaded BFA equivalent is included as a control. The level of A) IL-10 B) IL-6 C) TNF-α D) IL-12p70 secreted by BMDCs after 24 h.

3.3.3 Transcriptome analysis of FR response to Synergistic MP-TLR4_7 stimulation reveals upregulation of cell adhesion Genes

After assessing the *in vitro* signaling capabilities of FRs, we wanted to profile their transcriptome to determine the role of FRs beyond their initial cytokine release. We incubated BMDCs with the indicated MP for 16 h and isolated the FRs via FACS. We isolated the FRs RNA and sequenced on a NextSeq550 to obtain their transcriptional profile. Analysis of the FRs transcriptome indicates upregulation of many immune related genes after MP-TLR4_7 stimulation compared to the gene expression after MP-TL4 or MP-TLR7 stimulation. Using the criteria of *Fraser et al*. there is synergistic expression of TNFsf18 and TNFs13, which are two pro-inflammatory cytokines within the TNF superfamily.[19] Additionally, the RNA expression of IL-18 is additive. These cytokine data indicate that FRs continue to produce pro-inflammatory cytokines after their initial burst response, even if multiple pro-inflammatory cytokines are downregulated compared to FRs treated with MP-Blank at this time point. (Figure 3.3A, B). After analyzing the expression of immune related genes, we looked at synergistically regulated genes within the FRs after MP-TLR4_7 stimulation. We observed that multiple cell adhesion genes are synergistically upregulated, including CADM1, CD93, and LRMP. The upregulation of cell adhesion genes and pro-inflammatory cytokines highlights the signaling role that FRs have in the immune response.

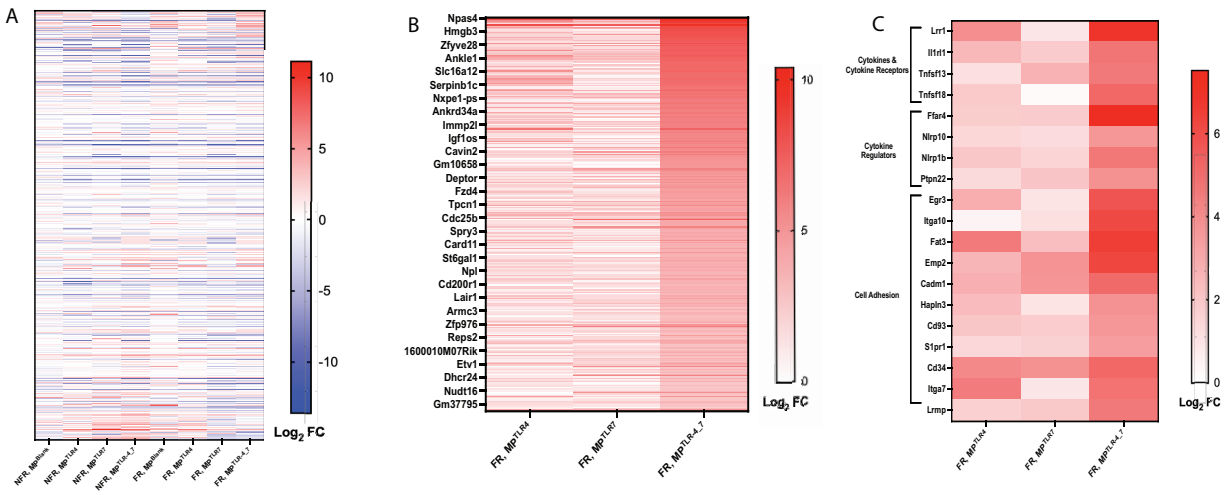

Figure 3.3: Transcriptome analysis of FRs and NFRs 16 h after synergistic MP stimulation A) Heatmap of immune related genes for FRs and NFRs upon MP-TLR stimulation. B) Heatmap of synergistically upregulated genes C) Heatmap of select synergistic genes. Many cell adhesion genes are synergistically upregulated.

3.4 Discussion and Conclusion

In this work, we build on the previous results of *Deak et al.,* which showed that FRs 1) release disproportionately high levels of cytokines compared to the average dendritic cell, 2) are critical to activating immune cell populations *in vitro*, and 3) are key to generating a powerful antibody response *in vivo*.[14] Knowing that FRs have these strong signaling capabilities, in this chapter, we demonstrate that FRs have a strong, initial cytokine response to synergistic MP-TLR4_7 stimulation, as well as soluble TLR 4/7 agonist, and reduced cytokine secretion using a BFA-TL microparticle to ablate FR signaling function. We also transcriptionally profiled the FRs to better understand their downstream immune signaling mechanisms to observe that FRs have synergistically upregulated cell adhesion genes 16 h after MP-TLR4_7 stimulation. Since intercellular adhesion is an essential component of immune processes, such as antigen presentation, we hypothesize that the signaling role of FRs has shifted focus from their initial pro-inflammatory burst to mechanical signaling that can help them present antigen, leading to

adaptive immune responses. These data highlight the powerful signaling role of FRs in the immune response to synergistic TLR stimulation.

Given technical challenges of simultaneously observing FR cytokine responses and population cytokine responses, we have not been able to quantitate the impact of FR cytokine release has on population cytokine expression in the case of synergy. We hope the BFA-TL system will help elucidate the FR's function in this respect. When we determine an effective way to ablate FR signaling, we can deduce the role of FR signaling in response to synergistic stimulation. Moreover, we can translate this BFA-TL technology *in vivo*, to hopefully reduce inflammatory side effects of vaccination, while maintaining a protective antibody response. These results will help vaccines be developed more optimally to enhance immune signaling produced by the cells that already have robust inflammation signaling capabilities.

3.5 Materials and Methods

Bone marrow derived DCs:

GM-CSF murine bone marrow cells were collected from 6-week-old female C57BL/6 mice. Red blood cells were lysed with RBC Lysis Buffer (BioLegend). BM cells were plated per well in deep petri dishes (VWR) at a concentration of 10^6/mL. Cells were cultured at 37°C and 5% CO2 in culture media: RPMI 1640 (Life Technologies), 10% HIFBS (Gibco), GM-CSF (20 ng/mL; recombinant Mouse GM-CSF (carrier-free) from BioLegend), 2 mM l-glutamine (Life Technologies), 1% antibiotic- antimycotic (Life Technologies). Media was replenished on day 3. Cells were used on day 5. For FLT-3L matured BMDCs, a similar procedure was used but replacing GM-CSF with 100 ng/mL of FLT-3L.

Silica-silane coated polystyrene microparticle (MP) synthesis:

PS MPs were synthesized and coated with a silica coating using a procedure from Moser et al.[13] Briefly, uniform, spherical, 2 μm diameter polystyrene microparticles were synthesized via controlled styrene polymerization. 2 g of polyvinylpyrrolidone, MW 40,000 and styrene (20 g), washed with NaOH and dried with MgSO4, was dissolved in EtOH (250 mL) and purged with nitrogen. AIBN (0.2 g) was added, the mixture stirred at 70°C and 200 rpm for 24 h. Mixture was purified by centrifugation (5000 RPM for 5 min, followed by washing 3X in 30 mL of EtOH to remove residual monomer, initiator, and stabilizer). The surfaces of MPs were modified with reactive thiol groups via Pickering emulsion reaction. A mixture of cyclohexane (45 mL), n-hexanol (10.8 mL), endotoxin free water (2 mL) and Triton X-114 (10.8 mL) were placed in a round-bottom flask and sonicated for 20 min. Particles (0.2 g) were added and the suspension was sonicated for 40 min. Tetraethyl-orthosilicate (TEOS) (400 μL) was added dropwise followed by 14 M aqueous ammonia (1.2 mL). The resulting solution was stirred for 30 min RT. Subsequently, 3-Mercaptosilane (200 μL) was added dropwise and stirred for 6 h. TEOS-mercaptosilane copolymer coated particles were then pelleted at 3,400 rpm for 30 min and washed 3× with EtOH. Particles were dried at 70°C and stored at 4°C.

TLR agonist surface functionalization:

Thiol bearing MPs were functionalized with MPLA and Pam_2 using thiol-maleimide chemistry. First MPs (5 mg) were swelled in ACN (500 uL) for 30 mins under sonication, then 1 mg of FITC in 500 uL of ACN was added for a final concentration of 1 mg/mL for 30 mins. MPs were then centrifuged for 1 min (5000 rcf), supernatant removed and washed 3x with PBS. For MPs conjugated with agonists to TLR7: FITC labeled MPs were dissolved in 500 uL of PBS, then 5 mg of Bismaleimide-PEG_3 was added and allowed to sonicate for 30 min, then washed 3x in PBS. During this 2BXY (0.1 mg/mL) was incubated for 5 mins with Traut's reagent (1 mg/mL)

in 500 uL of PBS. After washing, maleimide bearing MPs were incubated with thiol functionalized with either Traut's + 2BXY (500 uL) and sonicated for 30 mins, then washed 10 times, 3x with PBS, 4x with PBS with 0.1 Tween 20, and 3x with PBS. For TLR4 MPs, 1 mg of LPS was dissolved in 400 uL of DMF and 10 ug of p-maleimidophenyl isocyanate added and allowed to stir overnight under argon. Then PBS (400 uL) was added followed by 2,2'-(ethylenedioxy)diethanethiol (4 mg) and allowed to stir for 12 h. 100 uL of this mixture was added to the MP with 400 uL of PBS for 30 mins and similarly washed. After conjugation, all MPs were diluted in PBS + 0.05 %wt Tween20 at 20, 50 and 100X and then number of MPs in 10 uL counted using flow cytometry to determine a concentration. MP solutions were diluted to a concentration of 1 million MPs per uL of PBS and stored at 4°C until use.

Liposome synthesis:

Liposomes were synthesized via membrane extrusion method using a setup from Avanti polar lipids and 200 nm extrusion filters. DSPC, PEG2000 PE, Cholesterol, and/or DiD, Heparin-lipid, DAP12 peptide lipid and any TLR agonists/ Brefeldin A were combined in 1 mL methanol added, dried via lyophilization, and rehydrated in PBS to make a 10 mM total lipid, 200 uL solutions. OVA was added during rehydration. Solutions were gently rotated at 67°C and passed through a 70°C 200 nm filter 5 times. The liposome solution was dialyzed against PBS with a 3,500 Da filter for 24 hrs.

ICS determination of FR cytokine expression:

BMDCs were plated at 1million/ml in 200 uL in a 96 well plate in 10%HIFBS in DMEM with Golgiplug (Biolegend) to inhibit cytokine release from the cells for 1 h before addition of immune agonist. MP-TLRs and/or immune agonist were added as indicated. After the denoted

amount of time, the cells were fixed and permeabilized using a Cytofix/CytoPerm kit (BD Biosciences) per the manufacturers instructions. The cells were stained and run on a ACEA NovoCyte Flow cytometer.

Brefeldin Liposome (BFA-TL) Cytokine Inhibition Experiment

BMDCs were plated at 1 million/mL in 200 uL in a 96 well plate and were allowed to rest for at least 1 h. Agonist, BFA, and/or BFA-TLs were added as indicated. After 24 h the supernatant was removed and cytokines were sampled using a Mouse Inflammation CBA kit (BD Biosciences) according to the manufacturer's instructions.

mRNA Transcriptome Analysis:

For 16 h sequencing: BMDCs were incubated at a 1:1 ratio with MP^{TLR-X} (x = blank, 4, 7) for 16 h. The FRs and non-FRs were isolated via FACS. RNA was extracted using a Direct-zol RNA-Microprep kit (Zymo), prepped using SMARTer® Stranded Total RNA-Seq Kit v2 (Takara), and sequenced on a NextSeq550 (Illumina). RNA-Seq reads were mapped to GRCm38 mouse reference genome using STAR version 2.7.0b.[20] The resulting files from the alignment step above were taken to evaluate transcriptional expression using subread::featureCounts with gencode transcript annotation M19.[21] The obtained count table was normalized and log fold change in expression was generated using the edgeR package.[22] Using the Cell Surface Protein Atlas's database for mouse cell surface protein, we identified proteins that were most frequently upregulated in the most MP^{TLR-X} dosing conditions that met both the following criteria: 2-fold upregulation and pval <.05.[23] For time series sequencing: BMDCs were incubated at 1:1 ratio with MP^{TLR-4} for 15 min. The FRs and non-FRs were isolated via FACS, washed, and resuspended in media. At 0, 0.5, 1, 2, 4 h, the RNA was extracted using a Direct-zol RNA-

Microprep kit (Zymo). Sequencing was performed by the University of Chicago Genomics Core, and BasePairTech's DESEQ2 pipeline was used to align the reads to the mm10 genome, and compute the differential expression and Gene Set Enrichment Analysis. Using the Mouse Genomic Informatics database to acquire lists of genes with 1) immune function 2) antigen presentation the immune response of the FRs and non-FRs were profiled by analyzing the differential expression, using only genes with 2-fold differential expression change and pval < .05 for at least one of the timepoints.[24]

3.6 References

(1) Querec, T. D.; Pulendran, B. Understanding the Role of Innate Immunity in the Mechanism of Action of the Live Attenuated Yellow Fever Vaccine 17D. In *Crossroads between Innate and Adaptive Immunity*; Katsikis, P. D., Schoenberger, S. P., Pulendran, B., Eds.; Advances in Experimental Medicine and Biology; Springer US: Boston, MA, 2007; pp 43–53. https://doi.org/10.1007/978-0-387-34814-8_3.

(2) Querec, T.; Bennouna, S.; Alkan, S.; Laouar, Y.; Gorden, K.; Flavell, R.; Akira, S.; Ahmed, R.; Pulendran, B. Yellow Fever Vaccine YF-17D Activates Multiple Dendritic Cell Subsets via TLR2, 7, 8, and 9 to Stimulate Polyvalent Immunity. *J. Exp. Med.* **2006**, *203* (2), 413–424. https://doi.org/10.1084/jem.20051720.

(3) Gaucher, D.; Therrien, R.; Kettaf, N.; Angermann, B. R.; Boucher, G.; Filali-Mouhim, A.; Moser, J. M.; Mehta, R. S.; Drake, D. R., III; Castro, E.; Akondy, R.; Rinfret, A.; Yassine-Diab, B.; Said, E. A.; Chouikh, Y.; Cameron, M. J.; Clum, R.; Kelvin, D.; Somogyi, R.; Greller, L. D.; Balderas, R. S.; Wilkinson, P.; Pantaleo, G.; Tartaglia, J.; Haddad, E. K.; Sékaly, R.-P.

Yellow Fever Vaccine Induces Integrated Multilineage and Polyfunctional Immune Responses. *J. Exp. Med.* **2008**, *205* (13), 3119–3131. https://doi.org/10.1084/jem.20082292.

(4) Duggan, J. M.; You, D.; Cleaver, J. O.; Larson, D. T.; Garza, R. J.; Guzmán Pruneda, F. A.; Tuvim, M. J.; Zhang, J.; Dickey, B. F.; Evans, S. E. Synergistic Interactions of TLR2/6 and TLR9 Induce a High Level of Resistance to Lung Infection in Mice. *J. Immunol. Baltim. Md 1950* **2011**, *186* (10), 5916–5926. https://doi.org/10.4049/jimmunol.1002122.

(5) Beutler, E.; Gelbart, T.; West, C. Synergy between TLR2 and TLR4: A Safety Mechanism. *Blood Cells. Mol. Dis.* **2001**, *27* (4), 728–730. https://doi.org/10.1006/bcmd.2001.0441.

(6) Fischetti, L.; Zhong, Z.; Pinder, C. L.; Tregoning, J. S.; Shattock, R. J. The Synergistic Effects of Combining TLR Ligand Based Adjuvants on the Cytokine Response Are Dependent upon P38/JNK Signalling. *Cytokine* **2017**, *99*, 287–296. https://doi.org/10.1016/j.cyto.2017.08.009.

(7) Pavot, V.; Rochereau, N.; Rességuier, J.; Gutjahr, A.; Genin, C.; Tiraby, G.; Perouzel, E.; Lioux, T.; Vernejoul, F.; Verrier, B.; Paul, S. Cutting Edge: New Chimeric NOD2/TLR2 Adjuvant Drastically Increases Vaccine Immunogenicity. *J. Immunol. Baltim. Md 1950* **2014**, *193* (12), 5781–5785. https://doi.org/10.4049/jimmunol.1402184.

(8) Tom, J. K.; Dotsey, E. Y.; Wong, H. Y.; Stutts, L.; Moore, T.; Davies, D. H.; Felgner, P. L.; Esser-Kahn, A. P. Modulation of Innate Immune Responses via Covalently Linked TLR Agonists. *ACS Cent. Sci.* **2015**, *1* (8), 439–448. https://doi.org/10.1021/acscentsci.5b00274.

(9) Mogensen, T. H.; Paludan, S. R.; Kilian, M.; Ostergaard, L. Live Streptococcus Pneumoniae, Haemophilus Influenzae, and Neisseria Meningitidis Activate the Inflammatory

Response through Toll-like Receptors 2, 4, and 9 in Species-Specific Patterns. *J. Leukoc. Biol.* **2006**, *80* (2), 267–277. https://doi.org/10.1189/jlb.1105626.

(10) Madan-Lala, R.; Pradhan, P.; Roy, K. Combinatorial Delivery of Dual and Triple TLR Agonists via Polymeric Pathogen-like Particles Synergistically Enhances Innate and Adaptive Immune Responses. *Sci. Rep.* **2017**, *7* (1), 2530. https://doi.org/10.1038/s41598-017-02804-y.

(11) Kasturi, S. P.; Skountzou, I.; Albrecht, R. A.; Koutsonanos, D.; Hua, T.; Nakaya, H. I.; Ravindran, R.; Stewart, S.; Alam, M.; Kwissa, M.; Villinger, F.; Murthy, N.; Steel, J.; Jacob, J.; Hogan, R. J.; García-Sastre, A.; Compans, R.; Pulendran, B. Programming the Magnitude and Persistence of Antibody Responses with Innate Immunity. *Nature* **2011**, *470* (7335), 543–547. https://doi.org/10.1038/nature09737.

(12) Yang, K.; Whalen, B.; Tirabassi, R. S.; Selin, L.; Levchenko, T.; Torchilin, V. P.; Kislauskis, E. H.; Guberski, D. L. A DNA Vaccine Prime Followed By A Liposome-Encapsulated Protein Boost Confers Enhanced Mucosal Immune Responses And Protection. *J. Immunol. Baltim. Md 1950* **2008**, *180* (9), 6159–6167.

(13) Moser, B. A.; Steinhardt, R. C.; Esser-Kahn, A. P. Surface Coating of Nanoparticles Reduces Background Inflammatory Activity While Increasing Particle Uptake and Delivery. *ACS Biomater. Sci. Eng.* **2017**, *3* (2), 206–213. https://doi.org/10.1021/acsbiomaterials.6b00473.

(14) Deak, P. E.; Studnitzer, B.; Ung, T.; Steinhardt, R.; Swartz, M.; Esser-Kahn, A. Isolating and Targeting a Highly Active, Stochastic Dendritic Cell Subpopulation for Improved Immune Responses. Rochester, NY April 25, 2022. https://doi.org/10.2139/ssrn.4093302.

(15) Banchereau, J.; Steinman, R. M. Dendritic Cells and the Control of Immunity. *Nature* **1998**, *392* (6673), 245–252. https://doi.org/10.1038/32588.

(16) Collin, M.; Bigley, V. Human Dendritic Cell Subsets: An Update. *Immunology* **2018**, *154* (1), 3–20. https://doi.org/10.1111/imm.12888.

(17) Shalek, A. K.; Satija, R.; Shuga, J.; Trombetta, J. J.; Gennert, D.; Lu, D.; Chen, P.; Gertner, R. S.; Gaublomme, J. T.; Yosef, N.; Schwartz, S.; Fowler, B.; Weaver, S.; Wang, J.; Wang, X.; Ding, R.; Raychowdhury, R.; Friedman, N.; Hacohen, N.; Park, H.; May, A. P.; Regev, A. Single-Cell RNA-Seq Reveals Dynamic Paracrine Control of Cellular Variation. *Nature* **2014**, *510* (7505), 363–369. https://doi.org/10.1038/nature13437.

(18) Van Eyndhoven, L. C.; Singh, A.; Tel, J. Decoding the Dynamics of Multilayered Stochastic Antiviral IFN-I Responses. *Trends Immunol.* **2021**, *42* (9), 824–839. https://doi.org/10.1016/j.it.2021.07.004.

(19) Lin, B.; Dutta, B.; Fraser, I. D. C. Systematic Investigation of Multi-TLR Sensing Identifies Regulators of Sustained Gene Activation in Macrophages. *Cell Syst.* **2017**, *5* (1), 25-37.e3. https://doi.org/10.1016/j.cels.2017.06.014.

(20) Dobin, A.; Davis, C.A.; Schlesinger, F.; Drenkow, J.; Zaleski, C.; Jha, S.; Batut, P.; Chaisson, M.; Gingeras, T. R. STAR: Ultrafast Universal RNA-Seq Aligner, Bioinformatics, 29, 1, (2013), 15–21, Https://Doi.Org/10.1093/Bioinformatics/Bts635.

(21) Liao, Y.; Smyth, G. K.; Shi, W. The Subread Aligner: Fast, Accurate and Scalable Read Mapping by Seed-and-Vote. *Nucleic Acids Res.* **2013**, *41* (10), e108. https://doi.org/10.1093/nar/gkt214.

(22) Robinson, M. D.; McCarthy, D. J.; Smyth, G. K. EdgeR: A Bioconductor Package for Differential Expression Analysis of Digital Gene Expression Data. *Bioinformatics* **2010**, *26* (1), 139–140. https://doi.org/10.1093/bioinformatics/btp616.

(23) Bausch-Fluck D, Hofmann A, Bock T, Frei AP, Cerciello F, et al. A Mass Spectrometric-Derived Cell Surface Protein Atlas. *PLoS* **2015**, No. One 10: e0121314.

(24) Bult, C. J.; Blake, J. A.; Smith, C. L.; Kadin, J. A.; Richardson, J. E.; the Mouse Genome Database Group. Mouse Genome Database (MGD) 2019. *Nucleic Acids Res.* **2019**, *47* (D1), D801–D806. https://doi.org/10.1093/nar/gky1056.

Chapter 4: IRF3 plays key inflammatory role in allergic contact dermatitis

4.1 Summary

Allergic contact dermatitis (ACD) is a condition in which an individual has an inflammatory response to small compounds called contact allergens. ACD is estimated to affect up to 20 % of the USA's population and is characterized by a sensitization phase and elicitation phase. In this work, we identify IRF-3 is a key inflammatory transcription factor in the ACD response. We demonstrate that the addition of GSK-8612, an IRF-3 inhibitor, reduces IL-8 levels in THP-1 cells by 30-55% compared to the IL-8 levels induced by the contact allergen, only. When mice were treated with both GSK-8612 and DNCB in a local lymph node assay, we observed a net reduction in final ear widths of 20 % as well as a reduction in cutaneous IL-1β, compared to mice treated with DNCB alone. We are currently testing to see whether IRF3 plays an inflammatory role *in vivo* using IRF3-KO mice and WT mice.

4.2 Introduction

Allergic contact dermatitis (ACD) is estimated to affect up to 20 % of the population in the USA.[1] ACD is a delayed type IV hypersensitivity reaction that occurs after exposure to a contact allergen. These contact allergens react with epidermal proteins, such as HSP90, to form a haptenated protein.[2] This allergen-protein complex is recognized by the innate immune system, initiating an immune response.[3] The immune response in ACD is broken down into two phases: the sensitization phase and the elicitation phase. In the sensitization phase, the allergen-protein complex is detected by pattern recognition receptors (PRRs), such as Toll-like receptor 3 (TLR3) and Toll-like receptor (TLR4) on skin resident dendritic cells (DCs), resulting in cytokine release

and recruitment of T cells.[4] DCs present the allergen-protein complex to naïve CD4+ and CD8+ T cells, which leads to T cell activation, proliferation, and differentiation into allergen-specific T cells.[4] At this point, ACD is in the elicitation phase, which is characterized by rapid skin inflammation and pro-inflammatory cytokines upon re-exposure to the same contact allergen.[5]

Currently, there is no cure for ACD, and common treatments only mitigate symptoms.[6] Often a topical corticosteroid is applied to the site of inflammation, but the corticosteroid does not completely eradicate inflammation, and long-term use of corticosteroids has a myriad of negative side effects, including muscle atrophy and bone loss.[7,8,9] As a result, we want to better understanding the cellular pathways of ACD to both prevent sensitization and treat ACD.

Interferon regulating factor 3 (IRF3) is a key transcription factor in the antiviral host response. IRF3 is activated by multiple PRRs, including TLR3 and TLR4.[10] After PRR activation, IRF3 regulates many immune functions, such as type I interferon (IFN) and IL-8 expression.[11,12] We hypothesize that IRF3 has a role in biological processes of ACD for three main reasons. First, IRF3 is activated by TLR3 and TLR4, which are important PRRs in the onset of ACD.[13,14] Second, IRF3 regulates IL-8 expression, which is the key cytokine to recruit neutrophils to the site of inflammation in ACD – an essential step in both sensitization and elicitation –.[15,16] Third, our lab has previously inhibited the ACD response with geldanamycin, a small molecule that blocks HSP90 mediated activation of IRF3.[2,17] Given this information, we explored IRF3's role in ACD *in vitro* and *in vivo*, using GSK-8612, a small molecule inhibitor of the TBK1-IRF3 complex that is essential for IRF3 activation.[18] Additionally, we use IRF3-KO mice to demonstrate IRF3 is critical to the development of skin inflammation and proinflammatory cytokines in a local lymph node assay. These results elucidate the role of IRF3 in ACD, which promises to enable novel classes of treatments for ACD.

4.3 Results

4.3.1 GSK-8612, an inhibitor of IRF-3 activity, reduces IL-8 secretion in THP-1s upon co-stimulation with contact allergens

To assess whether IRF3 has a role in sensitization for ACD, we examined the secretion of IL-8 levels in THP-1 and IRF3-KO THP-1 Dual cells upon stimulation with multiple contact allergens. THP-1 cells are a human monocyte cell line and are a well-established platform for screening sensitization.[19,20] By screening IL-8 release in THP-1 cells, we can reliably determine the sensitization potential of contact allergens, since IL-8 is the primary cytokine involved in neutrophil recruitment, and neutrophil recruitment is essential to sensitization.[20,21] Thus, by evaluating IL-8 secretion *in vitro*, we can screen biological pathways that contribute to sensitization, such as IRF-3.

To test IRF-3's role in sensitization, we added the following contact allergens: dinitrochlorobenzene (DNCB), citral, citral, and 2-methyl-4-isothiazolin-3-one (MIST) – to THP-1s as indicated. Along with the contact allergen, we surveyed IL-8 levels using GSK-8612, a selective and potent inhibitor of TBK-1 – a kinase that binds to IRF-3 and is essential for IRF-3's activation–, to deduce whether IRF-3 has a role in sensitization.[18,22] For DNCB, citral, and MIST, significant reductions in IL-8 secretion was observed by the THP-1 cells treated with contact allergen and GSK-8612, compared to THP-1 cells that were just treated with the contact allergen, indicating that GSK-8612 reduces IL-8 secretion in THP-1 cells. For example, GSK-8612 reduced IL-8 levels by 32 % for DNCB, 50 % for citral, and 56 % for MIST. (Figure 4.1A-C). Additionally, there were lower levels of secreted IL-8 in IRF-3 KO THP-1 Dual cells compared to THP-1 cells, and GSK-8612 did not reduce IL-8 levels in the IRF-3 KO THP-1

Dual cells, demonstrating that GSK-8612 reduces IL-8 expression via an IRF-3 controlled mechanism. From these results, we conclude that IRF-3 contributes to IL-8 secretion *in vitro* and sought to determine if IRF-3 plays a role in sensitization *in vivo.*

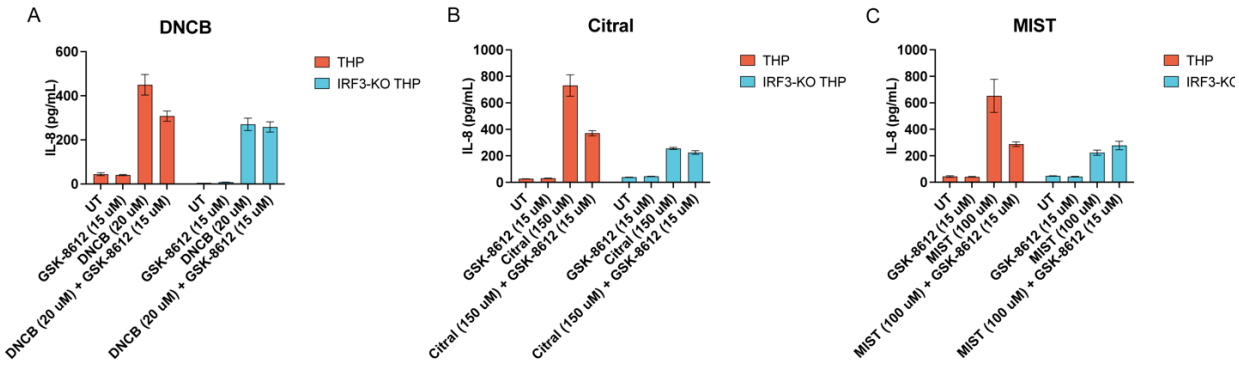

Figure 4.1: GSK-8612 reduces IL-8 secretion in THP-1 cells upon co-addition with multiple contact allergens at 20 h. IRF3-KO THP-1 cells have lower IL-8 secretion than THP-1 cells, and GSK-8612 does not reduce IL-8 secretion in IRF3-KO THP-1 cells for A) DNCB B) Citral and C) MIST. N=3.

4.3.2 GSK-8612 reduces ACD response to DNCB in mouse model

To study the effect of GSK-8612 on ACD, we performed a local lymph node assay (LLNA). The LLNA is a common procedure for examining ACD in a mouse model.[23,24] In this assay, a mouse is sensitized to a contact allergen, typically DNCB, by adding a solution containing the allergen on stomach of a mouse on days 0-1. On days 5-8, the same allergen is added to the back of the ear of the mouse to elicit the ACD response. On day 9, the final ear width is measured, and local cytokine production in the inflamed ear is assayed. For the LLNA, we used a 0.5 % w/v solution of DNCB in a solvent containing 4:1 acetone:olive oil.[25] In the sensitization phase – days 0-1 – of this experiment, 0.3% w/v of GSK-8612 was included to a control and DNCB sensitized experimental groups to determine whether IRF-3 is important to sensitization of DNCB. We chose 0.3 % w/v for GSK-8612, because this molar ratio of DNCB:GSK-8612 was found to maximally reduce IL-8 levels *in vitro*.

At the end of the LLNA, we observed roughly a 20% reduction in the final ear widths in mice that were subjected to DNCB + GSK-8612 during sensitization compared to mice that were only exposed to DNCB during sensitization. (Figure 4.2A-B). Moreover, in the DNCB + GSK-8612 sensitized mice, there was a significant decrease cutaneous for IL-1β levels, but not for TNF-α levels compared to mice sensitized with DNCB alone (Figure 4.2C-D). The reduction in both final ear widths and IL-1β levels indicate that GSK-8612 effectively reduces sensitization in mice.

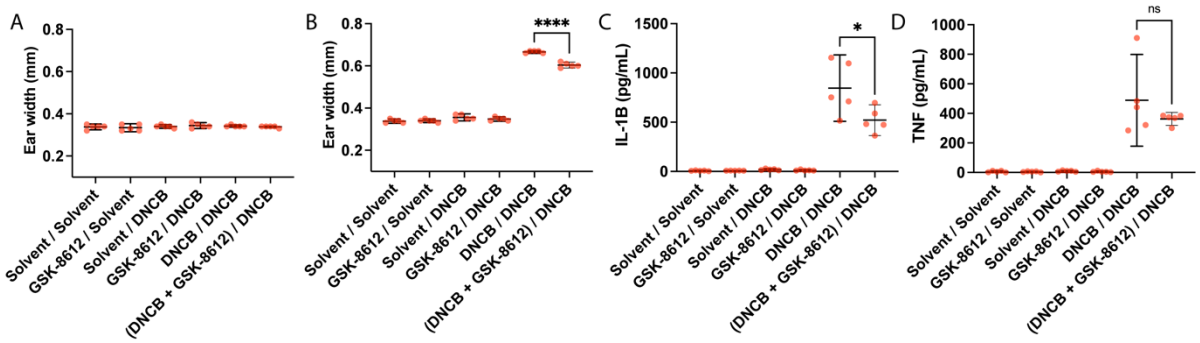

Figure 4.2: GSK-8612 reduces ACD response in a local lymph node assay model. A) Ear widths of mice before elicitation phase. Treatment groups are labeled as "Sensitization phase treatment / Elicitation phase treatment". For example, a group labeled "GSK-8612 / Solvent" received GSK-8612 during sensitization phase and the delivery solvent in the elicitation phase. B) Ear widths of the mice on day 9, just before sacrifice. C, D) Cytokines in the ear were measured on day 9, with significant results observed for IL-1β. N=5. *p<.05, **p<.01 ***p<.001, ****p<.0001.

4.3.3 IRF-3 KO mice have reduced response to contact allergens in local lymph node model

To directly assess the impact of IRF-3 on ACD, we screened IRF-3 KO mice and WT mice using a LLNA to see their response to DNCB. We used a 0.5 % w/v solution of DNCB in a solvent containing 4:1 acetone: olive oil to topically deliver DNCB to the mice. For days 0 - 1, 25 uL of DNCB solution was applied to the shaved mice's stomachs. On days 2-4, the mice rested, as time is needed for the mice to become sensitized to DNCB. On days 5-8, the mice

were challenged with the same DNCB solution applied to the back of the ear to observe a difference in ACD response between IRF-3 KO mice and WT mice. On day 9 we measured the final ear widths and cutaneous cytokines in the ear.

In this study, we did not observe a significant difference in final ear widths between WT and IRF-3 KO mice. Additionally, there was no significant difference in cutaneous cytokine levels of the pro-inflammatory cytokines IL-12p70 and MCP-1. Even though these results do not suggest a difference between the ACD response between WT and IRF-3 KO mice, this was the first attempt running this experiment, and if we compare these results to the LLNA results for DNCB / DNCB treated in Figure 4.2, there was less significantly inflammation in final ear widths and lower cytokines produced in this experimental attempt. Therefore, before drawing any conclusions about the role of IRF-3 in ACD, this experiment will be reattempted to try to induce an elicitation response that matches previous results.

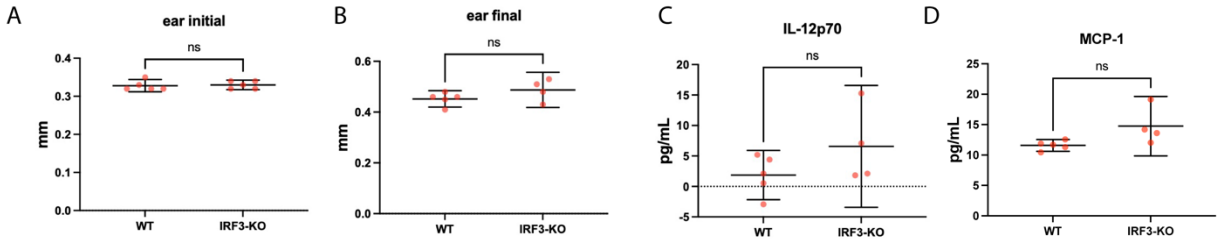

Figure 4.3: There is no difference in ACD response of IRF-3 KO mice compared to WT mice. Both groups received DNCB / DNCB treatment for their sensitization and elicitation phases. A) Ear widths of mice before elicitation phase. B) Ear widths of the mice on day 9, just before sacrifice. C, D) Cytokines in the ear were measured on day 9. N= 4 or 5. *p<.05, **p<.01 ***p<.001, ****p<.0001.

4.4 Discussion & Conclusion

In this study, we report that IRF-3 plays an inflammatory role in the ACD response to exposure to contact allergens. We screened GSK-8612, an IRF-3 inhibitor, to demonstrate that,

addition of GSK-8612 with contact allergens, reduces IL-8 secreted levels compared to the levels secreted for each the contact allergens tested. Additionally, we tested GSK-8612's impact on ACD *in vivo* using a local lymph node assay. We observed a decrease in final ear widths and IL-1β for (GSK-8612 + DNCB) / DNCB treated mice compared to DNCB / DNCB treated mice. After these results, we tested the ACD response in both WT and IRF-3 KO mice, and on first pass, observed no significant difference in ear widths or cytokines between WT and IRF-3 KO mice.

Activation of innate immunity is a key initial step in the ACD response. Within ACD, upstream activators of IRF-3, such as PRRs that recognize contact allergens, as well as downstream targets, such as cytokines, have been well characterized.[5,13,14] However, relatively little is known about the role transcription factors, such as IRF-3, in ACD. To better understand ACD, it is important to have a mechanistic understanding of the pathways that lead to inflammation. Since contact allergens have a variety of reactivities and each allergen can react with multiple proteins, it is hard to determine pathways of ACD that are independent of contact allergen. Because GSK-8612 reduced IL-8 levels for multiple contact allergens, we would expect IRF-3 to be important to the ACD response, regardless of the contact allergen. The mechanism by which IRF-3 activates in the ACD model remains unclear, but given that HSP90 is important in sensitization and is known to complex with TBK-1 to activate IRF-3, it is possible that HSP-90 could be one activator of IRF-3 activity in ACD.[2] By studying the role of IRF-3 in ACD, we have elucidated a key inflammatory pathway in ACD. We can leverage this information to develop novel, improved therapeutics for ACD.

4.5 Materials and Methods

All chemicals were bought from Sigma Aldrich unless otherwise noted. Honokiol was purchased from Tokyo Chemistry Industry. For the GSK-8612 / DNCB local lymph node assay, 6-week-old BALB/cByJ mice were purchased from Jackson Laboratory. For the IRF3-KO study, IRF-3 KO C57BL/6 were obtained from Wendy Walker at Texas Tech University, whose colony came from Yale, originating from Tadatsugu Taniguchi.[26,27,28] These mice were used at 6 weeks old, along with 6 week old wild type C57BL/6 mice from Jackson Laboratory. All mice were housed under controlled light, temperature, and humidity conditions. All experiments were conducted with the approval of the University of Chicago Institutional Animal Care and Use Committee, and animals were maintained in accordance with guidelines and regulations of the National Institutes of Health.

Cell Culture:

Human monocyte cell line THP-1 (American Type Culture Collection) and IRF3 KO Dual Reporter THP-1 Cell line (Invivogen) were grown in RPMC 1640 medium (Life Technologies) supplemented 10 % with fetal bovine serum (Thermo Fisher Scientific) and 1 % antibiotic-antimycotic (Thermo Fisher Scientific) at 37 ^{O}C in 5 % CO_2 incubator.

***In vitro* IL-8 Screening**:

For the assay, THP-1 cells were plated at 1 million/mL in a 24 well plate. GSK-8612 were added to the indicated samples to achieve a final concentration of 15 μM. After 5 min, the hapten was added. The THP-1s were incubated for 16-20 h. The cells were centrifuged at 300 x G for 5

mins, and the supernatant was subsequently collected to measure IL-8 secretion. IL-8 was quantified with IL-8 ELISAMAX (BioLegend) using the manufacturer's procedure, and absorbance was analyzed using a Multiskan FC plate reader (Thermo Scientific) at 450 nm.

Cell Viability:

At the end of IL-8 screen, the THP-1 cells were resuspended in 100 µL media. 5 mg of 3-(4,5-dimethylthiazol-2-yl)-2,5-diphenyltetrazolium bromide (MTT) was dissolved in 1 mL PBS. 10 µL MTT solution was added to the cells. After 3 hours, 65 µL of cell supernatant was added to 100 µL of DMSO and incubated at 37 ^{O}C for 10 min. The absorbances were analyzed using a Multiskan FC plate reader (Thermo Scientific) at 570 nm to assess viability.

Contact Hypersensitivity Animal Model:

Mice were allowed to acclimatize for 1 week prior to the start of experimentation and used at 6-8 weeks of age. The abdomen of the mice was shaved with a razor. On days 0 and 1, the mice were sensitized with 25 µL of solvent (1:4 v/v olive oil/acetone) containing 0.5 % w/v DNCB with 0.3% GSK-8612. After 3 days of rest, the mice were challenged on days 5-8 on the back of the ear with 10 µL solvent or solutions as indicated. On day 9, the final ear widths were measured, mice were sacrificed, and ears were excised. The ears were mechanically homogenized on ice in 0.5 mL of RPMI. The protein was retrieved by centrifuging at 20,000 g at 4 ^{O}C for 20 min and collecting the supernatant. Cutaneous cytokine levels were quantified using CBA Mouse Inflammation Kit (BD Biosciences) according to the manufacturer's procedure and analyzed on a NovoCyte Flow Cytometer (ACEA Biosciences).

4.6 References

(1) Adler, B. L.; Deleo, V. A. Allergic Contact Dermatitis. *JAMA Dermatol.* **2021**, *157* ((3):364). https://doi.org/doi:10.1001/jamadermatol.2020.5639.

(2) Kim, S.-M.; Studnitzer, B.; Esser-Kahn, A. Heat Shock Protein 90's Mechanistic Role in Contact Hypersensitivity. *J Immunol* **2022**. https://doi.org/10.4049/jimmunol.2101023.

(3) St. Mazard, P.; Rosieres, A.; Krasteva, M.; Berard, F.; Dubois, B.; Kaiserlian, D.; Nicolas, J.-F. Allergic Contact Dermatitis. *Eur J Dermatol* **2004**, *14*, 284–295.

(4) Kaplan, D. H.; Igyarto, B. Y.; Gaspari, A. A. Early Immune Events in the Induction of Allergic Contact Dermatitis. **2012**, *12* (2), 114–124.

(5) Kondo, S.; Pastore, S.; Shivji, G. M.; McKenzie, R. C.; Sauder, D. N. Characterization of Epidermal Cytokine Profiles in Sensitization and Elicitation Phases of Allergic Contact Dermatitis as Well as Irritant Contact Dermatitis in Mouse Skin. *Lymphokine Cytokine Res* **1994**, *13* (6), 367–475.

(6) Usatine, R. P.; Riojas, M. Diagnosis and Management of Contact Dermatitis. *Am. Fam. Physician* **2010**, *82* (3), 249–255.

(7) Vatti, R. R.; Ali, F.; Teuber, S.; Chang, C.; Gershwin, M. E. Hypersensitivity Reactions to Corticosteroids. *Clin Rev Allergy Immunol* **2014**, *47* (1), 36–37. https://doi.org/10.1007/s12016-013-8365-z.

(8) Braun, T. P.; Marks, D. L. The Regulation of Muscle Mass by Endogenous Glucocorticoids. *Front. Physiol.* **2015**. https://doi.org/10.3389/fphys.2015.00012.

(9) Picado, C.; Luengo, M. Corticosteroid-Induced Bone Loss. Prevention and Management. *Drug Saf.* **1996**, *15* (5), 347–359. https://doi.org/10.2165/00002018-199615050-00005.

(10) *Frontiers | Regulating IRFs in IFN Driven Disease*. https://www.frontiersin.org/articles/10.3389/fimmu.2019.00325/full#B40 (accessed 2022-11-03).

(11) *Innate Immune Sensing and Signaling of Cytosolic Nucleic Acids | Annual Review of Immunology*. https://www.annualreviews.org/doi/10.1146/annurev-immunol-032713-120156 (accessed 2022-11-03).

(12) Tarassishin, L.; Suh, H.-S.; Lee, S. C. Interferon Regulatory Factor 3 Plays an Anti-Inflammatory Role in Microglia by Activating the PI3K/Akt Pathway. *J. Neuroinflammation* **2011**, *8*, 187. https://doi.org/10.1186/1742-2094-8-187.

(13) Nakamura, N.; Tamagawa-Mineoka, R.; Ueta, M.; Kinoshita, S.; Katoh, N. Toll-like Receptor 3 Increases Allergic and Irritant Contact Dermatitis. *J. Invest. Dermatol.* **2015**, *135* (2), 411–417. https://doi.org/10.1038/jid.2014.402.

(14) Schmidt, M.; Raghavan, B.; Müller, V.; Vogl, T.; Fejer, G.; Tchaptchet, S.; Keck, S.; Kalis, C.; Nielsen, P. J.; Galanos, C.; Roth, J.; Skerra, A.; Martin, S. F.; Freudenberg, M. A.; Goebeler, M. Crucial Role for Human Toll-like Receptor 4 in the Development of Contact Allergy to Nickel. *Nat. Immunol.* **2010**, *11* (9), 814–819. https://doi.org/10.1038/ni.1919.

(15) Zhao, X.; Huo, R.; Yan, X.; Xu, T. IRF3 Negatively Regulates Toll-Like Receptor-Mediated NF-KB Signaling by Targeting TRIF for Degradation in Teleost Fish. *Front. Immunol.* **2018**, *9*.

(16) Weber, F. C.; Nemeth, T.; Csepregi, J. Z.; Dudeck, A.; Roers, A.; Ozsvari, E.; Puskas, L.; Thilo, J.; Mocsai, A.; Martin, S. F. Neutrophils Are Required for Both the Sensitization and Elicitation Phase of Contact Hypersensitivity. **2015**, *212* (1), 15–22. https://doi.org/10.1084/jem.20130062.

(17) Yang, K.; Shi, H.; Qi, R.; Sun, S.; Tang, Y.; Zhang, B.; Wang, C. Hsp90 Regulates Activation of Interferon Regulatory Factor 3 and TBK-1 Stabilization in Sendai Virus-Infected Cells. *Mol. Biol. Cell* **2006**, *17* (3), 1461–1471. https://doi.org/10.1091/mbc.e05-09-0853.

(18) Thomson, D. W.; Poeckel, D.; Zinn, N.; Rau, C.; Strohmer, K.; Wagner, A. J.; Graves, A. P.; Perrin, J.; Bantscheff, M.; Duempelfeld, B.; Kasparcova, V.; Ramanjulu, J. M.; Pesiridis, G. S.; Muelbaier, M.; Bergamini, G. Discovery of GSK8612, a Highly Selective and Potent TBK1 Inhibitor. *ACS Med. Chem. Lett.* **2019**, *10* (5), 780–785. https://doi.org/10.1021/acsmedchemlett.9b00027.

(19) Lambrechts, N.; Verstraelen, S.; Lodewyckx, H.; Felicio, A.; Hooyberghs, J.; Witters, H.; Van Tendeloo, V.; Van Cauwenberge, P.; Nelisson, I.; Van Den Heuvel, R.; Schoeters, G. THP-1 Monocytes but Not Macrophages as a Potential Alternative for CD34+ Dendritic Cells to Identify Chemical Skin Sensitizers. **2009**, *236* (2), 221–230. https://doi.org/10.1016/j.taap.2009.01.026.

(20) Mitjans, M.; Galbiati, V.; Lucchi, L.; Viviani, B.; Marinovich, M.; Galli, C. L.; Corsini, E. Use of IL-8 Release and P38 MAPK Activation in THP-1 Cells to Identify Allergens and to Assess Their Potency in Vitro. *Toxicol. Vitro Int. J. Publ. Assoc. BIBRA* **2010**, *24* (6), 1803–1809. https://doi.org/10.1016/j.tiv.2010.06.001.

(21) Helou, D. G.; Noel, B.; Gaudin, F.; Groux, H.; El Ali, Z.; Pallardy, M.; Chollet-Martin, S.; Kerdine-Romer, S. Cutting Edge: Nrf2 Regulates Neutrophil Recruitment and Accumulation in Skin during Contact Hypersensitivity. *J Immunol* **2019**, *202* (8), 2189–2194. https://doi.org/10.4049/jimmunol.1801065.

(22) Fitzgerald, K. A.; McWhirter, S. M.; Faia, K. L.; Rowe, D. C.; Latz, E.; Golenbock, D. T.; Coyle, A. J.; Liao, S.-M.; Maniatis, T. IKKε and TBK1 Are Essential Components of the IRF3 Signaling Pathway. *Nat. Immunol.* **2003**, *4* (5), 491–496. https://doi.org/10.1038/ni921.

(23) Gerberick, G. F.; Ryan, C. A.; Dearman, R.; Kimber, I. Local Lymph Node Assay (LLNA) for Detection of Sensitization Capacity of Chemicals. *Methods* **2007**, *41* (1), 54–60. https://doi.org/10.1016/j.ymeth.2006.07.006.

(24) Gerberick, G. F.; Ryan, C. A.; Kimber, I.; Dearman, R. J.; Lea, L. J.; Basketter, D. A. Local Lymph Node Assay: Validation Assessment for Regulatory Purposes. *Am. J. Contact Dermat. Off. J. Am. Contact Dermat. Soc.* **2000**, *11* (1), 3–18. https://doi.org/10.1053/ajcd.2000.0003.

(25) Kimber, I.; Dearman, R. J.; Scholes, E. W.; Basketter, D. A. The Local Lymph Node Assay: Developments and Applications. *Toxicology* **1994**, *93* (1), 13–31. https://doi.org/10.1016/0300-483x(94)90193-7.

(26) Walker, W. E.; Booth, C. J.; Goldstein, D. R. TLR9 and IRF3 Cooperate to Induce a Systemic Inflammatory Response in Mice Injected With Liposome:DNA. *Mol. Ther.* **2010**, *18* (4), 775–784. https://doi.org/10.1038/mt.2010.1.

(27) Heipertz, E. L.; Harper, J.; Goswami, D. G.; Lopez, C. A.; Nellikappallil, J.; Zamora, R.; Vodovotz, Y.; Walker, W. E. IRF3 Signaling within the Mouse Stroma Influences Sepsis Pathogenesis. *J. Immunol.* **2021**, *206* (2), 398–409. https://doi.org/10.4049/jimmunol.1900217.

(28) Sato, M.; Suemori, H.; Hata, N.; Asagiri, M.; Ogasawara, K.; Nakao, K.; Nakaya, T.; Katsuki, M.; Noguchi, S.; Tanaka, N.; Taniguchi, T. Distinct and Essential Roles of Transcription Factors IRF-3 and IRF-7 in Response to Viruses for IFN-Alpha/Beta Gene Induction. *Immunity* **2000**, *13* (4), 539–548. https://doi.org/10.1016/s1074-7613(00)00053-4.

Chapter 5: Honokiol Reduces Both Sensitization and Elicitation in Allergic Contact Dermatitis

5.1 Summary

Allergic contact dermatitis (ACD) is a condition in which an individual has an inflammatory response to small compounds called haptens. ACD affects up to 20 % of the USA's population and is characterized by a sensitization phase and elicitation phase. In this work, we identify honokiol (HON) as the first known compound to reduce both sensitization and elicitation to dinitrochlorobenzene (DNCB), a model hapten. When mice were treated with both HON and DNCB in the sensitization phase, we observed a net reduction in final ear widths of 24 % compared to mice treated with DNCB alone. In comparison, mice treated with DNCB + hydrocortisone (HC), a topical corticosteroid used to treat the elicitation phase of ACD, displayed no decrease in inflammation compared to DNCB sensitized mice. To test the effect of HON and HC on elicitation, mice challenged with HON + DNCB or HC + DNCB in the elicitation phase had a net reduction in final ear widths of 24 % for HON + DNCB and 68% for HC + DNCB, respectively, compared to DNCB alone. Moreover, we found lower levels of pro-inflammatory cytokines in the ears of both HON + DNCB and HC + DNCB treated mice, suggesting both HON and HC are viable treatments for reducing inflammation in the elicitation phase. We anticipate HON and HC reduce elicitation via their anti-inflammatory activity. From these experiments, we conclude that HON is effective at reducing both sensitization and elicitation. HON is less effective than HC at treating ACD in the elicitation phase but could be a useful alternate treatment in patients that have developed ACD to topical corticosteroids. Moreover, HON could be included in fragrance products to reduce sensitization toward haptens

commonly improved in these products, which could both reduce the prevalence of ACD in the general population and mitigate inflammation in individuals with ACD.

5.2 Introduction

Allergic contact dermatitis (ACD) is estimated to affect up to 20 % of the population in the USA.[1] ACD is typically caused by small, reactive molecules called haptens, which are commonly found in cosmetic and fragrance products. These haptens react with epidermal proteins, such as HSP90, to form a haptenated protein.[2] These haptenated proteins are recognized by the innate immune system, resulting in a pro-inflammatory response.[3] The ACD response occurs in two phases: the sensitization phase followed by the elicitation phase. In the sensitization phase, these haptenated proteins are detected by pattern recognition receptors (PRRs) on skin-resident dendritic cells (DCs), resulting recruitment of immune cells, with T cell and neutrophil recruitment being critical for sensitization.[4,5] These DCs present haptenated peptide to naïve T cells. These T cells become activated, proliferate, and differentiate into hapten-specific T cells.[4] Re-exposure to the same hapten can induce skin inflammation and pro-inflammatory cytokines, which are key characteristics of the elicitation phase.[6]

In addition to T cells, neutrophils are major players in acute inflammation and are essential for sensitization and elicitation.[5,7] After exposure to a hapten, neutrophils are recruited to the exposure site, resulting in further chemokine and cytokine release. A key mediator of this neutrophil recruitment in ACD is NRF2. [5,8] NRF2 is a transcription factor that regulates redox balance and homeostasis.[9] After hapten exposure, NRF2 activity results in upregulation of antioxidant genes and decreased chemokine production, leading to reduced inflammation.[8] As a result, NRF2 could be a potential therapeutic target for mitigating ACD.

Currently, topical corticosteroids are the most common treatment for inflammation in the elicitation phase. Topical corticosteroids are pleotropic compounds that signal through glucocorticoid receptors leading to strong anti-inflammatory biological activity.[10] However, they do not completely irradicate inflammation, long-term use can lead to muscle atrophy, and their role on the initial sensitization to haptens has not been studied.[11] Additionally, roughly 0.5 % of people treated with corticosteroids develop ACD to these compounds.[12] As such, there is a need to find alternative treatments for ACD.

Honokiol is a polyphenolic compound derived from magnolia tree bark and commonly used in Eastern medicine in a variety of therapeutic areas.[13] Recently, several groups have shown that honokiol inhibits the production of reactive oxygen species (ROS) in neutrophils by activating the NRF2 pathway.[14,15] Additionally, honokiol has anti-inflammatory activity through the inhibition of NF-κB, leading to reduction of pro-inflammatory cytokines.[16,17] Given honokiol's NRF2 activity and anti-inflammatory properties, we hypothesized that honokiol could reduce inflammation in the sensitization and elicitation phases of ACD.

5.3 Results

5.3.1 Honokiol & hydrocortisone reduce IL-8 in THP-1 cells after co-stimulation with haptens

To assess whether honokiol (HON) reduces sensitization, we examined its effect on IL-8 levels of THP-1 cells after co-stimulation with known haptens. THP-1 cells are a human monocyte cell line and are a well-established platform for screening sensitization.[18] By screening IL-8 release in THP-1 cells, we can reliably determine the sensitization potential of haptens, since IL-8 is the primary cytokine involved in neutrophil recruitment, and neutrophil recruitment

is essential to sensitization.[19,5] Thus, by evaluating reductions in IL-8 secretion *in vitro*, we can screen compounds, such as HON, to see if they would be potential candidates for reducing sensitization.[19]

To test whether HON could reduce the IL-8 response, we added the following haptens: dinitrochlorobenzene (DNCB), cinnamaldehyde (CINA), citral, and 2-methyl-4-isothiazolin-3-one (MIST) – to THP-1 cells along with HON or hydrocortisone (HC) as indicated. We included HC since it is a commercially available topical corticosteroid that is commonly used to treat ACD. For DNCB, CINA, citral, and MIST, significant reductions in IL-8 secretion was observed by the THP-1 cells that were treated with HON or HC (Figure 5.1). The largest observed decrease in IL-8 secretion was observed in THP-1 cells treated with citral, for which addition of HON or HC reduced IL-8 levels by ~ 70%. Despite the varying chemical reactivity of the haptens used in this screen, HON or HC were generally found to reduce IL-8 expression. We therefore sought to test whether HON and HC would function similarly *in vivo* to inhibit sensitization in a mouse model of ACD.

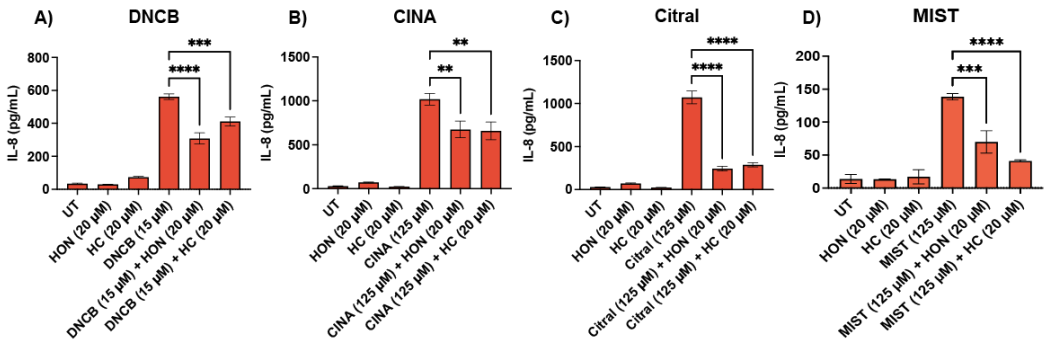

Figure 5.1: Honokiol and hydrocortisone reduce IL-8 levels *in vitro* for various haptens. THP-1s were incubated with indicated compounds for 20 h. IL-8 levels were significantly reduced by inclusion of honokiol or hydrocortisone for each of A) DNCB, B) CINA, C) citral, D) MIST treated cells. N=3. *p<.05, **p<.01, ***p<.001, ****p<.0001

5.3.2 Honokiol reduces sensitization to DNCB in mouse model, while hydrocortisone does not.

To study the effect of HON and HC on sensitization, we performed a local lymph node assay (LLNA). The LLNA is a common procedure for examining ACD in a mouse model.[20] In this assay, a mouse is sensitized to a hapten, typically DNCB, by adding a solution containing the hapten on stomach of a mouse on days 0-1. On days 5-8, the same hapten is added to the back of the ear of the mouse to elicit the ACD response. On day 9, the final ear width is measured, and local cytokine production in the inflamed ear is assayed (Figure 5.2A). For the LLNA, we used a 0.5 % w/v solution of DNCB in a solvent containing 4:1 acetone: olive oil. In the sensitization phase – days 0-1 – of this experiment, 0.7% w/v of HON and 1% w/v of HC were added to the control and DNCB sensitized experimental groups to observe their effect on sensitization. We chose 0.7 % w/v for HON and 1% w/v for HC because this molar ratio of DNCB:HON (or HC) was found to maximally reduce IL-8 levels *in vitro*. Conveniently, HC cream is also sold over the counter at 1% as a treatment for the elicitation phase of ACD.

At the end of the LLNA, we observed a 24% reduction in the final ear widths in mice that were subjected to HON + DNCB during sensitization compared to mice that were only exposed to DNCB during sensitization. (Figure 5.2B-C). Moreover, in the HON+DNCB sensitized mice, a significant decrease cutaneous TNF-α levels was observed compared to mice sensitized with DNCB alone (Figure 5.2D). The reduction in both final ear widths and TNF-α levels indicate that HON effectively reduces sensitization in mice. However, for HC+DNCB sensitized mice, there was no difference in final ear width compared to DNCB-sensitized mice. Additionally, in HC+DNCB sensitized mice, reduction of TNF-α and increase in MCP-1 production were

observed relative to DNCB mice. Based on these data, we conclude that HC does not reduce sensitization in mice, while HON does.

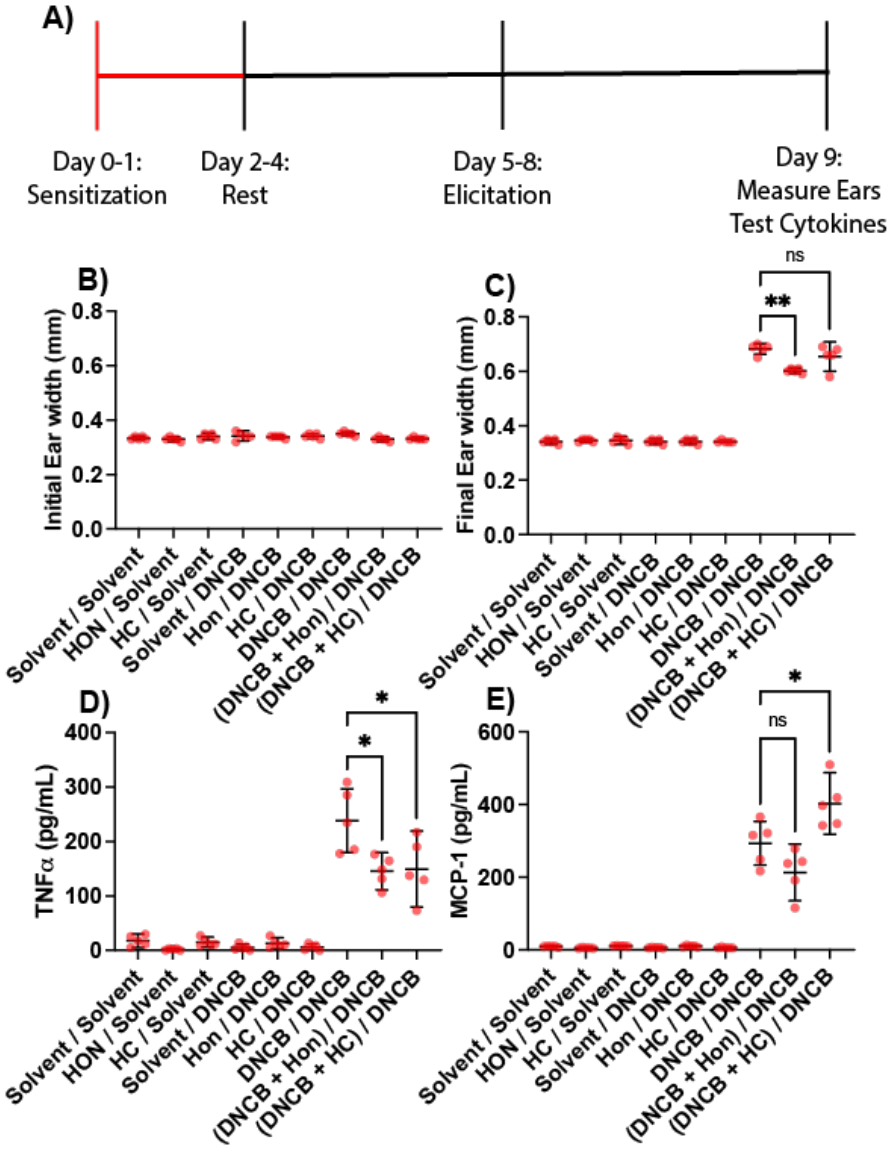

Figure 5.2: Honokiol reduces sensitization in mice; hydrocortisone does not. A) Experimental timeline, in which honokiol or hydrocortisone were added during the sensitization phase (highlighted in red) as indicated. B) Ear widths of mice before elicitation phase. Treatment groups are labeled as "Sensitization phase treatment / Elicitation phase treatment". For example, a group labeled "HON / Solvent" received honokiol during sensitization phase and the delivery solvent in the elicitation phase. C) Ear widths of the mice on day 9, just before sacrifice. D, E) Cytokines in the ear were measured on day 9, with significant results observed for TNF-α and MCP1. N=5. *p<.05, **p<.01.

5.3.3 Hydrocortisone and honokiol both reduce inflammation during the elicitation phase of ACD

After assessing whether HON and HC reduce sensitization, we thought it would be important to test whether they reduce elicitation since long-term use of topical corticosteroid use can have negative health effects. To study the effect of HON and HC on elicitation, we performed a similar LLNA. In this second iteration, no HON or HC was used during the sensitization phase; instead, we subjected the mice to HON or HC, along with DNCB, as indicated during the elicitation phase on days 5-8 (Figure 5.3A). For example, an experimental group denoted as DNCB/(HON+DNCB) was treated with DNCB during the sensitization phase, and then was subjected to HON + DNCB in the elicitation phase.

At the end of the elicitation phase, we observed significant 24 % decrease in the final ear widths of mice treated with DNCB/(HON+ DNCB) compared to the DNCB/DNCB mice (Figure 5.3B-C). Similarly, TNF-α and IL-6 levels were reduced for DNCB/(HON+ DNCB) mice (Figure 5.3D-F). For DNCB/(HC+ DNCB) mice, we observed a 68% decrease in net ear widths compared to DNCB/DNCB mice. Moreover, there were strong reductions in TNF-α, IL-6, and MCP-1 for DNCB/(HC+ DNCB) treated mice. This reduction in ear width and pro-inflammatory cytokine production is expected, as HC is already used to treat the elicitation phase in ACD. Compared to HON, HC more strongly reduced ear inflammation and pro-inflammatory cytokine production in the elicitation phase. However, it is important to note that HON is the first known compound to reduce both elicitation and sensitization phase in ACD. Consequently, the inclusion of HON in products with known haptens could reduce the impact of ACD on the general population.

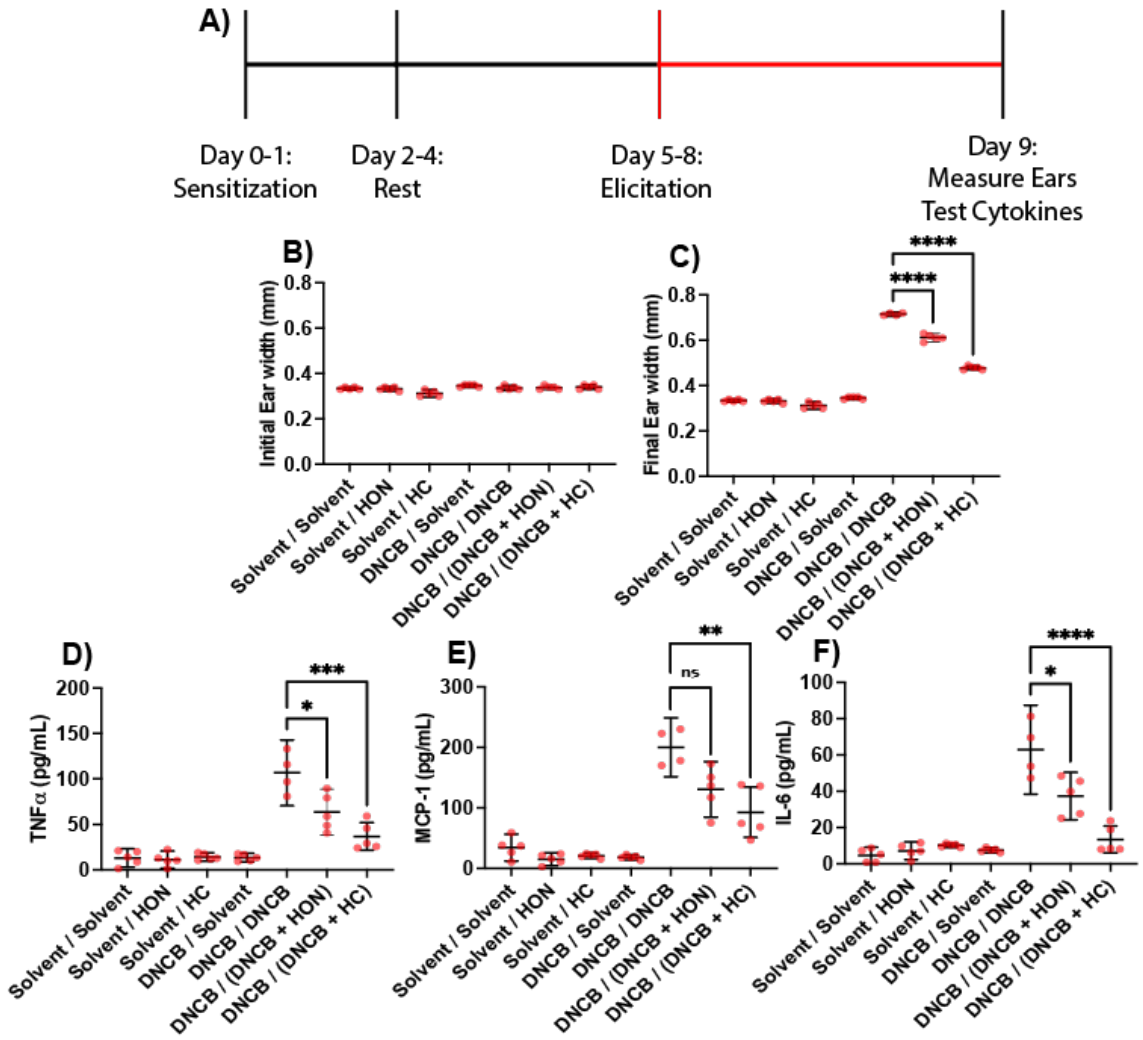

Figure 5.3) Honokiol and hydrocortisone reduce inflammation in elicitation. A) Experimental timeline, in which mice were treated with honokiol or hydrocortisone, as indicated, during the elicitation phase (highlighted in red). B) Ear widths of mice before elicitation phase. C) Ear widths of the mice on day 9, just before sacrifice. D,E, F) Cytokines in the ear were measured on day 9, with significant reduction observed in mice treated with DNCB + HON and DNCB + HC in the elicitation phase compared those treated with DNCB for TNF-α, MCP1, and IL-6. N=5. *p<.05, **p<.01, ***p<.001, ****p<.0001.

5.4 Discussion & Conclusion

In this study, we report that HON reduces both sensitization and elicitation to DNCB in a mouse model – the first known compound to reduce both phases of ACD. We first screened

HON and HC *in vitro* for their potential to reduce sensitization. After observing a decrease of secreted IL-8 in THP-1 monocytes treated with DNCB and either HON or HC compared to DNCB, we further screened these compounds' abilities to reduce sensitization *in vivo*. When mice were subjected to DNCB + HON in the sensitization phase, the final ear widths were reduced and there was lower cutaneous TNF-α levels than DNCB sensitized mice. We hypothesize that HON reduces sensitization through its NRF2 activity. NRF2 is a transcription factor that is activated to ameliorate oxidative stress.[21] Haptens are small, reactive molecules that induce oxidative stress in cells. As such, NRF2 inhibits sensitization by mitigating the oxidative stress experienced by cells after hapten exposure.[21] We expect HON's anti-inflammatory activity to play a lesser role in sensitization, since HC, a potent anti-inflammatory, did not reduce sensitization, even though inflammatory signaling is a key event in the early sensitization stage. One event that is critical for sensitization is neutrophil recruitment, and HC is known to increase neutrophil counts at the site of exposure for up to 24 h.[5,22] Since MCP-1 is involved in neutrophil recruitment and MCP-1 levels were increased for HC + DNCB sensitized mice, it is possible that neutrophil recruitment is counteracting HC's overall anti-inflammatory properties during sensitization.

In the elicitation phase, we observed reductions in inflammation in both DNCB/(DNCB + HON) and DNCB/(DNCB+HC) mice compared to DNCB/DNCB treated mice. The elicitation phase is characterized by the presence of skin inflammation and cytokine release upon re-exposure to haptens. As such, we expect the anti-inflammatory properties of HON and HC to be key to this reduction of ear widths and cytokine levels. As a common treatment for the elicitation phase of ACD, HC drastically reduced inflammation. However, roughly 0.5 % of patients that develop ACD to topical corticosteroids, and chronic exposure to topical

corticosteroids can lead to muscle atrophy, bone loss, and diabetes.[12,23,24,25] Notably, there was a significant reduction of elicitation in DNCB/(DNCB + HON) treated mice. Considering HON is already used in Eastern medicine without obvious toxicity, HON could be a valuable, alternate treatment for patients that develop negative side effects to topical corticosteroids. Since haptens are commonly found in fragrance products, HON could be included in these types of products to reduce sensitization to a breadth of haptens. Given these results, we hope that HON can ameliorate the impact of ACD in the general population.

5.5 Materials and Methods

All chemicals were bought from Sigma Aldrich unless otherwise noted. Honokiol was purchased from Tokyo Chemistry Industry. 6-week-old BALB/cByJ mice were purchased from Jackson Laboratory and housed under controlled light, temperature, and humidity conditions. All experiments were conducted with the approval of the University of Chicago Institutional Animal Care and Use Committee, and animals were maintained in accordance with guidelines and regulations of the National Institutes of Health.

Cell Culture:

Human monocyte cell line THP-1 was obtained from American Type Culture Collection and grown in RPMC 1640 medium (Life Technologies) supplemented 10 % with fetal bovine serum (Thermo Fisher Scientific) and 1 % antibiotic-antimycotic (Thermo Fisher Scientific) at 37 ^{O}C in 5 % CO_2 incubator.

***In vitro* IL-8 Screening:**

For the assay, THP-1 cells were plated at 1 million/mL in a 24 well plate. Honokiol or hydrocortisone were added to the indicated samples to achieve a final concentration of 20 μM.

After 5 min, the hapten was added. The THP-1s were incubated for 16-20 h. The cells were centrifuged at 300 x G for 5 mins, and the supernatant was subsequently collected to measure IL-8 secretion. IL-8 was quantified with IL-8 ELISAMAX (BioLegend) using the manufacturer's procedure, and absorbance was analyzed using a Multiskan FC plate reader (Thermo Scientific) at 450 nm.

Cell Viability:

At the end of IL-8 screen, the THP-1 cells were resuspended in 100 µL media. 5 mg of 3-(4,5-dimethylthiazol-2-yl)-2,5-diphenyltetrazolium bromide (MTT) was dissolved in 1 mL PBS. 10 µL MTT solution was added to the cells. After 3 hours, 65 µL of cell supernatant was added to 100 µL of DMSO and incubated at 37 ^{O}C for 10 min. The absorbances were analyzed using a Multiskan FC plate reader (Thermo Scientific) at 570 nm to assess viability.

Contact Hypersensitivity Animal Model:

Mice were allowed to acclimatize for 1 week prior to the start of experimentation and used at 6-8 weeks of age. The abdomen of the mice was shaved with a razor. On days 0 and 1, the mice were sensitized with 25 µL of solvent (1:4 v/v olive oil/acetone) containing 0.5 % w/v DNCB with 0.7% HON or 1% HC as indicated. After 3 days of rest, the mice were challenged on days 5-8 on the back of the ear with 10 µL solvent or solutions as indicated. On day 9, the final ear widths were measured, mice were sacrificed, and ears were excised. The ears were mechanically homogenized on ice in 0.5 mL of RPMI. The protein was retrieved by centrifuging at 20,000 g at 4 ^{O}C for 20 min and collecting the supernatant. Cutaneous cytokine levels were quantified using CBA Mouse Inflammation Kit (BD Biosciences) according to the manufacturer's procedure and analyzed on a NovoCyte Flow Cytometer (ACEA Biosciences).

Statistical Analyses: Statistical analyses were performed using GraphPad Prism. Comparisons between two or more groups were performed using two-way ANOVA with Tukey's multiple comparison test. Graphs report the mean with standard deviation unless noted otherwise in the caption.

5.6 References

(1) Adler, B. L.; Deleo, V. A. Allergic Contact Dermatitis. *JAMA Dermatol.* **2021**, *157* ((3):364). https://doi.org/doi:10.1001/jamadermatol.2020.5639.

(2) Kim, S.-M.; Studnitzer, B.; Esser-Kahn, A. Heat Shock Protein 90's Mechanistic Role in Contact Hypersensitivity. *J Immunol* **2022**. https://doi.org/10.4049/jimmunol.2101023.

(3) St. Mazard, P.; Rosieres, A.; Krasteva, M.; Berard, F.; Dubois, B.; Kaiserlian, D.; Nicolas, J.-F. Allergic Contact Dermatitis. *Eur J Dermatol* **2004**, *14*, 284–295.

(4) Kaplan, D. H.; Igyarto, B. Y.; Gaspari, A. A. Early Immune Events in the Induction of Allergic Contact Dermatitis. **2012**, *12* (2), 114–124.

(5) Weber, F. C.; Nemeth, T.; Csepregi, J. Z.; Dudeck, A.; Roers, A.; Ozsvari, E.; Puskas, L.; Thilo, J.; Mocsai, A.; Martin, S. F. Neutrophils Are Required for Both the Sensitization and Elicitation Phase of Contact Hypersensitivity. **2015**, *212* (1), 15–22. https://doi.org/10.1084/jem.20130062.

(6) Kondo, S.; Pastore, S.; Shivji, G. M.; McKenzie, R. C.; Sauder, D. N. Characterization of Epidermal Cytokine Profiles in Sensitization and Elicitation Phases of Allergic Contact Dermatitis as Well as Irritant Contact Dermatitis in Mouse Skin. *Lymphokine Cytokine Res* **1994**, *13* (6), 367–475.

(7) Kolaczkowska, E.; Kubes, P. Neutrophil Recruitment and Function in Health and Inflammation. *Nat Rev Immunol* **2013**, No. 13, 159–175.

(8) Helou, D. G.; Noel, B.; Gaudin, F.; Groux, H.; El Ali, Z.; Pallardy, M.; Chollet-Martin, S.; Kerdine-Romer, S. Cutting Edge: Nrf2 Regulates Neutrophil Recruitment and Accumulation in Skin during Contact Hypersensitivity. *J Immunol* **2019**, *202* (8), 2189–2194. https://doi.org/10.4049/jimmunol.1801065.

(9) Mia, Q. Role of Nrf2 in Oxidative Stress and Toxicity. *Annu Rev Pharmacol Toxicol.* **2013**, *53*, 401–426. https://doi.org/10.1146/annurev-pharmtox-011112-140320.

(10) Scheschowitsch, K.; Leite Alves, J.; Assreuy, J. New Insights in Glucocorticoid Receptor Signaling—More Than Just a Ligand-Binding Receptor. *Front Endocrinol* **2018**. https://doi.org/10.3389/fendo.2017.00016.

(11) Ference, J. D.; Last, A. R. Choosing Topical Corticosteroids. *Am Fam Physician.* **2009**, *79* (2), 135-140.

(12) Vatti, R. R.; Ali, F.; Teuber, S.; Chang, C.; Gershwin, M. E. Hypersensitivity Reactions to Corticosteroids. *Clin Rev Allergy Immunol* **2014**, *47* (1), 36–37. https://doi.org/10.1007/s12016-013-8365-z.

(13) Chen, C.; Zhang, Q.-W.; Ye, Y.; Lin, L.-G. Honokiol: A Naturally Occurring Lignan with Pleiotropic Bioactivities. *Chin J Nat Med* **2021**, *19* (7), 481–490. https://doi.org/10.1016/S1875-5364(21)60047-X.

(14) Liou, K.-T.; Shen, Y.-C.; Chen, C.-F.; Tsao, C.-M.; Tsai, S.-K. The Anti-Inflammatory Effect of Honokiol on Neutrophils: Mechanisms in the Inhibition of Reactive Oxygen Species

Production. *Eur J Pharmacol* **2003**, *475* (1–3), 19–27. https://doi.org/10.1016/s0014-2999(03)02121-6.

(15) Okayama, Y. Oxidative Stress in Allergic and Inflammatory Skin Diseases. *Curr Drug Targets Inflamm Allergy* **2005**, *4* (4), 517–519. https://doi.org/10.2174/1568010054526386.

(16) Fried, L. E.; Arbiser, J. L. Honokiol, a Multifunctional Antiangiogenic and Antitumor Agent. *Antioxid Redox Signal.* **2009**, *11* (5), 1139–1148. https://doi.org/10.1089/ars.2009.2440.

(17) Kai-Wing Tse, A.; Wan, C.-K.; Shen, X.-L.; Yang, M.; Fong, W.-F. Honokiol Inhibits TNF-Alpha-Stimulated NF-KappaB Activation and NF-KappaB-Regulated Gene Expression through Suppression of IKK Activation. *Biochem Pharmacol.* **2005**, *70* (10), 1443–1457. https://doi.org/10.1016/j.bcp.2005.08.011.

(18) Lambrechts, N.; Verstraelen, S.; Lodewyckx, H.; Felicio, A.; Hooyberghs, J.; Witters, H.; Van Tendeloo, V.; Van Cauwenberge, P.; Nelisson, I.; Van Den Heuvel, R.; Schoeters, G. THP-1 Monocytes but Not Macrophages as a Potential Alternative for CD34+ Dendritic Cells to Identify Chemical Skin Sensitizers. **2009**, *236* (2), 221–230. https://doi.org/10.1016/j.taap.2009.01.026.

(19) Mitjans, M.; Galbiati, V.; Lucchi, L.; Viviani, B.; Marinovich, M.; Galli, C. L.; Corsini, E. Use of IL-8 Release and P38 MAPK Activation in THP-1 Cells to Identify Allergens and to Assess Their Potency in Vitro. **2010**, *24*, 1803–1808. https://doi.org/10.1016/j.tiv.2010.06.001.

(20) Gerberick, G. F.; Ryan, C. A.; Dearman, R.; Kimber, I. Local Lymph Node Assay (LLNA) for Detection of Sensitization Capacity of Chemicals. *Methods* **2007**, *41* (1), 54–60. https://doi.org/10.1016/j.ymeth.2006.07.006.

(21) Helou, D. G.; Martin, S. F.; Pallardy, M.; Chollet-Martin, S.; Kerdine-Romer, S. Nrf2 Involvement in Chemical-Induced Skin Innate Immunity. *Front Immunol* **2019**, *10* (1004). https://doi.org/10.3389/fimmu.2019.01004.

(22) Olnes, M. J.; Kotliarov, Y.; Biancotto, A.; Cheung, F.; Chen, J.; Shi, R.; Zhou, H.; Wang, E.; Tsang, J. S.; Nussenblatt, R. Effects of Systemically Administered Hydrocortisone on the Human Immunome. *Sci Rep* **2016**, *6* (23002). https://doi.org/10.1038/srep23002.

(23) Braun, T. P.; Marks, D. L. The Regulation of Muscle Mass by Endogenous Glucocorticoids. *Front. Physiol.* **2015**. https://doi.org/10.3389/fphys.2015.00012.

(24) Picado, C.; Luengo, M. Corticosteroid-Induced Bone Loss. Prevention and Management. *Drug Saf.* **1996**, *15* (5), 347–359. https://doi.org/10.2165/00002018-199615050-00005.

(25) Phan, K.; Smith, S. D. Topical Corticosteroids and Risk of Diabetes Mellitus: Systematic Review and Meta-Analysis. *J Dermatolog Treat* **2021**, *32* (3). https://doi.org/10.1080/09546634.2019.1657224.

(26) Gerberick, G. F.; Ryan, C. A.; Kimber, I.; Dearman, R. J.; Lea, L. J.; Basketter, D. A. Local Lymph Node Assay: Validation Assessment for Regulatory Purposes. *Am. J. Contact Dermat. Off. J. Am. Contact Dermat. Soc.* **2000**, *11* (1), 3–18. https://doi.org/10.1053/ajcd.2000.0003.

(27) Kimber, I.; Dearman, R. J.; Scholes, E. W.; Basketter, D. A. The Local Lymph Node Assay: Developments and Applications. *Toxicology* **1994**, *93* (1), 13–31. https://doi.org/10.1016/0300-483x(94)90193-7.

(28) Schmidt, M.; Raghavan, B.; Müller, V.; Vogl, T.; Fejer, G.; Tchaptchet, S.; Keck, S.; Kalis, C.; Nielsen, P. J.; Galanos, C.; Roth, J.; Skerra, A.; Martin, S. F.; Freudenberg, M. A.; Goebeler, M. Crucial Role for Human Toll-like Receptor 4 in the Development of Contact Allergy to Nickel. *Nat. Immunol.* **2010**, *11* (9), 814–819. https://doi.org/10.1038/ni.1919.

Supplemental

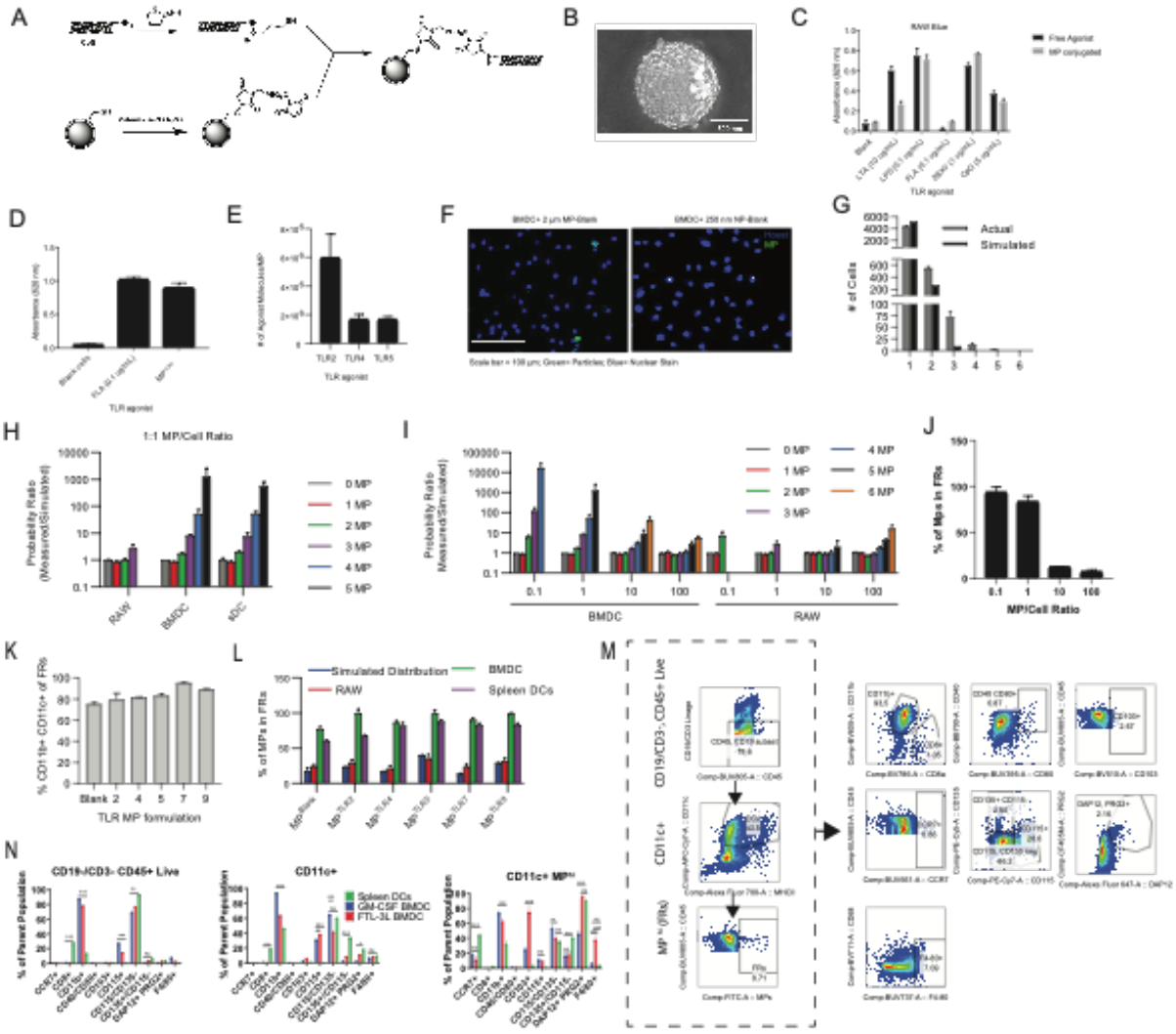

Figure S1. FRs contain a statically improbable number of TLR agonist-conjugated MPs. Related to Figure 1 and 2. (A) Chemistry schematic of the thiol-maleimide chemistry for TLR agonist conjugation (B)SEM of MPTLR4 , scale bar= 500 nm. (C) RAW Blue assay of TLR conjugated MP (grey) with free agonist (black) for comparison, note that RAWs do not express TLR5. (D) HEK-mTLR5 assay for free flagellin (FLA) and flagellin conjugated MPs. (E) Calculation of the number of molecules per MP via BCA assay using free agonists as standard curves. (F) Representative confocal images of BMDCs treated with either 2 µm MPs (MPblank, left) or unconjugated 250 nm NPs (right). (G) 100K Spleen DCs were incubated with 100K of varying MP formulations for 15 minutes, washed and then analyzed via ImageStream. The number of MPs uptaken by each cell was determined using the "spot counter" function on the IDEAS software and the percentage of all MPs in FRs was calculated. Simulated values estimate the number of MPs in the top 5% of MP signal using the Poisson distribution and the average number of MPs/Cells. The number of cells was normalized to 10k total MPs uptaken per sample. The number of cells with 1-6 MPs in these samples (actual) were compared to a random Poisson distribution (simulated). (H) This analysis was repeated and includes RAW cells and BMDCs and a ratio of the actual/simulated (probability ratio) was determined. (I) Repeated analysis from part H but varying the ratio of MPs to cells. (J) MP:Cell ratios change percentage of MP uptaken in FR populations. 1 million BMDCs were incubated with MPTLR4 at various cell to MP ratios for 15 mins, washed and then analyzed via Imagestream analysis (100K cells analyzed). The total number of MPs uptaken were calculated and compared to the MPs uptaken in the FR population (top 5% of MP signal). (K) 10 million splenocytes were incubated with 10 million MP conjugated with various TLR agonists for 15 mins, stained on ice and analyzed via spectral flow. The percent of cDC2 cells in the FR subpopulation was calculated. (L) Similar to fig 1B, the result from part K was compared to a random Poission distribution. (M) FRs are not selectively uptaken by a subset of BMDCs. BMDCs were generated via GM-CSF or FTL-3L or splenocytes were incubated with MP^{blank}(1:1 for BMDCs, 1:5 for splenocytes MP:cell) for 15 min, washed and stained for cell surface markers. Gating strategy. (N) % of cell population in various compartments for (left) all CD19/CD3- CD45+ live cells, (middle) all CD11c+ cells or (right) CD11c+ MP^{hi}population. part N; N=5 for all other N=3, error bars are ± SD. Significance was determined by two-way ANOVA *p<0.05, **p<0.01, ***p<1x10-4 and NS= not significant.

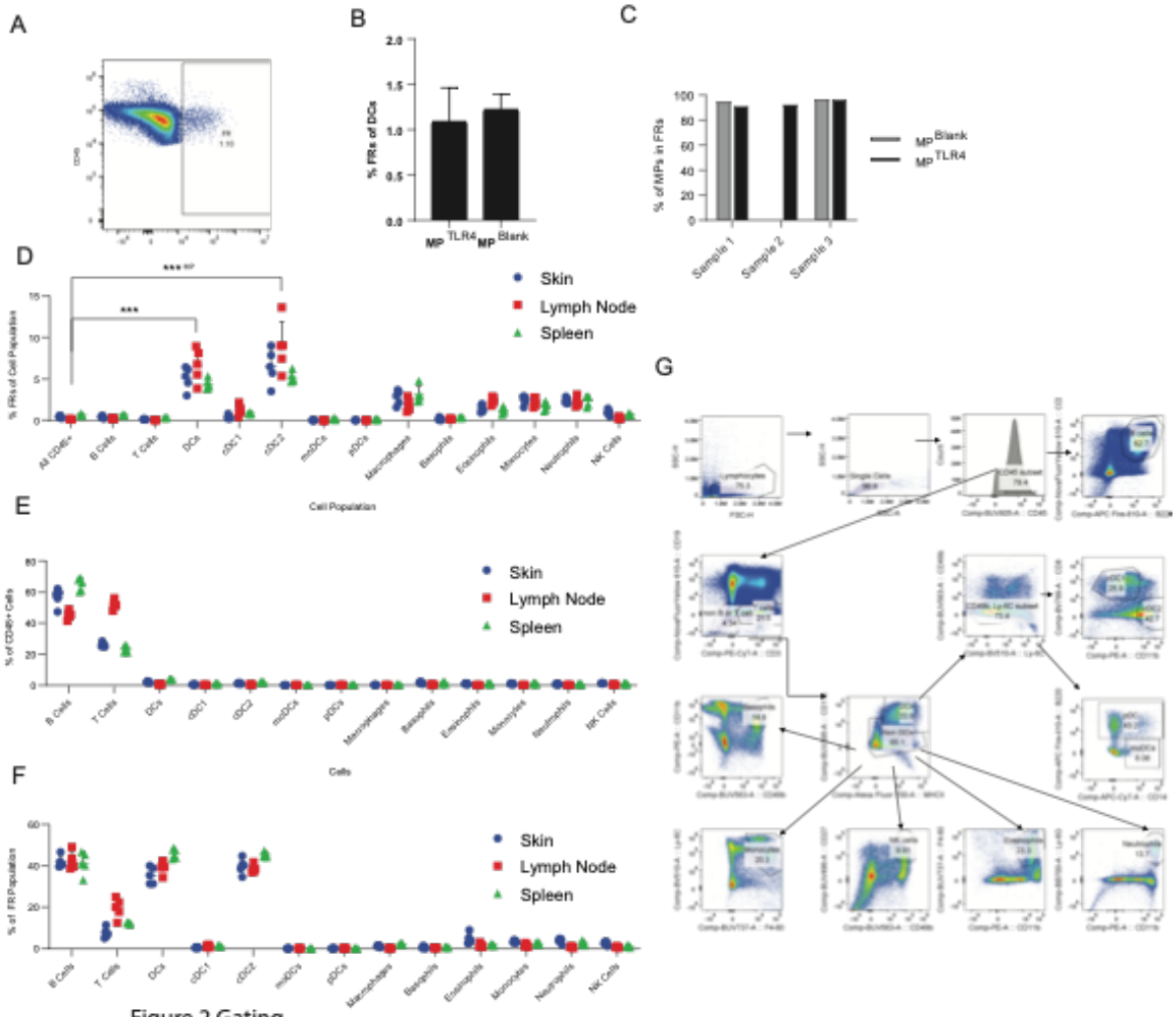

Figure 2 Gating

Figure S2. DCs are overrepresented in the FR substate when isolated via MP uptake and moDCs have FR populations. Related to figure 1 and 2. (A) Representative flow plot of MP uptake showing that the distinct FR population of about 1%. (B) Analysis of three different patient samples for FR % with uptake of MP-TLR4 or MP-Blank. (C) Imagestream analysis of moDC MP uptake. Samples from Figure 1C were gated on FR+ populations by high MP uptake (see figure 1A). (D) Percent FRs in various cell population. (E) Full cell breakdown of mouse samples (F) cells were gated on FRs then phenotyped into various population. (G) Splenocyte/lymph node/skin cell gating strategy for FR phenotyping experiment. Mouse spleens, lymph nodes and footpads were disassociated, treated with MPTLR4 at 1:1 MP:cell and stained for various immune markers. N=5 biological samples. (H) Gating strategy for ICS experiments in figure 2. (I) Controls for ICS experiments showing fully stained LPS stimulated splenocytes (red) and FMO control for intracellur cytokine (blue) for TNFa (left) or IFNb (right). Significance was determined by two-way ANOVA *p<0.05, **p<0.01, ***p<1x10-4 and NS= not significant.

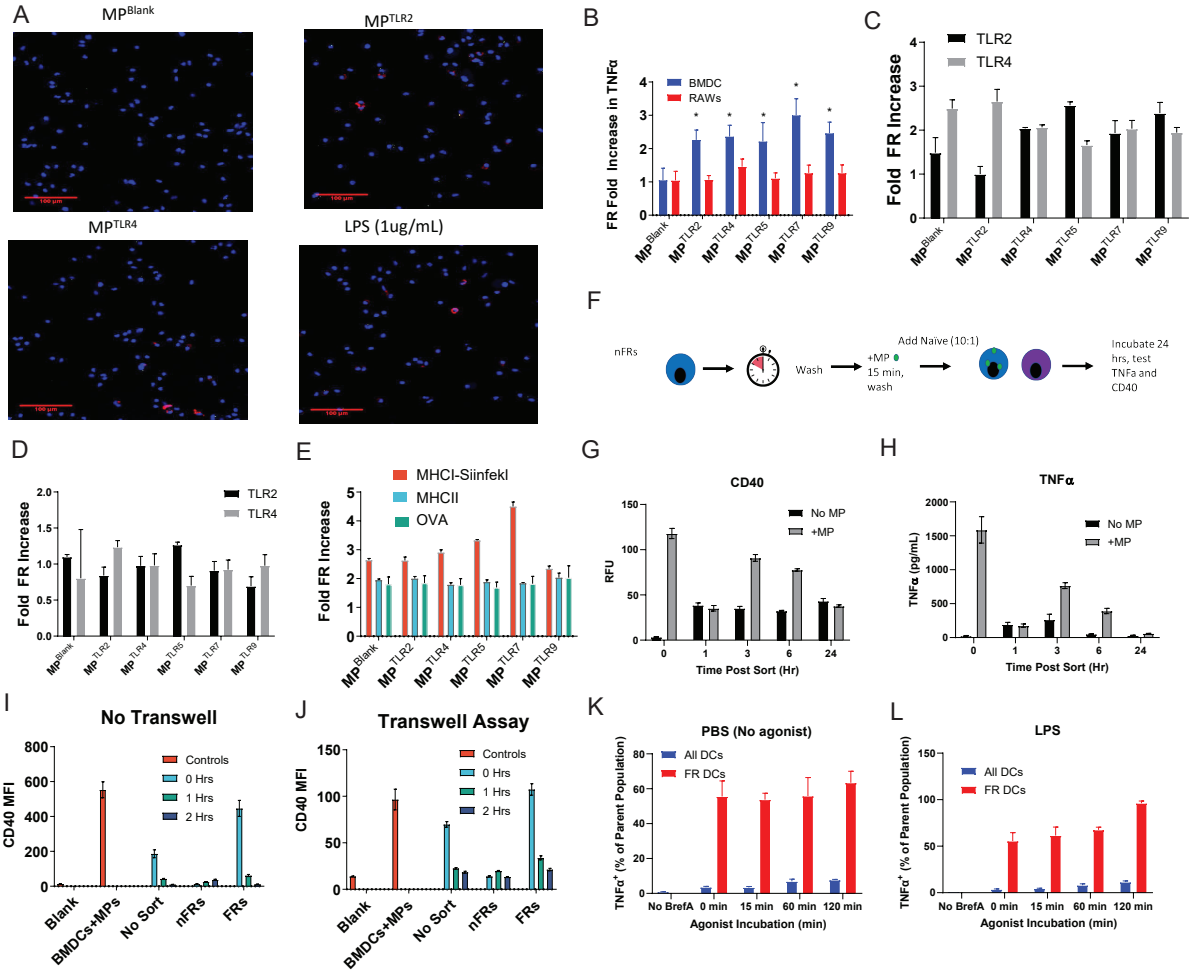

Figure S3. FRs have increased TNFα and MHC expression but not TLR and seem to cycle through FR populations. Related to figure 2. (A) 10k BMDCs were incubated on a coverslip and then treated with MP-Blank MP-TLR2, MP-TLR4 or free LPS (1 ug/mL) for 15 mins, then washed an incubated with brefeldin A for 4 hrs (0.5 ug/mL). Cells were then fixed, permeabilized and stained for TNFa (red) and the nucleus (Blue). Note that TNFα expression is concentrated in a small number of cells. (B) Expanded data from figure 2A, showing BMDCs treated with all TLR-MPs. FRs do not have increased TLR expression. 100k cells were incubated with various MP formulations for 15 mins in a 1:1 ratio, washed and then stained for either TLR2 and TLR4 expression. The fold TLR expression increase between FRs and nFRs is calculated. (C) BMDCs, (D) monocyte derived DCs (moDCs). Significance for C and D was calculated between untreated cell and MP treated cells. (E) FRs have increased MHC expression and antigen presentation in vitro. 1 million BMDCs were incubated with OVA-AF647 (10 ug/mL) for 3 hrs with 1 million MPs then stained for MHCII and MHCI-SIINFEKL. Fold increase calculated from CD11c+ cells FR/nFRs. (F) Schematic of experiment. (G) 100k non-FR (sorted out from experiment in figure 3C/D) were allowed to incubate for various timepoints, then restimulated with MPTLR4 for 15 mins (1:1), washed and then added to naïve BMDCs (10 naïve:1 non-FRs) then tested for CD40 expression or (H) TNFα. (I) Naïve BMDCs were stimulated at 1:1 ratio with MPTLR4 and isolated the FRs and non-FRs via FACS. After 0, 1, or 2 h incubation, FRs, non-FRs, and unsorted BMDCs were added to 1 million naïve BMDCs in a 1:10 ratio. After 16 hr, CD40 expression was measured via conventional flow cytometry. (J) Same experiment as I, but the naïve BMDCs were plated on the bottom section of a transwell assay and the MP-stimulated FRs, non-FRs, and unsorted BMDCs were plated on top of the membrane. Kinetic ICS of FRs vs all DCs. Raw data used to generate ratios in figure 2G. Splenocytes were treated with (K) PBS, (L) 100 ng/mL LPS in the FR kinetic experiment described in figure 2G. Results showing TNFα+ populations for all DCs (blue) vs FRs (red). N=5 mice per group. +/- indicate SD. Significance was determined by two-way ANOVA *p<0.05, **p<0.01, ***p<1x10-4 and NS= not significant.

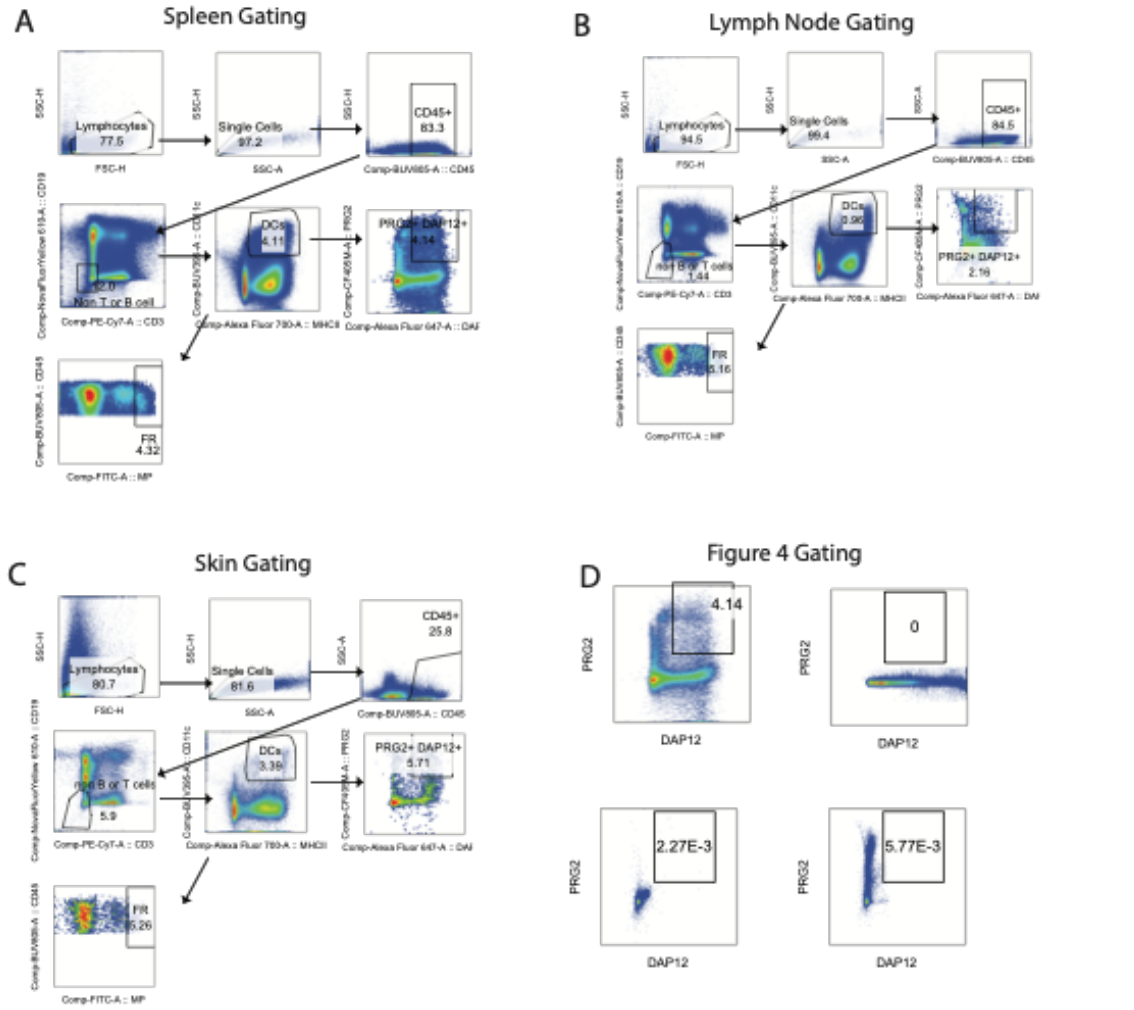

Figure S4. Gating Strategy for FR flow cytometry analysis. Related to figure 2, 4 and 5. Gating strategies for murine tissue analyzed in figure 4 for (A) spenocytes, (B) lymph nodes or (C) skin. (D) Controls for figure 4 flow cytometry. (top left) full stain control for FR surface markers, gated on single, CD45+ CD11c+, MHCII hi splenocytes. (top right) FMO control of same cells without PRG2 antibody (bottom right) FMO control of same cells without DAP12 antibody. (bottom left) isotype control without gating. (E) (top) gating strategy for PRG2+ cells, DAP12+ cells and liposome + cells. (bottom) FMO controls without MP (shown in blue) or without (left) PRG2, (middle) DAP12 or (right) liposome (shown in red).

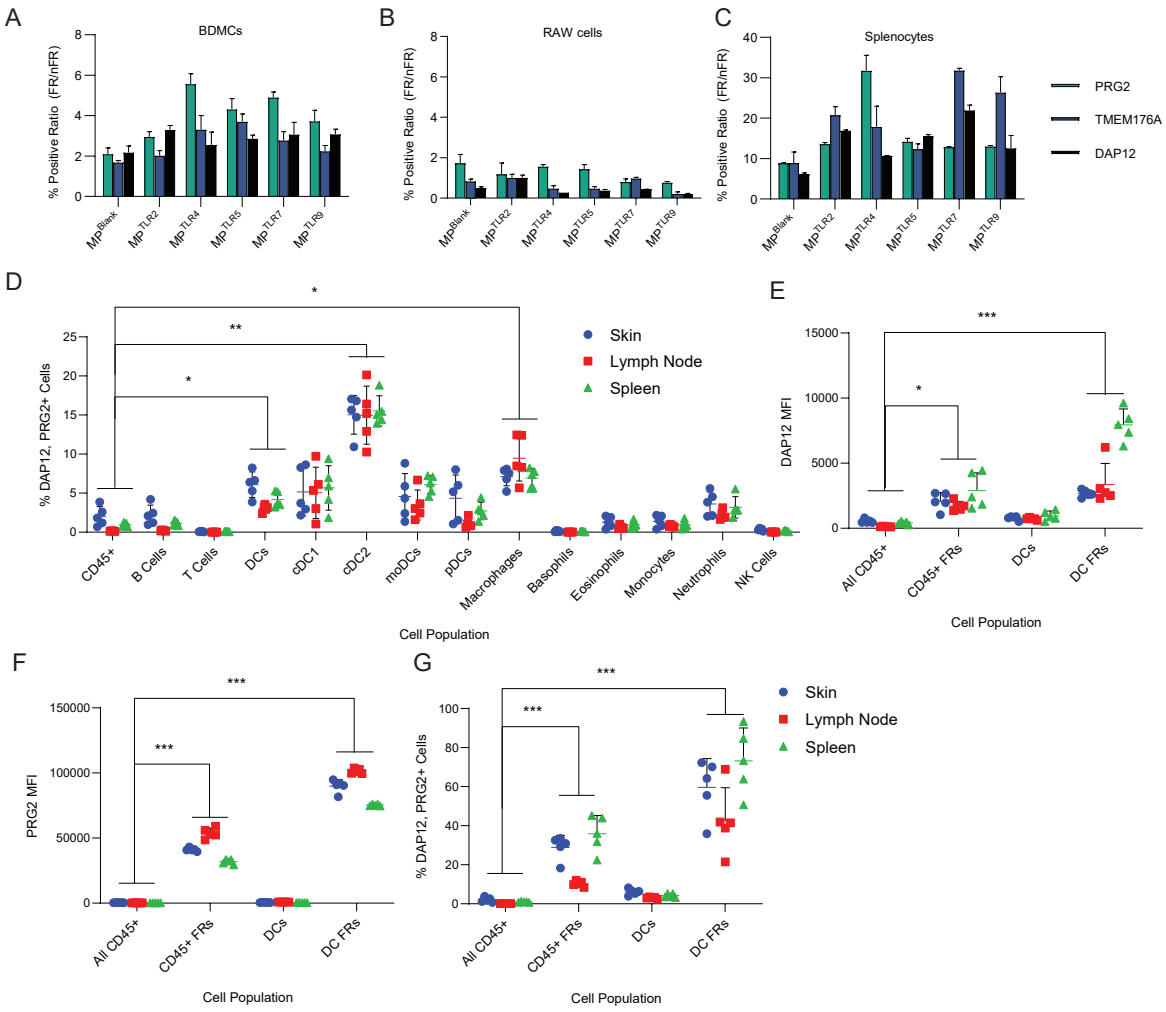

Figure S5. FRs overexpress FR related cell surface markers. (A) 1 million BMDCs, (B) 1 million RAW cells or (C) 1 million splenocytes were incubated with MP of various formulations for 15 mins, washed and stained for antibodies for the listed cellular markers as well as CD11c+. Note that A and C were gated on CD11c+ populations. The ratio of protein positive cells in "FR" population (i.e. cells with the top 5% of MP signal) were divided by non-FR population to calculate FRs overexpress PRG2 and DAP12 receptor, while most cell do not. (D-G) Skin, lymph node and spleen cells from figure 4 were phenotyped for immune cell populations and DAP12/PRG2 coexpression. (D) Coexpression of DAP12/PRG2 on various immune cell populations. (E) DAP12 MFI (F) PRG2 MFI and (G) DAP12/PRG2+ cell population for all CD45 cell or DCs, both all cells and FR populations. Each group had N=5 mice, error bars indicate ±SD. Significance was determined by two-way ANOVA *p<0.05, **p<0.01, ***p<1x10-4 and NS= not significant. Related to Figure 4.

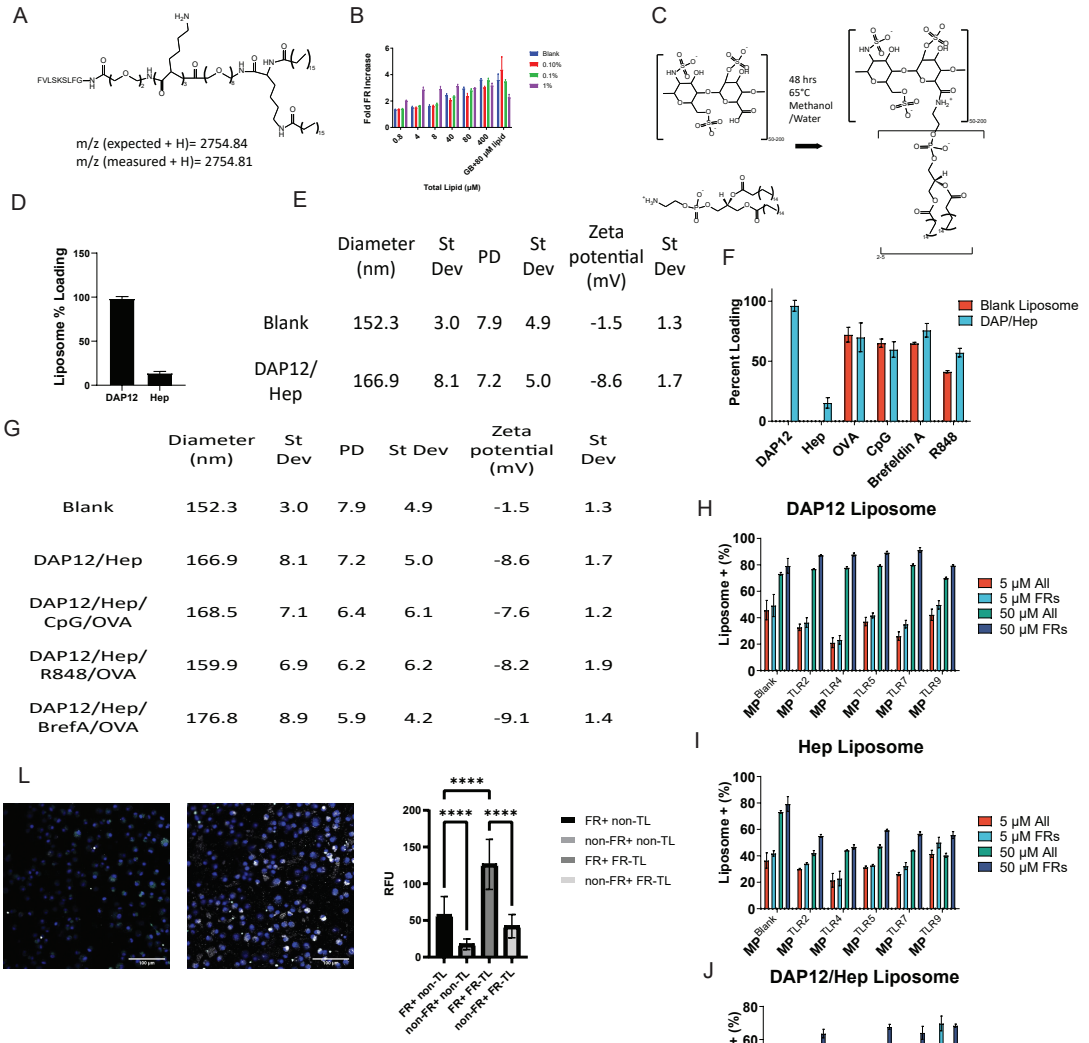

Figure S6. FR Targeting liposome characterization. Related to figure 5. (A) DAP12 targeting peptide was conjugated to a palmitic acid tail, purified via HPLC and characterized via MS. (B) DAP12 lipid was loaded at 0.01, 0.1 and 1 % and with 0.1% DiD and incubated with BMDCs for 15 mins, washed and then incubated with MPTLR4 (1:1) for 15 mins, washed and analyzed via flow cytometry. (C) Chemistry of heparin sulfate-lipid. (D) HPLC analysis of DAP12/heparin lipid. Liposomes were synthesized with DAP12 peptide (1%) and heparin at (10%) (DAP/Hep) and then dialyzed with 10kDa filters in PBS for 24 hrs. Loading was calculated against a standard curve via HPLC. (E) DLS analysis of 200 nm liposomes. (F-G) 200 nm liposomes were synthesized at 10 mM total lipid and loaded with OVA (1 mg/mL) and OVA plus CpG (.2 mg/mL), R848 (.2 mg/mL) or Brefeldin A (1 mg/mL), dialyzed for 24 hrs with a 10 kDa membrane against PBS. (F) HPLC analysis of loading and (G) DLS analysis of liposomes. (H-I) FR targeting liposomes are most effective with both DAP12 targeting and heparin sulfate-lipid. DiD loaded (0.1%) liposomes were prepare with (H) DAP12 targeted peptide-lipid at 1% (I) heparin-lipid at 1% or (J) both. BMDCs were incubated with liposomes for 15 mins, washed and then incubated with MPs (1:1) for 15 mins then washed and analyzed via flow. (K) Brefeldin A loaded liposomes suppress global DC activation only when targeted to FRs. 500k BMDCs were incubated with liposomes with or without targeted loaded with brefeldin A (loaded at 1% total lipid) the incubated for 1 hr and washed and incubated with 1 ug/mL of R848 for 16 hrs, then tested for CD40 expression via flow cytometry. (L) Quantification of FR-TL confocal experiment in Figure 5F. (left) wide field microscopy image of non-TL (10 uM)+ MP+BMDCs (middle) image of FR-TL (10 uM) + MP + BMDCs. (Right) Quantification of images. 3 images from three separate wells with >100 cells per image were analyzed via Fuji and average RFU of liposome intensity calculated. All experiments were performed in biological triplicates, error bars indicate ±SD.Significance was determined by two-way ANOVA *p<0.05, **p<0.01, ***p<1x10-4 and NS= not significant

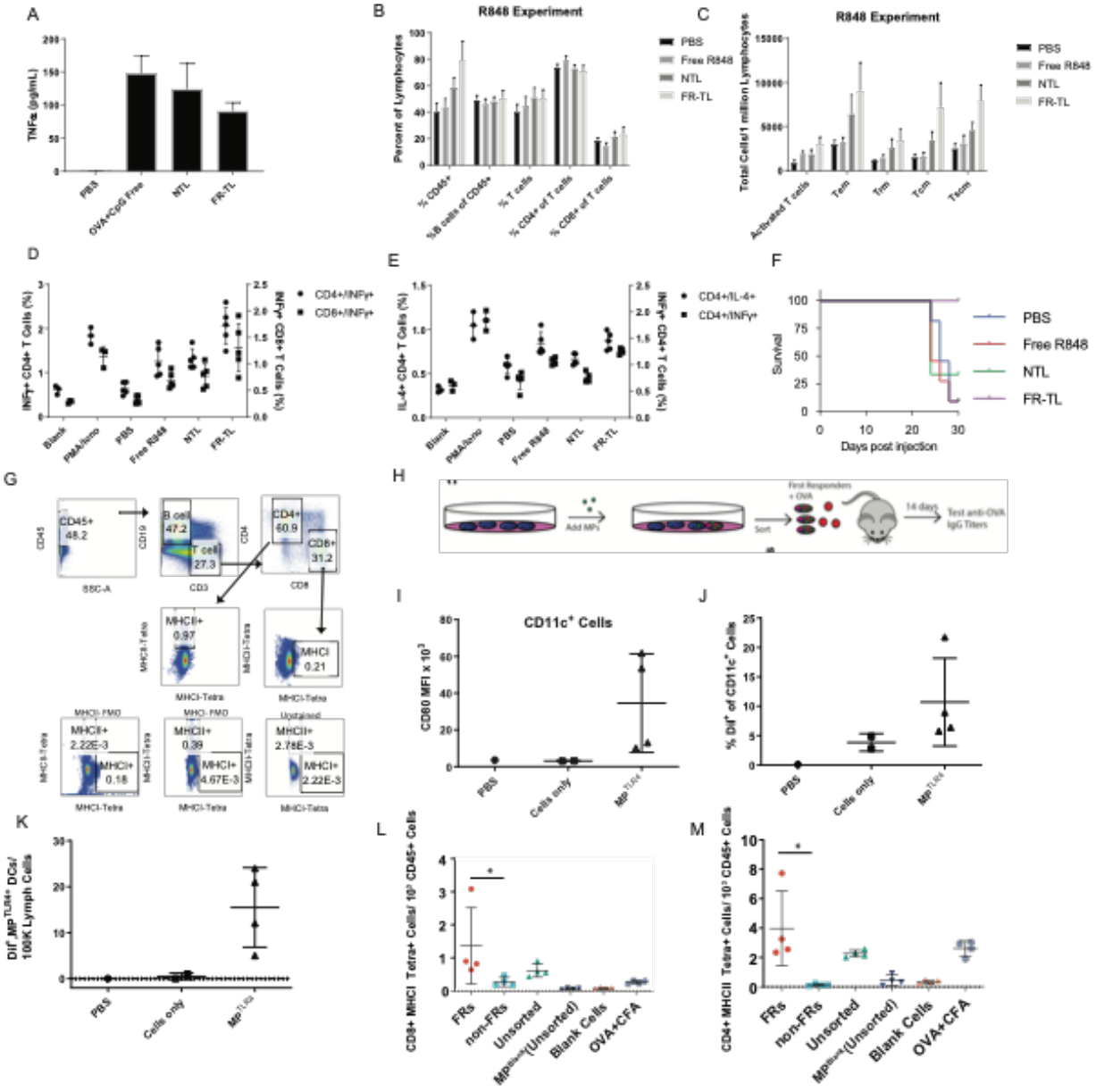

Figure S7. In vivo analysis of FR-TL formulations and ex vivo FR analysis. Related to figure 6. (A) Systemic TNFa levels in vivo after CpG/OVA liposome injection. 1 h after 100 uL liposome injection or free CpG/OVA equivalent (10 ug/ 100 ug) or PBS control serum samples were taken and analyzed via CBA. Error bars represent +/- SD of 5 mice per group (B-C) Aurora analysis of lymph nodes from R848 in vivo experiment in Fig 6E. (B) % of all lymph cells that were CD45+, CD3+/CD45+ (T cells), CD4/CD3/CD45+ or CD8/CD3/CD45+ (C) T cells were further divided into Activated T cells (CD25/CD44/CD69+), effector memory (Tem, CD45+/CD62L-), resident memory (Trm, CD27-/CD62L-/CD44+/CD69+), central memory (Tcm, CD27+/CD28+/CD44+/CD127+/CD62L+) or stem cell memory (Tscm, CD27+/CD28+/CD62L+/CD127+/CD69-) (D-E) Intracellular staining analysis of R848 in vivo experiment. Spenocytes taken from mice in figure 6B were incubated for 12 h with monensin and either (D) the major MHCI OVA epitope (OVA 257-264) tetramer or (E) the major MHCII OVA epitope (OVA 323-339) and stained for CD8/CD4 and for IL-4/IFNγ using ICS. (F) Survival curve for E7-OVA experiment in figure 6G. Mice were sacrificed with tumor was >20 mm in any direction N=10. (G) Representative flow plots showing gating strategy for tetramer staining in figure 6C/F. Bottom row shows FMO controls for both MHCI and MHCII and blank. (H) Schematic of FR adoptive transfer experiment. BMDCs were incubated 1:1 with MPTLR4 for 15 minutes in media with tracker DiI dye washed and sorted into FR or nFR populations. Both hind leg footpads of a C57BL/6 mouse were injected with either 100K FRs, 1 million nFRs, 1 million unsorted MP incubated BMDCs, untreated BMDCs, CFA (positive control) or PBS (negative control). All samples except PBS contained OVA (10 ug per footpad). (I-K) Data from preliminary validation (N=3) where C57BL/6 mice were injected with unsorted MP+BMDC+OVA+DiI and 24 h later inguanal lymph nodes tested via ISX for (I) CD80 expression on CD11c+ cell, (J) DiI+ CD11c+ cells and (K) MP+, DiI+ DCs. (L) CD8+ T cells positive for a MHCI tetramer to the major MHCI epitope OVA 257-264. (M) CD4+ T cells positive for a MHCII tetramer to the major MHCII epitope OVA 323-339. Error bars indicate ±SD. Significance was determined by two-way ANOVA *p<0.05, **p<0.01, ***p<1x10-4 and NS= not significantError bars indicate +/- SD of N=5 unless otherwise noted.